Laminated Partially-Composite Plate Theory (LPCPT)-An extension of the classical laminated plate theory for flexible n-layer plates with partial

Composite Structures 380 (2026) 119951

Contents lists available at ScienceDirect

Composite Structures

journal homepage: www.elsevier.com/locate/compstruct

Laminated Partially-Composite Plate Theory (LPCPT)—An extension of the classical laminated plate theory for flexible *n*-layer plates with partial interlayer interaction

S.R. Atashipour [a,b,*], N. Challamel [c], P.D. Folkow [a], U.A. Girhammar [d]

[a] Division of Dynamics, Department of Mechanics and Maritime Sciences (M2), Chalmers University of Technology, SE-412 96 Gothenburg, Sweden
[b] Division of Vehicular Systems, Department of Electrical Engineering, Linköping University, 58183 Linköping, Sweden
[c] Université de Bretagne Sud, UBS – Institut de Recherche Dupuy de Lôme IRDL (CNRS UMR 6027), Centre de Recherche, Rue de Saint Maudé, BP 92116, 56321 Lorient Cedex, France
[d] Department of Engineering Sciences and Mathematics, Division of Wood Science and Engineering, Luleå University of Technology, Skellefteå, Sweden

ARTICLE INFO

Keywords:
Partial-composite plate model
Orthotropic layers
Interlayer interaction imperfection
Higher-order theory results
Mono- and bi-axial buckling
Free vibrations

ABSTRACT

This paper introduces the Laminated Partial-Composite Plate Theory (LPCPT), as an extension of the classical laminated plate theory (CLPT), incorporating the effects of partial-interaction imperfection at the constituting layers' interfaces. The interlayer interaction effects are modelled through out-of-plane shear stresses based on a shear spring model in terms of the relative displacements/slips at the interfaces. The proposed LPCPT extends a recently developed model for multilayer composite beam/column elements with interlayer partial-interaction imperfection. The model's governing equations, as well as the extended classical boundary conditions, are formulated. Analytical solution schemes are introduced for free vibrations and buckling of partial-composite plates. The analytical solutions can flexibly capture any number of constituent layers. The validity and high accuracy of the established approach are demonstrated via comparative numerical results based on 3-D finite element analysis (FEA). It is shown how the buckling loads and natural vibration frequencies degrade from those predicted based on CLPT with perfect-bonding ideal assumptions, considering different levels of interlayer interaction. For a special case where the interlayer interaction modulus is set to the equivalent layers' transverse shear modulus, the results of the present model are shown to match those of thick integrated plates based on higher-order shear deformation theory (HSDT).

1. Introduction

Layered plates are key structural elements omnipresent in different branches of modern technology, from marine engineering [1–4] and automotive industries [5–7] to aviation and aerospace structures [8–11] and advanced structural building applications [12–14]. This widespread application is due to their superior properties over traditional monolithic structures, such as high stiffness- and strength-to-weight ratios and flexibility in design for different applications. However, due to the abrupt through-thickness changes of constituent materials and mismatches in mechanical properties at the layer interfaces, their structural performance may degrade from an ideally bonded and fully integrated structure.

Despite the existence of a wide variety of frequently-used conventional theories for the structural static and dynamic analyses of laminated plates, the vast majority rely on the key assumption of kinematic and strain continuity conditions; i.e., the idealized perfect-bonding condition at the interlayers. This can be evidenced, e.g., from the simplest Reissner-Stavsky classical laminated plate theory [15] based on the Kirchhoff-Love kinematics, to the extensions of Mindlin's first-order shear deformable theory [16] for the laminated plates [17], and different refined higher-order shear deformation theories such as those of Levinsson [18], Librescu [19], Reddy [20] based on a parabolic model, Touratier [21] based on a trigonometric model, Karama et al. [22] and Mechab [23], based on hyperbolic models for the through-thickness shear strains, etc. Several refined models and modified forms of the conventional laminated plate theories have also been introduced in the past decades, mainly focusing on improvement and more

* Corresponding author at: Division of Dynamics, Department of Mechanics and Maritime Sciences (M2), Chalmers University of Technology, SE-412 96 Gothenburg, Sweden.
E-mail address: rasoul.atashipour@liu.se (S.R. Atashipour).

https://doi.org/10.1016/j.compstruct.2025.119951
Received 7 August 2025; Received in revised form 10 November 2025; Accepted 12 December 2025
Available online 14 December 2025

flexibility of the displacement field functions for easier implementation into the numerical approaches; e.g., the category of C° higher-order shear deformation theories of five to seven variables, initially presented by Shankara et al. [24]; also their extensions for the category of quasi-3D plate theories by describing the transverse displacement component using higher-order polynomials with respect to the thickness coordinate (see e.g., [25,26]).

In the standard class of zig-zag theories, formulated as a superposition of a conventional first-, second-, and/or higher-order displacement fields and a local zig-zag function [27–29], the drawback associated with an imposed ideal out-of-plane shear and in-plane normal deformation patterns is inherently addressed, but not the effects of non-perfect interactions between individual layers. Evidently, the mentioned theories are incapable of capturing the realistic mechanical behaviour of the layered plates when the partial interfacial interaction effects cannot be dismissed, e.g., when the layered structures are susceptible to debonding/delamination [30,31], or the constituting layers are bonded through relatively soft adhesives [32,33] and/or connected via discrete mechanical connectors and fasteners [34–36], etc. The class of layerwise theories [37], including the categories of displacement-based and mixed displacement-and-stress variable types, treat each layer individually, and therefore, have been extensively utilized to model such non-perfect interfacial interaction behaviour [38–42], however, at the expense of a relatively high computational cost [43], particularly by increasing the number of layers, while gaining analytical solutions is cumbersome. Compromising between accuracy and efficiency, several refined and hybrid zig-zag-layerwise theories have been proposed [37,43–45].

Imperfections in layered composite elements may be geometrical (such as initial deflection and out-of-straightness [46–49], geometrical gaps and waviness/wrinkles in the layers [50–52], variations in layer thickness [53,54], and loading eccentricity and boundary condition imperfections/irregularities [55–57]), or of material and constructional type (e.g., cracks and partial delamination [58–60], interfacial bonding defects such as incomplete/uneven/poor bonding, or interfacial shear slip [61–68], etc.). The influence of interfacial bonding imperfection on the mechanical behaviour of layered structures has been extensively studied by many researchers, modelling imperfect bonding behaviour using linear spring-like models [69–71] or based on nonlinear elastic/ elastoplastic/ viscoelastic models [66,72,73] in computational simulations.

In some applications, various types of discrete mechanical connectors, such as bolts, screws, nails, dowels, or different types of adhesives, are used to keep the integrity of the layered composite elements (e.g., in laminated timber composite applications). Therefore, their structural behaviour and performance may deviate from those of ideal composites (i.e., perfectly bonded or the so-called fully-composite laminates) due to the relative interlayer slips [74,75]. This specific type of interfacial imperfection, in the form of interlayer partial-composite interaction, is known as the "partial-composite" behaviour. For a detailed literature background on the partial-composite phenomenon, readers are referred to [76]. The present study aims to introduce the Laminated Partial-Composite Plate Theory (LPCPT), focusing on this specific type of imperfection. Consequently, any other forms of interfacial bonding imperfections are beyond the scope of this theory.

The present paper addresses the mentioned challenge associated with treating partial interlayer interaction effects through a new innovative approach by introducing the Laminated Partial-Composite Plate Theory (LPCPT) as an extension of the known classical laminated plate theory (CLPT), and accompanied by an exact analytical solution scheme. The established LPCPT-based analytical solution scheme provides reliable and accurate results at negligible computational cost, without any increase in the computational burden as the number of layers increases, unlike other existing approaches based on, e.g., layerwise theories. The partial interfacial interaction effects are included in the form of out-of-plane shear stresses based on a shear spring model in terms of the relative displacements/slips at the interfaces. Similar to the broad class of layerwise theories [37,77], the introduced simplest Laminated Partial-Composite Plate Theory (LPCPT) may serve as a foundational framework for a potential series of refined extensions based on different shear deformable kinematic models (ranging from Mindlin-Reissner to higher-order models) for the internal shear deformations at each individual layer.

The LPCPT-based solutions in the present paper are devoted to the problems of stability and dynamics of elastic multilayered plates composed of n layers, partially connected at each layer interface, or equivalently connected through shear layers; also referred to as a connection with imperfect bonding. The earliest relevant effort can be attributed to Hoff [78] for the bending and buckling analyses of a symmetric sandwich plate. Hoff's sandwich plate is composed of two identical layers for the faces, each assumed to be governed by an elastic extensible Kirchhoff-Love or Germain-Lagrange plate model, connected by a pure shear layer as the core of the sandwich plate [78]. A similar study was carried out by Rzhanitsyn [79] for a sandwich plate with unsymmetrical layers (see also the historical review of Challamel *et al.* [80]). Such a sandwich plate is equivalent to a two-layer plate connected by a soft shear layer of zero thickness in the asymptotic limit, which may be referred to as the concept of the laminated plate with partial interaction. Recently, a number of research studies have been conducted to investigate the structural behaviour of two-layer plates with partial interlayer interaction. Andrade et al. [81] and Barroso et al. [82] employed Hoff's sandwich approach for the bending, buckling, and vibration analyses of two-layer partial composite plates, with application to glass structural members. Boutin [83] showed that a tri-Laplacian governing equation can also be derived for unsymmetrical three-layer sandwich plates with two homogeneous faces, or equivalently, two-layer composite plates with interlayer slip. Shen et al. [84] investigated the static bending of a multilayered plate with approximate kinematic fields, as a reconsideration of the study first conducted by Bolotin [85,86] for the bending of multilayered plates with interlayer slip under transversal distributed loading. Shaat et al. [87,88] developed an analytical model for static responses of multilayer beams and plates subjected to thermal and mechanical loading using a slip-interface model. Wu et al. [89] formulated the principle of virtual work and the reciprocal theorem for laminated plates accounting for interlayer slip, and subsequently derived the principles of minimum potential and complementary energy. Shen et al. [90] studied the large deflection bending of multilayer two-dimensional structures having interlayer slips. Recently, Atashipour et al. [34] developed a Timoshenko/ Engesser-kinematic-based model for composite beam/column elements with interlayer partial interaction imperfection, complemented by exact analytical solutions for the structural stability and dynamic analyses, without any limitation on the number of constituent layers. No such work appears to exist in the literature for flexible n-layer plates. The present study aims to address this apparent gap by formulating the Laminated Partial-Composite Plate Theory (LPCPT) and the accompanied exact stability and vibration solutions for the n-layer partial-composite plates. A unique formulation of the model is presented for the first time. The governing differential equations of the model, as well as the corresponding extended classical boundary conditions, are extracted and formulated using the extended Hamilton's energy principle. The problems of free vibrations and buckling of partial composite plates under mono- or bi-axial compressive in-plane loads are treated analytically. The analytical solutions are general in nature and can flexibly capture any arbitrary number of identical orthotropic constituent layers. Furthermore, direct analytical solution alternatives for laminated plates with a specified number of constituent layers are presented, treating laminated plates with non-identical layers. It is demonstrated how the buckling loads and natural vibration frequencies are degraded from those predicted based on CLPT with ideal bonding assumptions, considering different levels of interlayer interaction.

2. Laminated partially-composite plate model

2.1. Problem description and model formulation

Assume a laminated plate consisting of n layers of uniform thickness (Fig. 1), in which the layers are imperfectly bonded to one another at their interfaces. Thus, each layer interacts partially with the adjacent layers at their interfaces when the laminated plate is loaded. Depending on the level of interlayer interaction, the structural performance of the laminate is expected to be degraded when compared to an ideal perfectly-bonded case.

For each layer, a local coordinate system $(\chi_i, \upsilon_i, \zeta_i)$ is defined here such that the planar axes (χ_i, υ_i) are coincident with the layer's mid-plane, as illustrated in Fig. 1. Furthermore, the global coordinate system (x, y, z) is established where its origin is located in a specific transversal location to fulfil the uncoupling conditions between the bending and stretching effects of the laminate; e.g., for a symmetrically laid-up, the origin of the $z-$axis is located at the geometric transverse centroid of the laminate.

The planar components of the displacement field for the i-th layer of the laminated plate, u_i and v_i, can be expressed based on the kinematics of the classical plate theory, as

$$\begin{aligned} u_i(x,y,z,t) &= u_{0,i}(x,y,t) - \zeta_i \partial w(x,y,t)/\partial x \\ v_i(x,y,z,t) &= v_{0,i}(x,y,t) - \zeta_i \partial w(x,y,t)/\partial y \end{aligned} \tag{1}$$

where $u_{0,i}$ and $v_{0,i}$ are the displacements of the i-th layer's mid-plane along x and y directions, respectively, and ζ_i is the local transverse coordinate variable (i.e., along $z-$axis) for the i-th layer with an origin located at the mid-plane. Also, $w(x,y,t)$ is the transverse displacement/deflection of the plate at the planar coordinates (x,y) and the time t.

Assuming a relative slip between the laminated plate's layers due to imperfect bonding and partial interaction effects, the components of the displacement field for the i-th layer can also be described in terms of the global transverse displacement in the form:

$$\begin{aligned} u_i(x,y,z,t) &= u_{0,i}^{\text{Slip}}(x,y,t) - z\partial w(x,y,t)/\partial x \\ v_i(x,y,z,t) &= v_{0,i}^{\text{Slip}}(x,y,t) - z\partial w(x,y,t)/\partial y \end{aligned} \tag{2}$$

The model's kinematics of deformations and the internal load resultants are illustrated in Fig. 2.

In Eq. (2), $u_{0,i}^{\text{Slip}}$ and $v_{0,i}^{\text{Slip}}$ are the absolute in-plane displacements (in the global coordinate system) of the i-th layer, respectively, along x and y directions, which may be affected by the relative slips at the interfaces due to the partial interlayer interaction. Each layer's mid-plane has a different distance from neutral plane of the entire laminate's cross-section ($z_i = z - \zeta_i$; i.e., the difference between the vertical axes of the global and local coordinate system at any transverse level). Therefore, at a deformed state due to the dynamic motions or external loads, the aforementioned planar displacements at each layer may be formulated as the sum of the in-plane displacements of the i-th layer's mid-plane and those due to the transverse displacements; i.e.,

$$\begin{aligned} u_{0,i}^{\text{Slip}} &= u_{0,i} + (z - \zeta_i)\frac{\partial w}{\partial x} = u_{0,i} + z_i \frac{\partial w}{\partial x} \\ v_{0,i}^{\text{Slip}} &= v_{0,i} + (z - \zeta_i)\frac{\partial w}{\partial y} = v_{0,i} + z_i \frac{\partial w}{\partial y} \end{aligned} \tag{3}$$

where z_i is the transverse distance between the i-th layer's mid-plane and the location of the origin of the global coordinate system (see Fig. 1). The linear strain components may be directly deduced from Eq. (1) for the small displacements as follows

$$\begin{aligned} \varepsilon_{x,i} &= \frac{\partial u_{0,i}}{\partial x} - \zeta_i \frac{\partial^2 w}{\partial x^2} \\ \varepsilon_{y,i} &= \frac{\partial v_{0,i}}{\partial y} - \zeta_i \frac{\partial^2 w}{\partial y^2} \\ \gamma_{xy,i} &= \frac{\partial u_{0,i}}{\partial y} + \frac{\partial v_{0,i}}{\partial x} - 2\zeta_i \frac{\partial^2 w}{\partial x \partial y} \end{aligned} \tag{4}$$

The constitutive relations for a laminate composed of orthotropic layers,

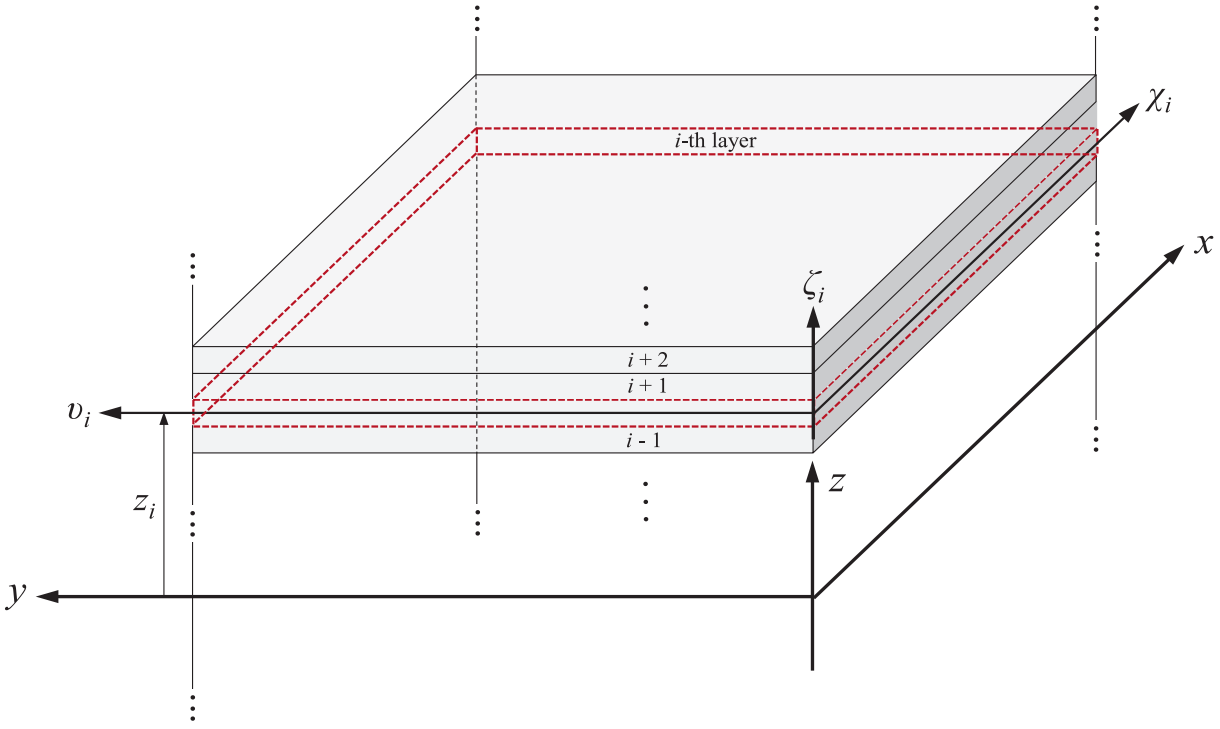

Fig. 1. Global and local coordinate systems, and their correlation in a laminated configuration.

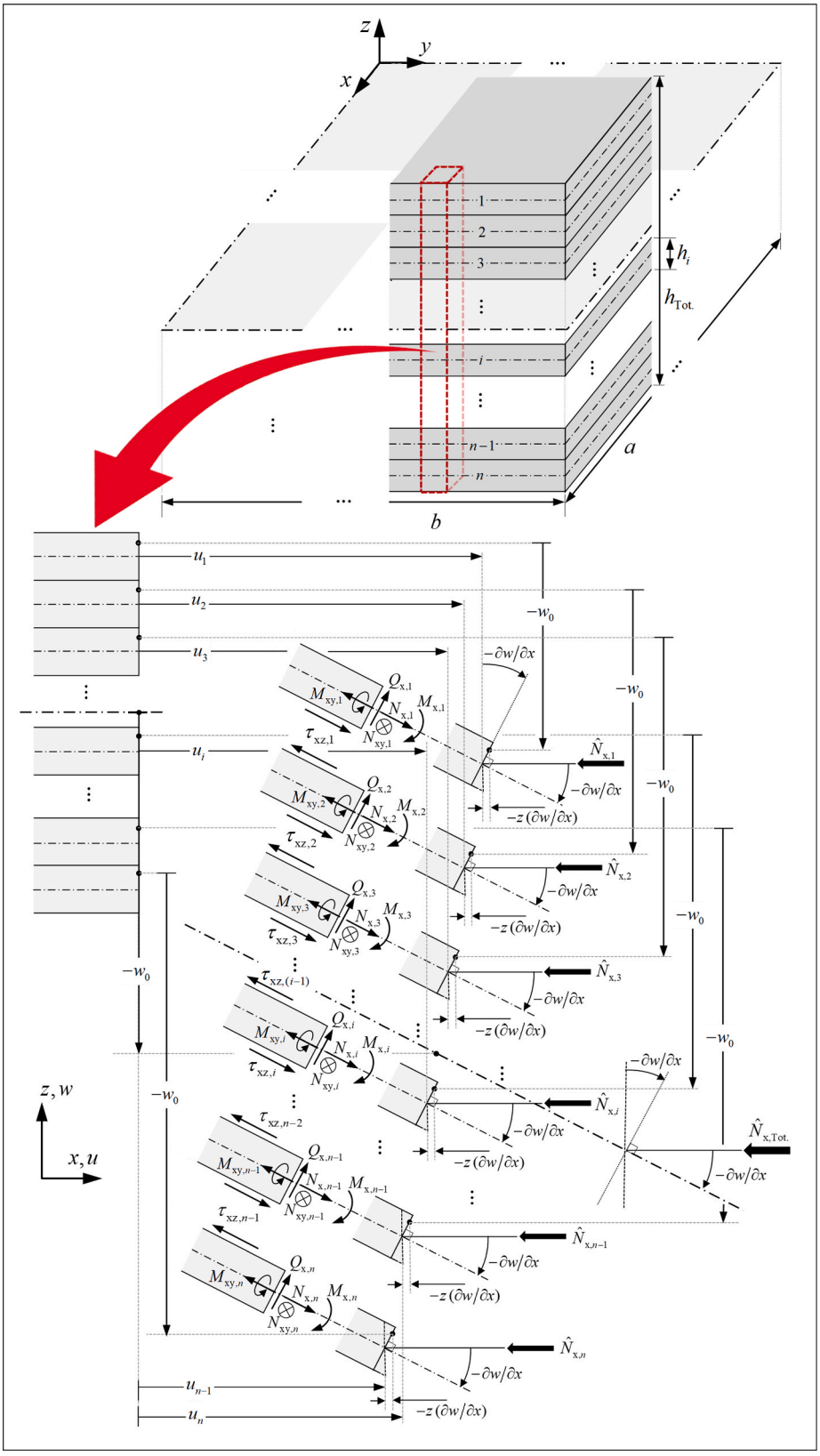

Fig. 2. The model's kinematics of deformations and the internal force and stress resultant assumptions. At the i-th interface, the relative slip represents the displacement discontinuity between the bottom surface of the i-th layer and the top surface of the $(i + 1)$-th layer.

oriented arbitrarily with respect to the layers' plane, based on the 2-D plane-stress Hooke's law under the assumption of linear elastic behavior for small deformations, after replacing Eq. (4), are expressed as

$$\begin{aligned}\sigma_{x,i} &= \frac{E_{x,i}}{1-\nu_{xy,i}\nu_{yx,i}}(\varepsilon_{x,i}+\nu_{yx,i}\varepsilon_{y,i}) = \frac{E_{x,i}}{1-\nu_{xy,i}\nu_{yx,i}}\left[\left(\frac{\partial u_{0,i}}{\partial x}+\nu_{yx,i}\frac{\partial v_{0,i}}{\partial y}\right)\right.\\ &\left.-\zeta_i\left(\frac{\partial^2 w}{\partial x^2}+\nu_{yx,i}\frac{\partial^2 w}{\partial y^2}\right)\right]\\ \sigma_{y,i} &= \frac{E_{y,i}}{1-\nu_{xy,i}\nu_{yx,i}}(\nu_{xy,i}\varepsilon_{x,i}+\varepsilon_{y,i}) = \frac{E_{y,i}}{1-\nu_{xy,i}\nu_{yx,i}}\left[\left(\nu_{xy,i}\frac{\partial u_{0,i}}{\partial x}+\frac{\partial v_{0,i}}{\partial y}\right)\right.\\ &\left.-\zeta_i\left(\nu_{xy,i}\frac{\partial^2 w}{\partial x^2}+\frac{\partial^2 w}{\partial y^2}\right)\right]\\ \tau_{xy,i} &= G_{xy,i}\gamma_{xy,i} = G_{xy,i}\left(\frac{\partial u_{0,i}}{\partial y}+\frac{\partial v_{0,i}}{\partial x}-2\zeta_i\frac{\partial^2 w}{\partial x\partial y}\right)\end{aligned} \tag{5}$$

Based on the simplest Kirchhoff-Love kinematic assumptions, the out-of-plane strains in each layer are zero due to the shear rigidity assumptions in the inherence of the displacement field. Therefore, the non-zero transverse shear stresses based on the present model are those to be attributed to the interlayer slip due to a non-perfect partial interaction and relative shear displacements between the layers. This can be formulated via a linear elastic state in terms of a constant slip modulus k_n [N/m^3] in the form:

$$\begin{aligned}\tau_{xz,i} &= k_i\left(u_{0,i+1}^{\text{Slip}}-u_{0,i}^{\text{Slip}}\right)\\ \tau_{yz,i} &= k_i\left(v_{0,i+1}^{\text{Slip}}-v_{0,i}^{\text{Slip}}\right)\end{aligned} \tag{6}$$

Replacing the slip displacement relations from Eq. (3) into Eq. (6) yields

$$\begin{aligned}\tau_{xz,i} &= k_i\left(u_{0,i+1}-u_{0,i}+d_i\frac{\partial w}{\partial x}\right)\\ \tau_{yz,i} &= k_i\left(v_{0,i+1}-v_{0,i}+d_i\frac{\partial w}{\partial y}\right)\end{aligned} \tag{7}$$

where

$$d_i = z_{i+1}-z_i = \frac{1}{2}(h_i+h_{i+1}) \tag{8}$$

The governing differential equations of the described model are developed in the following.

2.2. Governing equations of the model

To formulate the governing differential equations of motion of the model, the extended Hamilton's energy principle [91] is employed here as

$$\delta\int_{t_1}^{t_2}[T-(U_{\text{str.}}+U_{\text{ext.}})]\mathrm{d}t = 0 \tag{9}$$

where δ is the variational operator, T is the system's kinetic energy, and $U_{\text{str.}}$ is the elastic strain energy. Also, $U_{\text{ext.}}$ represents the potential energy of the external loads, including the bending and axial effects of the applied in-plane compressive edge forces per unit length at each individual layer: $\widehat{N}_{x,i}$ and $\widehat{N}_{y,i}$ $(i=1,2,\ldots,n)$. Obviously, the total applied in-plane compressive forces per unit edge length acting on the entire laminate are $\widehat{N}_{x,\text{Tot.}}=\sum_{i=1}^{n}\widehat{N}_{x,i}$ and $\widehat{N}_{y,\text{Tot.}}=\sum_{i=1}^{n}\widehat{N}_{y,i}$. The aforementioned energy terms are defined as follows

$$U_{\text{str.}} = \frac{1}{2}\iiint_V\left(\sigma_x\varepsilon_x+\sigma_y\varepsilon_y+\tau_{xy}\gamma_{xy}\right)\mathrm{d}V+\frac{1}{2}\iint_{S^*}(\tau_{xz}\Delta u+\tau_{yz}\Delta v)\mathrm{d}S^* \tag{10a}$$

$$U_{\text{ext.}} = -\iint_S q(x,y)w\,\mathrm{d}S-\frac{1}{2}\iint_S\left[\widehat{N}_{x,\text{Tot.}}(\partial w/\partial x)^2+\widehat{N}_{y,\text{Tot.}}(\partial w/\partial y)^2\right]\mathrm{d}S+\sum_{i=1}^{n}\iint_S\left[\widehat{N}_{x,i}(\partial u_{0,i}/\partial x)+\widehat{N}_{y,i}(\partial v_{0,i}/\partial y)\right]\mathrm{d}S \tag{10b}$$

$$T = \frac{1}{2}\iiint_V\rho(\dot{u}^2+\dot{v}^2+\dot{w}^2)\mathrm{d}V \tag{10c}$$

in which ρ is the material density; $\mathrm{d}S$ is the 2-D (in-plane) differential element, $\mathrm{d}V$ is the volume element of the laminated plate, and $\mathrm{d}S^*$ is the surface differential element at the layers' interfaces. Substituting Eqs. (4) through (8) into Eq. (10a), and assuming the principal material coordinates for each layer coincide with those of the plate in the global system (i.e., the specially-orthotropic), the strain energy is given as

$$\begin{aligned}U_{\text{str.}} =& \frac{1}{2}\sum_{i=1}^{n}\iint_S\left[A_{11,i}\left(\frac{\partial u_{0,i}}{\partial x}\right)^2+A_{66,i}\left(\frac{\partial u_{0,i}}{\partial y}\right)^2+2A_{12,i}\left(\frac{\partial u_{0,i}}{\partial x}\right)\left(\frac{\partial v_{0,i}}{\partial y}\right)\right.\\ &\left.+2A_{66,i}\left(\frac{\partial u_{0,i}}{\partial y}\right)\left(\frac{\partial v_{0,i}}{\partial x}\right)+A_{66,i}\left(\frac{\partial v_{0,i}}{\partial x}\right)^2+A_{22,i}\left(\frac{\partial v_{0,i}}{\partial y}\right)^2\right]\mathrm{d}S\\ &-\frac{1}{2}\sum_{i=1}^{n}\iint_S\left[2\left(B_{11,i}\frac{\partial u_{0,i}}{\partial x}+B_{12,i}\frac{\partial v_{0,i}}{\partial y}\right)\left(\frac{\partial^2 w}{\partial x^2}\right)+2\left(B_{12,i}\frac{\partial u_{0,i}}{\partial x}+B_{22,i}\frac{\partial v_{0,i}}{\partial y}\right)\left(\frac{\partial^2 w}{\partial y^2}\right)\right.\\ &\left.+4B_{66,i}\left(\frac{\partial u_{0,i}}{\partial y}+\frac{\partial v_{0,i}}{\partial x}\right)\left(\frac{\partial^2 w}{\partial x\partial y}\right)\right]\mathrm{d}S\\ &+\frac{1}{2}\sum_{i=1}^{n}\iint_S\left[D_{11,i}\left(\frac{\partial^2 w}{\partial x^2}\right)^2+2D_{12,i}\left(\frac{\partial^2 w}{\partial x^2}\right)\left(\frac{\partial^2 w}{\partial y^2}\right)+D_{22,i}\left(\frac{\partial^2 w}{\partial y^2}\right)^2\right.\\ &\left.+4D_{66,i}\left(\frac{\partial^2 w}{\partial x\partial y}\right)^2\right]\mathrm{d}S\\ &+\frac{1}{2}\sum_{i=1}^{n-1}k_i\iint_S\left[\left(u_{0,i+1}-u_{0,i}+d_i\frac{\partial w}{\partial x}\right)^2+\left(v_{0,i+1}-v_{0,i}+d_i\frac{\partial w}{\partial y}\right)^2\right]\mathrm{d}S\end{aligned} \tag{11}$$

where the coefficients $A_{rs,i}$, $B_{rs,i}$, and $D_{rs,i}$ $(r,s\in\{1,2,6\})$ are the axial stiffnesses per unit length, stretching-bending stiffness, and the bending stiffness of the i-th layer of the plate, and are determined as

$$\begin{aligned}(A_{11,i},A_{12,i},A_{22,i},A_{66,i}) &= \int_{z_i-\frac{h_i}{2}}^{z_i+\frac{h_i}{2}}(Q_{xx,i},Q_{xy,i},Q_{yy,i},G_{xy,i})\mathrm{d}z\\ &= \left(\frac{E_{x,i}h_i}{1-\nu_{xy,i}\nu_{yx,i}},\frac{\nu_{xy,i}E_{y,i}h_i}{1-\nu_{xy,i}\nu_{yx,i}}=\frac{\nu_{yx,i}E_{x,i}h_i}{1-\nu_{xy,i}\nu_{yx,i}},\frac{E_{y,i}h_i}{1-\nu_{xy,i}\nu_{yx,i}},G_{xy,i}h_i\right)\\ (B_{11,i},B_{12,i},B_{22,i},B_{66,i}) &= \int_{z_i-\frac{h_i}{2}}^{z_i+\frac{h_i}{2}}(Q_{xx,i},Q_{xy,i},Q_{yy,i},G_{12,i})\zeta_n\mathrm{d}z = 0\\ (D_{11,i},D_{12,i},D_{22,i},D_{66,i}) &= \int_{z_i-\frac{h_i}{2}}^{z_i+\frac{h_i}{2}}(Q_{xx,i},Q_{xy,i},Q_{yy,i},G_{xy,i})\zeta_i^2\mathrm{d}z\\ &= \left(\frac{E_{x,i}h_i^3}{12(1-\nu_{xy,i}\nu_{yx,i})},\frac{\nu_{xy,i}E_{y,i}h_i^3}{12(1-\nu_{xy,i}\nu_{yx,i})}=\frac{\nu_{yx,i}E_{x,i}h_i^3}{12(1-\nu_{xy,i}\nu_{yx,i})},\frac{E_{y,i}h_i^3}{12(1-\nu_{xy,i}\nu_{yx,i})},\right.\\ &\left.\frac{1}{12}G_{xy,i}h_i^3\right),\quad(\zeta_i=z-z_i)\end{aligned} \tag{12}$$

where

$$Q_{xx,i} = \frac{E_{x,i}}{1-\nu_{xy,i}\nu_{yx,i}}$$
$$Q_{yy,i} = \frac{E_{y,i}}{1-\nu_{xy,i}\nu_{yx,i}} \tag{13}$$
$$Q_{xy,i} = \frac{\nu_{xy,i}E_{y,i}}{1-\nu_{xy,i}\nu_{yx,i}} = \frac{\nu_{yx,i}E_{x,i}}{1-\nu_{xy,i}\nu_{yx,i}}$$

The kinetic energy of the model can be formulated by replacing Eq. (1) into Eq. (10c) as follows

$$T = \frac{1}{2}\sum_{i=1}^{n} I_{0,i}\iint_S \left(\dot{u}_{0,i}^2 + \dot{v}_{0,i}^2 + \dot{w}^2\right)\mathrm{d}S$$
$$-\sum_{i=1}^{n} I_{1,i}\iint_S \left[\dot{u}_{0,i}(\partial\dot{w}/\partial x) + \dot{v}_{0,i}(\partial\dot{w}/\partial y)\right]\mathrm{d}S \tag{14}$$
$$+\frac{1}{2}\sum_{i=1}^{n} I_{2,i}\iint_S \left[(\partial\dot{w}/\partial x)^2 + (\partial\dot{w}/\partial y)^2\right]\mathrm{d}S$$

in which the mass and rotary inertia terms for each layer are defined as

$$I_{0,i} = \int_{z_i-\frac{h_i}{2}}^{z_i+\frac{h_i}{2}} \rho_i \mathrm{d}z = \rho_i h_i$$
$$I_{1,i} = \int_{z_i-\frac{h_i}{2}}^{z_i+\frac{h_i}{2}} \rho_i \zeta_i \mathrm{d}z = 0 \tag{15}$$
$$I_{2,i} = \int_{z_i-\frac{h_i}{2}}^{z_i+\frac{h_i}{2}} \rho_i \zeta_i^2 \mathrm{d}z = \frac{1}{12}\rho_i h_i^3, \qquad (\zeta_i = z - z_i)$$

It is noteworthy that since each layer is assumed to be homogeneous and of a rectangular section, the coupling stretching-bending term, B_i, as well as the coupling effects of translational-rotational inertia, $I_{1,i}$, for each individual layer obviously vanish. Furthermore, to eliminate the stretching-bending coupling effects for the entire laminate, we consider the origin of the global coordinate axis z at a location to fulfil the following condition:

$$\int_{z_1-\frac{h_1}{2}}^{z_N+\frac{h_N}{2}} \frac{E_i}{1-\nu_i^2}\zeta_n \mathrm{d}z = \sum_{i=1}^{n} \frac{E_i h_i}{1-\nu_i^2} z_i = 0 \tag{16}$$

Applying the extended Hamilton's principle (9) to Eqs. (10b), (11)-(15) yields a set of $2n+1$ governing differential equations of motion of the model as follows

$$\delta u_{0,1} : \frac{\partial N_{x,1}}{\partial x} + \frac{\partial N_{xy,1}}{\partial y} + \tau_{xz,1} = I_{0,1}\ddot{u}_{0,1} \tag{17a}$$

$$\delta v_{0,1} : \frac{\partial N_{xy,1}}{\partial x} + \frac{\partial N_{y,1}}{\partial y} + \tau_{yz,1} = I_{0,1}\ddot{v}_{0,1} \tag{17b}$$

$$\left\{\delta u_{0,i} : \frac{\partial N_{x,i}}{\partial x} + \frac{\partial N_{xy,i}}{\partial y} + \tau_{xz,i} - \tau_{xz,i-1} = I_{0,i}\ddot{u}_{0,i}, \qquad (i = 2,3,\ldots,n-1)\right. \tag{17c}$$

$$\left\{\delta v_{0,i} : \frac{\partial N_{xy,i}}{\partial x} + \frac{\partial N_{y,i}}{\partial y} + \tau_{yz,i} - \tau_{yz,i-1} = I_{0,i}\ddot{v}_{0,i}, \qquad (i = 2,3,\ldots,n-1)\right. \tag{17d}$$

$$\delta u_{0,n} : \frac{\partial N_{x,n}}{\partial x} + \frac{\partial N_{xy,n}}{\partial y} - \tau_{xz,n-1} = I_{0,n}\ddot{u}_{0,n} \tag{17e}$$

$$\delta v_{0,n} : \frac{\partial N_{xy,n}}{\partial x} + \frac{\partial N_{y,n}}{\partial y} - \tau_{yz,n-1} = I_{0,n}\ddot{v}_{0,n} \tag{17f}$$

$$\delta w : \frac{\partial^2 M_x^{(0)}}{\partial x^2} + 2\frac{\partial^2 M_{xy}^{(0)}}{\partial x \partial y} + \frac{\partial^2 M_y^{(0)}}{\partial y^2} + \sum_{i=1}^{n-1} d_i\left(\frac{\partial \tau_{xz,i}}{\partial x} + \frac{\partial \tau_{yz,i}}{\partial y}\right)$$
$$-\widehat{N}_{x,\mathrm{Tot.}}\left(\frac{\partial^2 w}{\partial x^2}\right) - \widehat{N}_{y,\mathrm{Tot.}}\left(\frac{\partial^2 w}{\partial y^2}\right) + q(x,y) = I_0\ddot{w} - I_{2,0}\nabla^2\ddot{w} \tag{17g}$$

where the stress resultants $N_{x,i}, N_{y,i}, N_{xy,i}$ $(i = 1,2,\ldots,n)$ are the normal and shear forces per unit length in each layer of the plate, and are obtained in the form:

$$N_{x,i} = A_{11,i}\frac{\partial u_{0,i}}{\partial x} + A_{12,i}\frac{\partial v_{0,i}}{\partial y}$$
$$N_{y,i} = A_{12,i}\frac{\partial u_{0,i}}{\partial x} + A_{22,i}\frac{\partial v_{0,i}}{\partial y} \tag{18}$$
$$N_{xy,i} = A_{66,i}\left(\frac{\partial u_{0,i}}{\partial y} + \frac{\partial v_{0,i}}{\partial x}\right), \qquad (i = 1,2,\ldots,n)$$

Also, the stress resultants $(M_x^{(0)}, M_y^{(0)}, M_{xy}^{(0)})$ are the bending and twisting moments per unit length of laminated plates, and are obtained as

$$M_x^{(0)} = -\sum_{i=1}^{n}\left(D_{11,i}\frac{\partial^2 w}{\partial x^2} + D_{12,i}\frac{\partial^2 w}{\partial y^2}\right) = -D_{11}^{(0)}\frac{\partial^2 w}{\partial x^2} - D_{12}^{(0)}\frac{\partial^2 w}{\partial y^2}$$
$$M_y^{(0)} = -\sum_{i=1}^{n}\left(D_{12,i}\frac{\partial^2 w}{\partial x^2} + D_{22,i}\frac{\partial^2 w}{\partial y^2}\right) = -D_{12}^{(0)}\frac{\partial^2 w}{\partial x^2} - D_{22}^{(0)}\frac{\partial^2 w}{\partial y^2} \tag{19}$$
$$M_{xy}^{(0)} = -2\sum_{i=1}^{n} D_{66,i}\left(\frac{\partial^2 w}{\partial x \partial y}\right) = -2D_{66}^{(0)}\frac{\partial^2 w}{\partial x \partial y}$$

in which

$$(D_{11}^{(0)}, D_{12}^{(0)}, D_{22}^{(0)}, D_{66}^{(0)}) = \sum_{i=1}^{n}(D_{11,i}, D_{12,i}, D_{22,i}, D_{66,i}) \tag{20}$$

where $D_{rs}^{(0)}$ $(r,s = 1,2,6)$ are different bending/twisting stiffness components of the laminated composite plate with no interlayer interaction. The superscript '(0)' denotes the "non-composite" condition, i.e., a case in which the frictionless layers are laid one another with no relative shear interaction; in other words, zero-interaction between the layers at their interfaces, corresponding to a fully-debonded laminate.

Substituting the above stress resultants as well as Eq. (7) into Eqs. (17a)-g), the governing differential equations of the described extended classical plate model are obtained in the form:

$$\delta u_{0,1} : A_{11,1}\frac{\partial^2 u_{0,1}}{\partial x^2} + A_{66,1}\frac{\partial^2 u_{0,1}}{\partial y^2} - k_1 u_{0,1} + k_1 u_{0,2} + (A_{12,1} + A_{66,1})\frac{\partial^2 v_{0,1}}{\partial x \partial y}$$
$$+ k_1 d_1 \frac{\partial w}{\partial x} = I_{0,1}\ddot{u}_{0,1} \tag{21a}$$

$$\delta v_{0,1}: (A_{12,1}+A_{66,1})\frac{\partial^2 u_{0,1}}{\partial x\partial y} + A_{66,1}\frac{\partial^2 v_{0,1}}{\partial x^2} + A_{22,1}\frac{\partial^2 v_{0,1}}{\partial y^2} - k_1 v_{0,1} + k_1 v_{0,2} + k_1 d_1 \frac{\partial w}{\partial y} = I_{0,1}\ddot{v}_{0,1} \tag{21b}$$

$$\delta u_{0,i}: \begin{cases} A_{11,i}\dfrac{\partial^2 u_{0,i}}{\partial x^2} + A_{66,i}\dfrac{\partial^2 u_{0,i}}{\partial y^2} + k_{i-1}u_{0,i-1} - (k_{i-1}+k_i)u_{0,i} + k_i u_{0,i+1} \\ +\left(A_{12,i}+A_{66,i}\right)\dfrac{\partial^2 v_{0,i}}{\partial x\partial y} + (k_i d_i - k_{i-1}d_{i-1})\dfrac{\partial w}{\partial x} = I_{0,i}\ddot{u}_{0,i}, \\ \quad (i=2,3,...,n-1) \end{cases} \tag{21c}$$

$$\delta v_{0,i}: \begin{cases} \left(A_{12,i}+A_{66,i}\right)\dfrac{\partial^2 u_{0,i}}{\partial x\partial y} + A_{66,i}\dfrac{\partial^2 v_{0,i}}{\partial x^2} + A_{22,i}\dfrac{\partial^2 v_{0,i}}{\partial y^2} + k_{i-1}v_{0,i-1} \\ -(k_{i-1}+k_i)v_{0,i} + k_i v_{0,i+1} + (k_i d_i - k_{i-1}d_{i-1})\dfrac{\partial w}{\partial y} = I_{0,i}\ddot{v}_{0,i}, \\ \quad (i=2,3,...,n-1) \end{cases} \tag{21d}$$

$$\delta u_{0,n}: A_{11,n}\frac{\partial^2 u_{0,n}}{\partial x^2} + A_{66,n}\frac{\partial^2 u_{0,n}}{\partial y^2} + k_{n-1}u_{0,n-1} - k_{n-1}u_{0,n} + (A_{12,n}+A_{66,n})\frac{\partial^2 v_{0,n}}{\partial x\partial y} - k_{n-1}d_{n-1}\frac{\partial w}{\partial x} = I_{0,n}\ddot{u}_{0,n} \tag{21e}$$

$$\delta v_{0,n}: (A_{12,n}+A_{66,n})\frac{\partial^2 u_{0,n}}{\partial x\partial y} + A_{66,n}\frac{\partial^2 v_{0,n}}{\partial x^2} + A_{22,n}\frac{\partial^2 v_{0,n}}{\partial y^2} + k_{n-1}v_{0,n-1} - k_{n-1}v_{0,n} - k_{n-1}d_{n-1}\frac{\partial w}{\partial y} = I_{0,n}\ddot{v}_{0,n} \tag{21f}$$

$$\delta w: \left[D_{11}^{(0)}\frac{\partial^4 w}{\partial x^4} + 2(D_{12}^{(0)}+2D_{66}^{(0)})\frac{\partial^4 w}{\partial x^2\partial y^2} + D_{22}^{(0)}\frac{\partial^4 w}{\partial y^4}\right] + I_0\ddot{w} - I_{2,0}\nabla^2\ddot{w} - \sum_{i=1}^{n-1} k_i d_i\left(\frac{\partial u_{0,i+1}}{\partial x} - \frac{\partial u_{0,i}}{\partial x} + d_i\frac{\partial^2 w}{\partial x^2}\right) - \sum_{i=1}^{n-1} k_i d_i\left(\frac{\partial v_{0,i+1}}{\partial y} - \frac{\partial v_{0,i}}{\partial y} + d_i\frac{\partial^2 w}{\partial y^2}\right) + \widehat{N}_{x,\mathrm{Tot.}}\left(\frac{\partial^2 w}{\partial x^2}\right) + \widehat{N}_{y,\mathrm{Tot.}}\left(\frac{\partial^2 w}{\partial y^2}\right) = q(x,y) \tag{21g}$$

where $I_{2,0}$ is the non-composite rotary inertia of the laminate, and is given as

$$I_{2,0} = \sum_{i=1}^{n} I_{2,i} = \sum_{i=1}^{n}\frac{1}{12}\rho_i h_i^3 \tag{22}$$

Furthermore, I_0 is the translational mass inertia of the entire laminate, and is expressed as

$$I_0 = \sum_{i=1}^{n} I_{0,i} = \sum_{i=1}^{n}\rho_i h_i \tag{23}$$

2.3. Extended classical boundary conditions

Using the extended Hamilton's energy principle (9) in conjunction with the energy terms (10), (11) and (14), the geometric/essential and natural boundary equations are directly deduced for the classical edges as follows,

$$\text{at } x=0,a: \begin{cases} \text{either} \quad \delta u_{0,1}=0 \quad \text{or} \quad N_{x,1} = -\widehat{N}_{x,1} \\ \text{either} \quad \delta v_{0,1}=0 \quad \text{or} \quad N_{xy,1}=0 \\ \text{either} \quad \delta u_{0,2}=0 \quad \text{or} \quad N_{x,2} = -\widehat{N}_{x,2} \\ \text{either} \quad \delta v_{0,2}=0 \quad \text{or} \quad N_{xy,2}=0 \\ \ldots \\ \text{either} \quad \delta u_{0,i}=0 \quad \text{or} \quad N_{x,i} = -\widehat{N}_{x,i} \\ \text{either} \quad \delta v_{0,i}=0 \quad \text{or} \quad N_{xy,i}=0 \\ \ldots \\ \text{either} \quad \delta u_{0,n-1}=0 \quad \text{or} \quad N_{x,n-1} = -\widehat{N}_{x,n-1} \\ \text{either} \quad \delta v_{0,n-1}=0 \quad \text{or} \quad N_{xy,n-1}=0 \\ \text{either} \quad \delta u_{0,n}=0 \quad \text{or} \quad N_{x,n} = -\widehat{N}_{x,n} \\ \text{either} \quad \delta v_{0,n}=0 \quad \text{or} \quad N_{xy,n}=0 \\ \text{either} \quad \delta w=0 \quad \text{or} \quad V_x^{(\mathrm{PC})}=0 \\ \text{either} \quad \delta(\partial w/\partial x)=0 \quad \text{or} \quad M_x^{(0)}=0 \\ \text{either} \quad \delta(\partial w/\partial y)=0 \quad \text{or} \quad M_{xy}^{(0)}=0 \end{cases} \tag{24a}$$

and

$$\text{at } y=0,b: \begin{cases} \text{either} \quad \delta v_{0,1}=0 \quad \text{or} \quad N_{y,1} = -\widehat{N}_{y,1} \\ \text{either} \quad \delta u_{0,1}=0 \quad \text{or} \quad N_{xy,1}=0 \\ \text{either} \quad \delta v_{0,2}=0 \quad \text{or} \quad N_{y,2} = -\widehat{N}_{y,2} \\ \text{either} \quad \delta u_{0,2}=0 \quad \text{or} \quad N_{xy,2}=0 \\ \ldots \\ \text{either} \quad \delta v_{0,i}=0 \quad \text{or} \quad N_{y,i} = -\widehat{N}_{y,i} \\ \text{either} \quad \delta u_{0,i}=0 \quad \text{or} \quad N_{xy,i}=0 \\ \ldots \\ \text{either} \quad \delta v_{0,n-1}=0 \quad \text{or} \quad N_{y,n-1} = -\widehat{N}_{y,n-1} \\ \text{either} \quad \delta u_{0,n-1}=0 \quad \text{or} \quad N_{xy,n-1}=0 \\ \text{either} \quad \delta v_{0,n}=0 \quad \text{or} \quad N_{y,n} = -\widehat{N}_{y,n} \\ \text{either} \quad \delta u_{0,n}=0 \quad \text{or} \quad N_{xy,n}=0 \\ \text{either} \quad \delta w=0 \quad \text{or} \quad V_y^{(\mathrm{PC})}=0 \\ \text{either} \quad \delta(\partial w/\partial y)=0 \quad \text{or} \quad M_y^{(0)}=0 \\ \text{either} \quad \delta(\partial w/\partial x)=0 \quad \text{or} \quad M_{xy}^{(0)}=0 \end{cases} \tag{24b}$$

where the stress resultants $(N_{x,i}, N_{y,i}, N_{xy,i})$ and $(M_x^{(0)}, M_y^{(0)}, M_{xy}^{(0)})$ $(i=1,2,...,N)$ are defined by Eqs. (18) and (19), respectively. Furthermore, $Q_x^{(\mathrm{PC})}$ and $Q_y^{(\mathrm{PC})}$ are the transverse shear forces per unit length, corresponding to a laminated plate with "partial-composite" interaction at the interlayers, and are deduced as follows,

$$\begin{aligned} Q_x^{(\mathrm{PC})} &= -\frac{\partial}{\partial x}\left[D_{11}^{(0)}\frac{\partial^2 w}{\partial x^2} + (D_{12}^{(0)}+2D_{66}^{(0)})\frac{\partial^2 w}{\partial y^2}\right] + \sum_{i=1}^{n-1} k_i d_i\left(u_{0,i+1} - u_{0,i} + d_i\frac{\partial w}{\partial x}\right) - \widehat{N}_{x,\mathrm{Tot.}}\left(\frac{\partial w}{\partial x}\right) \\ Q_y^{(\mathrm{PC})} &= -\frac{\partial}{\partial y}\left[(D_{12}^{(0)}+2D_{66}^{(0)})\frac{\partial^2 w}{\partial x^2} + D_{22}^{(0)}\frac{\partial^2 w}{\partial y^2}\right] + \sum_{i=1}^{n-1} k_i d_i\left(v_{0,i+1} - v_{0,i} + d_i\frac{\partial w}{\partial y}\right) - \widehat{N}_{y,\mathrm{Tot.}}\left(\frac{\partial w}{\partial y}\right) \end{aligned} \tag{25}$$

It is noteworthy that, similar to the classical laminated plate theory, only two conditions from the common three out-of-plane boundary condi-

tions (the three last of Eqs. (24a) and (24b)) can be satisfied at each edge of the plate. Thus, the twisting moment and transverse shear force conditions may commonly be replaced by an equivalent force as follows:

$$\begin{aligned} V_{\mathrm{x}}^{(\mathrm{PC})} &= Q_{\mathrm{x}}^{(\mathrm{PC})} + \frac{\partial M_{\mathrm{xy}}^{(0)}}{\partial y} = -D_{11}^{(0)}\left(\frac{\partial^3 w}{\partial x^3} + \alpha_1^{(0)}\frac{\partial^3 w}{\partial x \partial y^2}\right) \\ &\quad + \sum_{i=1}^{n-1} k_i d_i \left(u_{0,i+1} - u_{0,i} + d_i \frac{\partial w}{\partial x}\right) - \widehat{N}_{\mathrm{x,Tot.}}\left(\frac{\partial w}{\partial x}\right) \\ V_{\mathrm{y}}^{(\mathrm{PC})} &= Q_{\mathrm{y}}^{(\mathrm{PC})} + \frac{\partial M_{\mathrm{xy}}^{(0)}}{\partial x} = -D_{22}^{(0)}\left(\frac{\partial^3 w}{\partial y^3} + \alpha_2^{(0)}\frac{\partial^3 w}{\partial x^2 \partial y}\right) \\ &\quad + \sum_{i=1}^{n-1} k_i d_i \left(v_{0,i+1} - v_{0,i} + d_i \frac{\partial w}{\partial y}\right) - \widehat{N}_{\mathrm{y,Tot.}}\left(\frac{\partial w}{\partial y}\right) \end{aligned} \tag{26}$$

where

$$\begin{aligned} \alpha_1^{(0)} &= \frac{1}{D_{11}^{(0)}}(D_{12}^{(0)} + 4D_{66}^{(0)}) \\ \alpha_2^{(0)} &= \frac{1}{D_{22}^{(0)}}(D_{12}^{(0)} + 4D_{66}^{(0)}) \end{aligned} \tag{27}$$

3. Analytical solution approaches

3.1. Flexible n-layer laminated orthotropic plates with identical layers

In this section, analytical solutions are conducted for the problems of structural buckling under mono- and bi-axial compressive edge loads, as well as the free vibrations for flexible *n*-layer laminated partial composite plates. It should also be clarified that as the focus of the present study is on introducing the laminated partially-composite plate theory (LPCPT) based on the described model, the effect of different lay-up patterns stands outside the scope of the present research. Thus, first we conduct analytical solutions for the multilayers composed of any arbitrary number of constituent layers with identical orthotropic material properties to investigate the influence of the imperfect interlayer interaction and partial composite effects at the interfaces, only. (i.e., $\wp_1 = \wp_2 = \ldots = \wp_\ell = \text{const.}$, in which $\wp_\ell$ is any of the geometric or material property parameters of a constituting layer, where the subscript ℓ then refers to the case of identical layers). Furthermore, the interlayer shear interaction/slip moduli are considered to be the same for all the interfaces ($k_i\,(i = 1, 2, \ldots, n-1) = k = \text{const.}$). Next, laminated plates with non-identical orthotropic layers are treated via direct analytical solution alternatives for laminated plates with a specified number of constituent layers.

3.1.1. Buckling of partial-composite plates under mono- or bi-axial compressive in-plane loads

Consider a rectangular partial composite plate of uniform thickness $h_{\mathrm{Tot.}}$, length a, and width b, consisting of n layers, each of thickness h_ℓ, as illustrated in Fig. 2. Each layer of the plate is assumed to be subjected to the in-plane edge load per unit length $\widehat{N}_{\mathrm{x},i}$ along the x direction, as a result of a global applied edge load $\widehat{N}_{\mathrm{x,Tot.}}$. The layered partial-composite may also be subjected to bi-axial compressive edge loads, and thus, each layer under an in-plane edge load per unit length $\widehat{N}_{\mathrm{y},i}$ along the y direction (Fig. 2). For a simply-supported laminated partial composite plate, under mono- or bi-axial compressive edge-load conditions, the following boundary conditions are deduced from Eqs. (24a),b):

$$\text{at } x = 0, a: \begin{cases} N_{\mathrm{x},1} = -\widehat{N}_{\mathrm{x},1} \\ v_{0,1} = 0 \\ N_{\mathrm{x},2} = -\widehat{N}_{\mathrm{x},2} \\ v_{0,2} = 0 \\ \ldots \\ N_{\mathrm{x},i} = -\widehat{N}_{\mathrm{x},i} \\ v_{0,i} = 0 \\ \ldots \\ N_{\mathrm{x},n-1} = -\widehat{N}_{\mathrm{x},n-1} \\ v_{0,n-1} = 0 \\ N_{\mathrm{x},n} = -\widehat{N}_{\mathrm{x},n} \\ v_{0,n} = 0 \\ w = 0 \\ M_{\mathrm{x}}^{(0)} = 0 \end{cases} \tag{28a}$$

$$\text{at } y = 0, b: \begin{cases} N_{\mathrm{y},1} = -\widehat{N}_{\mathrm{y},1} \\ u_{0,1} = 0 \\ N_{\mathrm{y},2} = -\widehat{N}_{\mathrm{y},2} \\ u_{0,2} = 0 \\ \ldots \\ N_{\mathrm{y},i} = -\widehat{N}_{\mathrm{y},i} \\ u_{0,i} = 0 \\ \ldots \\ N_{\mathrm{y},n-1} = -\widehat{N}_{\mathrm{y},n-1} \\ u_{0,n-1} = 0 \\ N_{\mathrm{y},n} = -\widehat{N}_{\mathrm{y},n} \\ u_{0,n} = 0 \\ w = 0 \\ M_{\mathrm{y}}^{(0)} = 0 \end{cases} \tag{28b}$$

A solution for the components of the displacement field may be proposed in the form (see Appendix A for details):

$$\begin{cases} u_{0,i} = \dfrac{1}{E_{\mathrm{x},\ell} h_\ell}\left(\widehat{N}_{\mathrm{x},i} - \nu_{\mathrm{xy},\ell}\widehat{N}_{\mathrm{y},i}\right)(a/2 - x) + U_{0,i}\cos(\alpha_{\mathrm{m1}}x)\sin(\beta_{\mathrm{m2}}y), \\ v_{0,i} = \dfrac{1}{E_{\mathrm{y},\ell} h_\ell}\left(\widehat{N}_{\mathrm{y},i} - \nu_{\mathrm{yx},\ell}\widehat{N}_{\mathrm{x},i}\right)(b/2 - y) + V_{0,i}\sin(\alpha_{\mathrm{m1}}x)\cos(\beta_{\mathrm{m2}}y), \\ \qquad i \in \{1, 2, \ldots, n\} \\ w = W_0 \sin(\alpha_{\mathrm{m1}}x)\sin(\beta_{\mathrm{m2}}y) \end{cases} \tag{29}$$

in which the coefficients α_{m1} and β_{m2} are given by

$$\begin{aligned} \alpha_{\mathrm{m1}} &= m_1\pi/a \\ \beta_{\mathrm{m2}} &= m_2\pi/b \end{aligned} \tag{30}$$

where m_1 and m_2 are number of buckling modes' half-waves in the $x-$ and $y-$directions, respectively. Evidently, the proposed solution can exactly satisfy all the boundary conditions (28a),b) (see Appendix A).

Substituting the proposed solution (29) into Eqs. (21c),d) in the absence of any dynamic term yields

$$\begin{cases} kU_{0,i-1} - \left(\alpha_{m1}^2 A_{11,\ell} + \beta_{m2}^2 A_{66,\ell} + 2k\right) U_{0,i} + kU_{0,i+1} \\ \quad -\alpha_{m1}\beta_{m2}(A_{12,\ell} + A_{66,\ell}) V_{0,i} = 0 \\ (i = 2, 3, ..., n-1) \end{cases} \tag{31a}$$

$$\begin{cases} kV_{0,i-1} - \left(\alpha_{m1}^2 A_{66,\ell} + \beta_{m2}^2 A_{22,\ell} + 2k\right) V_{0,i} + kV_{0,i+1} \\ \quad -\alpha_{m1}\beta_{m2}(A_{12,\ell} + A_{66,\ell}) U_{0,i} = 0, \\ (i = 2, 3, ..., n-1) \end{cases} \tag{31b}$$

It should be clarified that based on the present model's fundamental assumptions, the distribution of the axial compressive edge loads $\widehat{N}_{x,i}$ and $\widehat{N}_{y,i}$ $(i = 1, 2, ..., n)$, respectively, parallel to x and y directions, are proportional to each layer's relative axial stiffness along that direction, which is a true assumption for the linear elastic deformations (see [34,92] for a detailed discussion on the assumption); i.e.,

$$\frac{\widehat{N}_{x,1}}{A_{11,1}} = \frac{\widehat{N}_{x,2}}{A_{11,2}} = ... = \frac{\widehat{N}_{x,i}}{A_{11,i}} = ... = \frac{\widehat{N}_{x,N}}{A_{11,N}} = \frac{\sum_{i=1}^{n} \widehat{N}_{x,i}}{\sum_{i=1}^{n} A_{11,i}} = \frac{\widehat{N}_{x,\text{Tot.}}}{A_{11,0}} \tag{32a}$$

$$\frac{\widehat{N}_{y,1}}{A_{22,1}} = \frac{\widehat{N}_{y,2}}{A_{22,2}} = ... = \frac{\widehat{N}_{y,i}}{A_{22,i}} = ... = \frac{\widehat{N}_{y,N}}{A_{22,N}} = \frac{\sum_{i=1}^{n} \widehat{N}_{y,i}}{\sum_{i=1}^{n} A_{22,i}} = \frac{\widehat{N}_{y,\text{Tot.}}}{A_{22,0}} \tag{32b}$$

in which $A_{11,i}$ and $A_{22,i}$ are the axial stiffness of each layer along x and y directions, respectively, whereas $A_{11,0}$ and $A_{22,0}$ are those of the entire laminate, and are defined as

$$\begin{aligned} A_{11,0} &= \sum_{i=1}^{n} A_{11,i} = \sum_{i=1}^{n} \frac{E_{x,i} h_i}{1 - \nu_{xy,i}\nu_{yx,i}} \\ A_{22,0} &= \sum_{i=1}^{n} A_{22,i} = \sum_{i=1}^{n} \frac{E_{y,i} h_i}{1 - \nu_{xy,i}\nu_{yx,i}} \end{aligned} \tag{33}$$

The set of coupled difference Eqs. (31a),b) can be exactly fulfilled if we set (see Appendix B for details on the solution):

$$\begin{cases} U_{0,i} = \chi_{1U}\cosh i\theta + \chi_{2U}\sinh i\theta, \\ V_{0,i} = \chi_{1V}\cosh i\theta + \chi_{2V}\sinh i\theta, \\ i \in \{1, 2, 3, ..., n\} \end{cases} \tag{34}$$

in which θ is an unknown parameter to be determined. Substituting the above solution into the set of difference equations (31a),b), and applying the standard hyperbolic angle addition/subtraction formulae, yield:

$$\begin{bmatrix} 2k(1-\cosh\theta) + c_{11,\ell}^{m12} & c_{12,\ell}^{m12} \\ c_{12,\ell}^{m12} & 2k(1-\cosh\theta) + c_{22,\ell}^{m12} \end{bmatrix} \begin{Bmatrix} U_{0,i} \\ V_{0,i} \end{Bmatrix} = 0 \tag{35}$$

where

$$\begin{aligned} c_{11,\ell}^{m12} &= \alpha_{m1}^2 A_{11,\ell} + \beta_{m2}^2 A_{66,\ell} \\ c_{22,\ell}^{m12} &= \alpha_{m1}^2 A_{66,\ell} + \beta_{m2}^2 A_{22,\ell} \\ c_{12,\ell}^{m12} &= \alpha_{m1}\beta_{m2}(A_{12,\ell} + A_{66,\ell}) \end{aligned} \tag{36}$$

Applying a nontrivial solution to Eqs. (35) and performing some mathematical manipulations, the unknown parameter θ will be determined in the form:

$$\theta = \cosh^{-1}\left[1 + \frac{1}{4k}\left(c_{11,\ell}^{m12} + c_{22,\ell}^{m12} - \sqrt{(c_{11,\ell}^{m12} - c_{22,\ell}^{m12})^2 + 4(c_{12,\ell}^{m12})^2}\right)\right] \tag{37}$$

It can be shown that Eq. (37) for a laminated plate with isotropic layers is simplified as

$$\theta = \cosh^{-1}\left[1 + \frac{\pi^2 h_\ell E_\ell}{2k(1-\nu_\ell^2)}\left(\frac{m_1^2}{a^2} + \frac{m_2^2}{b^2}\right)\right] \tag{38}$$

Next, the remaining governing equations (21a),b) and (21e-g) are to be fulfilled. To this end, we substitute the proposed solution for the displacement field components (29) into the mentioned equations in the absence of the dynamic terms and the transverse distributed load, and obtain:

$$-\left(\alpha_{m1}^2 A_{11,\ell} + \beta_{m2}^2 A_{66,\ell} + k\right) U_{0,1} + kU_{0,2} - \alpha_{m1}\beta_{m2}(A_{12,\ell} + A_{66,\ell}) V_{0,1} + \alpha_{m1} h_\ell k W_0 = 0 \tag{39a}$$

$$-\alpha_{m1}\beta_{m2}(A_{12,\ell} + A_{66,\ell}) U_{0,1} - \left(\alpha_{m1}^2 A_{66,\ell} + \beta_{m2}^2 A_{22,\ell} + k\right) V_{0,1} + kV_{0,2} + \beta_{m2} h_\ell k W_0 = 0 \tag{39b}$$

$$kU_{0,n-1} - \left(\alpha_{m1}^2 A_{11,\ell} + \beta_{m2}^2 A_{66,\ell} + k\right) U_{0,n} - \alpha_{m1}\beta_{m2}(A_{12,\ell} + A_{66,\ell}) V_{0,n} - \alpha_{m1} h_\ell k W = 0 \tag{39c}$$

$$-\alpha_{m1}\beta_{m2}(A_{12,\ell} + A_{66,\ell}) U_{0,n} + kV_{0,n-1} - \left(\alpha_{m1}^2 A_{66,\ell} + \beta_{m2}^2 A_{22,\ell} + k\right) V_{0,n} - \beta_{m2} h_\ell k W_0 = 0 \tag{39d}$$

$$\begin{aligned} &-\alpha_{m1} U_{0,1} + \alpha_{m1} U_{0,n} - \beta_{m2} V_{0,1} + \beta_{m2} V_{0,n} \\ &+\frac{1}{h_\ell k}\left[\alpha_{m1}^4 D_{11}^{(0)} + 2\alpha_{m1}^2\beta_{m2}^2 (D_{12}^{(0)} + 2D_{66}^{(0)}) + \beta_{m2}^4 D_{22}^{(0)}\right] W_0 \\ &+(n-1)\gamma_{m12}^2 h_\ell W_0 - \frac{1}{h_\ell k}(\alpha_{m1}^2 \widehat{N}_{x,\text{Tot.}} + \beta_{m2}^2 \widehat{N}_{y,\text{Tot.}}) W_0 = 0 \end{aligned} \tag{39e}$$

where

$$\gamma_{m12} = \sqrt{\alpha_{m1}^2 + \beta_{m2}^2} \tag{40}$$

Substituting the solution by Eq. (34) into Eqs. (39a)-e) and collecting the coefficients of χ_{1U}, χ_{2U}, χ_{1V}, χ_{2V} and W_0 result in the following non-trivial solution for the critical buckling load $\widehat{N}_{cr}$:

$$\begin{aligned} &|\boldsymbol{M}_{5\times5}| = 0 : \\ &[\boldsymbol{M}_{5\times5}][\chi_{1U} \quad \chi_{2U} \quad \chi_{1V} \quad \chi_{2V} \quad W_0]^{\mathrm{T}} = \boldsymbol{0} \end{aligned} \tag{41}$$

in which the coefficient matrix $\mathbf{M}$ is given in Appendix C. The compressive load may be applied monoaxially on any pair of parallel edges of the plate, or biaxially with different intensity values, ξ_1 and ξ_2 along the x and y directions, respectively.

$$\begin{aligned} \widehat{N}_{x,\text{Tot.}} &= -\xi_1 \widehat{N}_{cr} \\ \widehat{N}_{y,\text{Tot.}} &= -\xi_2 \widehat{N}_{cr} \end{aligned} \tag{42}$$

Obviously, for a mono-axial load case, it is set $\xi_2 = 0$ (or $\xi_1 = 0$).

3.1.2. Free vibrations of partial composite plates

Apparently, under the assumption of small-amplitude oscillating vibrations and harmonic motions with an angular frequency of ω, the components of the displacement field (1) can be described using the separation of variables method for the dynamic effects as

$$\begin{cases} u_{0,i}(x,y,t) = \widetilde{u}_{0,i}(x,y)\, e^{j\omega t} \\ v_{0,i}(x,y,t) = \widetilde{v}_{0,i}(x,y)\, e^{j\omega t} \\ w(x,y,t) = \widetilde{w}_{0,i}(x,y)\, e^{j\omega t}, \quad j = \sqrt{-1} \\ , i \in \{1, 2, ..., n\} \end{cases} \tag{43}$$

Substituting Eq. (43) into the set of governing equations of motion (21a-

g), in the absence of any external forces and applying layers equality assumptions, as mentioned in the previous section, yields

$$A_{11,\ell}\frac{\partial^2\widetilde{u}_{0,1}}{\partial x^2}+A_{66,\ell}\frac{\partial^2\widetilde{u}_{0,1}}{\partial y^2}+(\omega^2 I_{0,\ell}-k)\widetilde{u}_{0,1}+k\widetilde{u}_{0,2}+(A_{12,\ell}+A_{66,\ell})\frac{\partial^2\widetilde{v}_{0,1}}{\partial x\partial y}+h_\ell k\frac{\partial\widetilde{w}}{\partial x}=0 \tag{44a}$$

$$(A_{12,\ell}+A_{66,\ell})\frac{\partial^2\widetilde{u}_{0,1}}{\partial x\partial y}+A_{66,\ell}\frac{\partial^2\widetilde{v}_{0,1}}{\partial x^2}+A_{22,\ell}\frac{\partial^2\widetilde{v}_{0,1}}{\partial y^2}+(\omega^2 I_{0,\ell}-k)\widetilde{v}_{0,1}+k\widetilde{v}_{0,2}+h_\ell k\frac{\partial\widetilde{w}}{\partial y}=0 \tag{44b}$$

$$\begin{cases} A_{11,\ell}\dfrac{\partial^2\widetilde{u}_{0,i}}{\partial x^2}+A_{66,\ell}\dfrac{\partial^2\widetilde{u}_{0,i}}{\partial y^2}+k\widetilde{u}_{0,i-1}+(\omega^2 I_{0,\ell}-2k)\widetilde{u}_{0,i}+k\widetilde{u}_{0,i+1}+(A_{12,\ell}+A_{66,\ell})\dfrac{\partial^2\widetilde{v}_{0,i}}{\partial x\partial y}=0, \\ (i=2,3,\ldots,n-1) \end{cases} \tag{44c}$$

$$\begin{cases} (A_{12,\ell}+A_{66,\ell})\dfrac{\partial^2\widetilde{u}_{0,i}}{\partial x\partial y}+A_{66,\ell}\dfrac{\partial^2\widetilde{v}_{0,i}}{\partial x^2}+A_{22,\ell}\dfrac{\partial^2\widetilde{v}_{0,i}}{\partial y^2}+k\widetilde{v}_{0,i-1}+(\omega^2 I_{0,\ell}-2k)\widetilde{v}_{0,i}+k\widetilde{v}_{0,i+1}=0, \\ (i=2,3,\ldots,n-1) \end{cases} \tag{44d}$$

$$A_{11,\ell}\frac{\partial^2\widetilde{u}_{0,n}}{\partial x^2}+A_{66,\ell}\frac{\partial^2\widetilde{u}_{0,n}}{\partial y^2}+k\widetilde{u}_{0,n-1}+(\omega^2 I_{0,\ell}-k)\widetilde{u}_{0,n}+(A_{12,\ell}+A_{66,\ell})\frac{\partial^2\widetilde{v}_{0,n}}{\partial x\partial y}-h_\ell k\frac{\partial\widetilde{w}}{\partial x}=0 \tag{44e}$$

$$(A_{12,\ell}+A_{66,\ell})\frac{\partial^2\widetilde{u}_{0,n}}{\partial x\partial y}+A_{66,\ell}\frac{\partial^2\widetilde{v}_{0,n}}{\partial x^2}+A_{22,\ell}\frac{\partial^2\widetilde{v}_{0,n}}{\partial y^2}+k\widetilde{v}_{0,n-1}+(\omega^2 I_{0,\ell}-k)\widetilde{v}_{0,n}-h_\ell k\frac{\partial\widetilde{w}}{\partial y}=0 \tag{44f}$$

$$\frac{1}{h_\ell k}\left[D_{11}^{(0)}\frac{\partial^4\widetilde{w}}{\partial x^4}+2(D_{12}^{(0)}+2D_{66}^{(0)})\frac{\partial^4\widetilde{w}}{\partial x^2\partial y^2}+D_{22}^{(0)}\frac{\partial^4\widetilde{w}}{\partial y^4}\right]+\left[\frac{\omega^2 I_{2,0}}{h_\ell k}-(n-1)h_\ell\right]\nabla^2 w-\frac{\omega^2 I_0}{h_\ell k}\widetilde{w}+\frac{\partial}{\partial x}(u_{0,1}-u_{0,n})+\frac{\partial}{\partial y}(v_{0,1}-v_{0,n})=0 \tag{44g}$$

The components of the displacement field can be described via double Fourier series as

$$\begin{cases} \widetilde{u}_{0,i}=\sum_{m_1=1}^{\infty}\sum_{m_2=1}^{\infty}\widetilde{U}_{0,im_1m_2}\cos(\alpha_{m1}x)\sin(\beta_{m2}y), \\ \quad i\in\{1,2,\ldots,n\} \\ \widetilde{v}_{0,i}=\sum_{m_1=1}^{\infty}\sum_{m_2=1}^{\infty}\widetilde{V}_{0,im_1m_2}\sin(\alpha_{m1}x)\cos(\beta_{m2}y), \\ \quad i\in\{1,2,\ldots,n\} \\ \widetilde{w}=\sum_{m_1=1}^{\infty}\sum_{m_2=1}^{\infty}\widetilde{W}_{0,m_1m_2}\sin(\alpha_{m1}x)\sin(\beta_{m2}y) \end{cases} \tag{45}$$

in which $\alpha_{m1}=m_1\pi/a$ and $\beta_{m2}=m_2\pi/b$ in terms of the number of vibration mode-shapes' half-waves, m_1 and m_2, along the $x-$ and $y-$directions, respectively. It is easy to show that the proposed solution (45) exactly satisfies the simply-supported boundary conditions at the plates' edges.

With inspiration from the introduced exact analytical solution in the previous section for the buckling problem, the set of Eqs. (44c) and (44d) can be exactly fulfilled if we set:

$$\begin{cases} \widetilde{U}_{0,im_1m_2}=\widetilde{\chi}_{1Um_1m_2}\cosh i\widetilde{\theta}+\widetilde{\chi}_{2Um_1m_2}\sinh i\widetilde{\theta}, \\ \widetilde{V}_{0,im_1m_2}=\widetilde{\chi}_{1Vm_1m_2}\cosh i\widetilde{\theta}+\widetilde{\chi}_{2Vm_1m_2}\sinh i\widetilde{\theta}, \\ i\in\{1,2,3,\ldots,n\} \end{cases} \tag{46}$$

where $\widetilde{\theta}$ is an unknown parameter in terms of the natural frequency ω to be determined. Upon substitution of the solution (45) in conjunction with the relations (46) into the set of Eqs. (44c),d), and using some standard hyperbolic angle addition/subtraction formulae, a set of equations in terms of the coefficients $\widetilde{U}_{0,im_1m_2}$ and $\widetilde{V}_{0,im_1m_2}$ are deduced as follows

$$\begin{bmatrix} 2k(1-\cosh\widetilde{\theta})+c_{11,\ell}^{m12}-\omega^2 I_{0,\ell} & c_{12,\ell}^{m12} \\ c_{12,\ell}^{m12} & 2k(1-\cosh\widetilde{\theta})+c_{22,\ell}^{m12}-\omega^2 I_{0,\ell} \end{bmatrix}\begin{Bmatrix}\widetilde{U}_{0,im_1m_2}\\ \widetilde{V}_{0,im_1m_2}\end{Bmatrix}=0 \tag{47}$$

in which the coefficients $c_{11,\ell}^{m12}$, $c_{22,\ell}^{m12}$ and $c_{12,\ell}^{m12}$ are given by Eq. (33). The unknown coefficient $\widetilde{\theta}$ will be determined via applying a non-trivial solution to the above set of equations, in the form:

$$\widetilde{\theta}=\cosh^{-1}\left[1+\frac{1}{4k}\left(c_{11,\ell}^{m12}+c_{22,\ell}^{m12}-\sqrt{(c_{11,\ell}^{m12}-c_{22,\ell}^{m12})^2+4(c_{12,\ell}^{m12})^2}\right)-\frac{1}{2k}\omega^2 I_{0,\ell}\right] \tag{48}$$

The rest of the governing Eqs. (44a),b,e-g) are to be satisfied by replacing the solution (45) in conjunction with Eq. (46) and the relation (48) for $\widetilde{\theta}$, leading to a nonlinear characteristic equation from a non-trivial solution, whose roots are the natural frequencies of the partial-composite plate. The determinant characteristic equation from the matrix of collected coefficients of the vector $\begin{bmatrix}\widetilde{\chi}_{1Um_1m_2} & \widetilde{\chi}_{2Um_1m_2} & \widetilde{\chi}_{1Vm_1m_2} & \widetilde{\chi}_{2Vm_1m_2} & \widetilde{W}_{0,m_1m_2}\end{bmatrix}^{\mathrm{T}}$ can be represented as

$$\begin{vmatrix} \widetilde{\Lambda}_{11}\cosh\widetilde{\theta}-k\cosh 2\widetilde{\theta} & \widetilde{\Lambda}_{11}\sinh\widetilde{\theta}-k\sinh 2\widetilde{\theta} & c_{12}^{m12}\cosh\widetilde{\theta} & c_{12}^{m12}\sinh\widetilde{\theta} & -\alpha_{m1}h_\ell k \\ c_{12}^{m12}\cosh\widetilde{\theta} & c_{12}^{m12}A_\ell\sinh\widetilde{\theta} & \widetilde{\Lambda}_{22}\cosh\widetilde{\theta}-k\cosh 2\widetilde{\theta} & \widetilde{\Lambda}_{22}\sinh\widetilde{\theta}-k\sinh 2\widetilde{\theta} & -\beta_{m2}^2 h_\ell k \\ \widetilde{\Lambda}_{11}\cosh n\widetilde{\theta}-k\cosh[(n-1)\widetilde{\theta}] & \widetilde{\Lambda}_{11}\sinh n\widetilde{\theta}-k\sinh[(n-1)\widetilde{\theta}] & c_{12}^{m12}\cosh n\widetilde{\theta} & c_{12}^{m12}\sinh n\widetilde{\theta} & \alpha_{m1}h_\ell k \\ c_{12}^{m12}\cosh n\widetilde{\theta} & c_{12}^{m12}\sinh n\widetilde{\theta} & \widetilde{\Lambda}_{22}\cosh n\widetilde{\theta}-k\cosh[(n-1)\widetilde{\theta}] & \widetilde{\Lambda}_{22}\sinh n\widetilde{\theta}-k\sinh[[(n-1)\widetilde{\theta}] & \beta_{m2}h_\ell k \\ \alpha_{m1}\left(\cosh n\widetilde{\theta}-\cosh\widetilde{\theta}\right) & \alpha_{m1}\left(\sinh n\widetilde{\theta}-\sinh\widetilde{\theta}\right) & \beta_{m2}\left(\cosh n\widetilde{\theta}-\cosh\widetilde{\theta}\right) & \beta_{m2}\left(\sinh n\widetilde{\theta}-\sinh\widetilde{\theta}\right) & \widetilde{\Lambda}_{33} \end{vmatrix}=0 \tag{49}$$

in which

$$\begin{aligned}\widetilde{\Lambda}_{11} &= \alpha_{m1}^2 A_{11,\ell} + \beta_{m2}^2 A_{66,\ell} + k - I_{0,\ell}\omega^2 \\ \widetilde{\Lambda}_{22} &= \alpha_{m1}^2 A_{66,\ell} + \beta_{m2}^2 A_{22,\ell} + k - I_{0,\ell}\omega^2 \\ \widetilde{\Lambda}_{33} &= \frac{1}{h_\ell k}\left[\alpha_{m1}^4 D_{11}^{(0)} + 2\alpha_{m1}^2\beta_{m2}^2(D_{12}^{(0)} + 2D_{66}^{(0)}) + \beta_{m2}^4 D_{22}^{(0)}\right] \\ &\quad + (n-1)\gamma_{m12}^2 h_\ell - \frac{1}{h_\ell k}\left(I_0 + I_{2,0}\gamma_{m12}^2\right)\omega^2\end{aligned} \tag{50}$$

The roots of the characteristic equation (49) represent the natural frequencies of the laminated plate with interlayer partial-composite interaction based on the introduced model.

3.1.3. Higher-order shear deformation theory results as a special case of the introduced LPCPT

It can be shown that the kinematic field of the introduced LPCPT evolves into a hyperbolic form for the out-of-plane shear strains through the thickness direction as a special case of the present model, while it vanishes on the laminate top and bottom surfaces, similar to a higher-order shear deformation theory. In other words, the contribution of the material's shear rigidity to the structural responses can be incorporated based on the present model by setting the interlayer partial shear interaction modulus, k, to be equivalent to the fraction of the material shear modulus to the thickness of the lamella (see Eq. (6) for the definition of the interlayer shear stresses); i.e.,

$$k^* = \frac{G_\ell}{h_\ell} = \frac{nE_\ell}{2(1+\nu_\ell)h_{Tot}} \tag{51}$$

The asymptotic results based on the present model in which the interlayer interaction modulus k is set to be k^* is, therefore, expected to capture those based on the hyperbolic higher-order shear deformation theory. This is due to the fact that based on the fundamental assumptions of the present model, the upper/bottom surfaces of the laminate are shear-stress-free while it possesses a non-zero value at the interfaces, and consequently, lead to non-uniform through-thickness transverse shear stresses. The difference between the present asymptotic model and the three-dimensional theory of elasticity may be negligible and only sensible for very thick plates. This discrepancy may be attributed to the non-symmetric/anti-symmetric distribution of different stress components through the thickness of a monolithic plate/shell which inherently increases for the thicker plates according to the elasticity theory. In other words, the concept of the neutral plane is not valid any longer; for the aforementioned extremely thick plate/shell asymmetric stress effects, readers are referred to the discussions in [93]). Apparently, all types of plate/shell theories are incapable of incorporating the aforementioned asymmetry effects.

It can be shown that the asymptotic limit of the buckling load, obtained from the solution of the determinant equation (41), when $k = k^*$ and the number of constituting layers approaches infinity while their thicknesses approach zero for a fixed total plate thickness h_{Tot}, is derived in the form:

$$\begin{aligned}&\lim_{n\to\infty} N_{cr}(k = k^*) \\ &= \frac{\sqrt{\alpha_{m1}^2 + \beta_{m2}^2}\left[\sqrt{2(1-\nu_\ell)} + h_{Tot}\sqrt{\alpha_{m1}^2 + \beta_{m2}^2}\right]E_\ell}{2(1+\nu_\ell)(\xi_1\alpha_{m1}^2 + \xi_2\beta_{m2}^2)} \\ &\tanh\left(h_{Tot}\sqrt{\frac{\alpha_{m1}^2 + \beta_{m2}^2}{2(1-\nu)}}\right)\end{aligned} \tag{52}$$

which is numerically comparable—as will be demonstrated in the numerical comparative results—to the critical buckling load formulae based on Reddy's higher-order shear deformation theory, reported in [94]:

$$N_{cr} = \frac{\alpha_{12} + \alpha_{11}(\alpha_{m1}^2 + \beta_{m2}^2)}{(\xi_1\alpha_{m1}^2 + \xi_2\beta_{m2}^2)[1 + \alpha_{13}(\alpha_{m1}^2 + \beta_{m2}^2)]}(\alpha_{m1}^2 + \beta_{m2}^2)^2 \tag{53}$$

For mathematically small total thickness, h_{Tot}, the buckling load formula (52) is equivalent to:

$$\lim_{n\to\infty} N_{cr}\Big|_{h_{Tot}\to 0} = \frac{E_\ell h_{Tot}^3}{12(1-\nu_\ell^2)}\frac{(\alpha_{m1}^2 + \beta_{m2}^2)^2}{(\xi_1\alpha_{m1}^2 + \xi_2\beta_{m2}^2)} = D_\infty\frac{(\alpha_{m1}^2 + \beta_{m2}^2)^2}{\xi_1\alpha_{m1}^2 + \xi_2\beta_{m2}^2} \tag{54}$$

which is identical to the buckling load formula based on the classical plate theory (CPT). A comparison of the numerical buckling and vibration results based on the described present special case and those of the 3-D elasticity, as well as the conventional Reddy's higher-order shear deformation theory (HSDT), is presented and discussed in Section 4.

3.2. Laminated orthotropic plates with non-identical layers

The developed analytical solutions in the preceding subsections for the structural stability and dynamic analyses of laminated partial-composite plates based on the introduced LPCP model for an arbitrary number of constituting layers (n) may not be applicable to the laminates with non-identical layers. To evaluate the validity and performance of the proposed LPCP model for such cases and to study the influence of the non-idealised/partial interlayer interaction, direct analytical solution alternatives may be conducted for laminated plates with a specified number of constituent layers.

Consider a simply-supported laminated composite plate composed of n non-identical layers of uniform thickness h. The previously defined displacement fields, given by Eq. (29) together with Eq. (42) for the buckling, and by Eqs. (43) and (45) for the vibration analysis are recalled in their general form, without assuming identical mechanical properties. Substituting the mentioned displacement fields into the governing equations of the LPCP model yields two systems of $2n+1$ algebraic equations (see Appendix D). The critical buckling loads and natural vibration frequencies of a laminated orthotropic plate having n non-identical layers can subsequently be extracted from the resulting polynomial characteristic equations by vanishing the determinant of the coefficient matrices; i.e.,

$$|\boldsymbol{M}_{(2n+1)\times(2n+1)}| = 0 \tag{55}$$

in which $\boldsymbol{M}$ is the matrix of coefficients of the vectors:

$$[\,[U_{0,1}\ \ V_{0,1}]\ \ [U_{0,2}\ \ V_{0,2}]\ \ \cdots\ \ [U_{0,i}\ \ V_{0,i}]\ \ \cdots\ \ [U_{0,n}\ \ V_{0,n}]\ \ W_0\,]_{2n+1}^{T} \quad \text{(for buckling)} \tag{56a}$$

$$[\,[\widetilde{U}_{0,1m_1m_2}\ \ \widetilde{V}_{0,1m_1m_2}]\ \ [\widetilde{U}_{0,2m_1m_2}\ \ \widetilde{V}_{0,2m_1m_2}]\ \ \cdots\ \ [\widetilde{U}_{0,im_1m_2}\ \ \widetilde{V}_{0,im_1m_2}]\ \ \cdots\ \ [\widetilde{U}_{0,nm_1m_2}\ \widetilde{V}_{0,nm_1m_2}]\widetilde{W}_{0,m_1m_2}\,]_{2n+1}^{T} \ \text{(for vibration)} \tag{56b}$$

3.3. A remark on methods for determining interlayer partial-interaction moduli

The established laminated partial-composite plate (LPCP) model and the presented solutions rely on the key parameter of the interlayer interaction modulus, k. Therefore, accurate determination of its values is essential to ensure reliable predictions of the structural behaviour and response of layered plates and panels with imperfect interlayer bonding in various applications, based on the LPCPT. Similar to what was described in [34] for the laminated beam/column elements, the interlayer moduli for layered plates and panels can be experimentally determined through standard test techniques on small 1-D beam-like specimens, such as the three-point bending test in conjunction with static partial-composite beam theory [76] or the double shear joint test. It is noteworthy that two beam specimens, cut along orthogonal planar directions, should be tested if the level of interlayer interaction differs

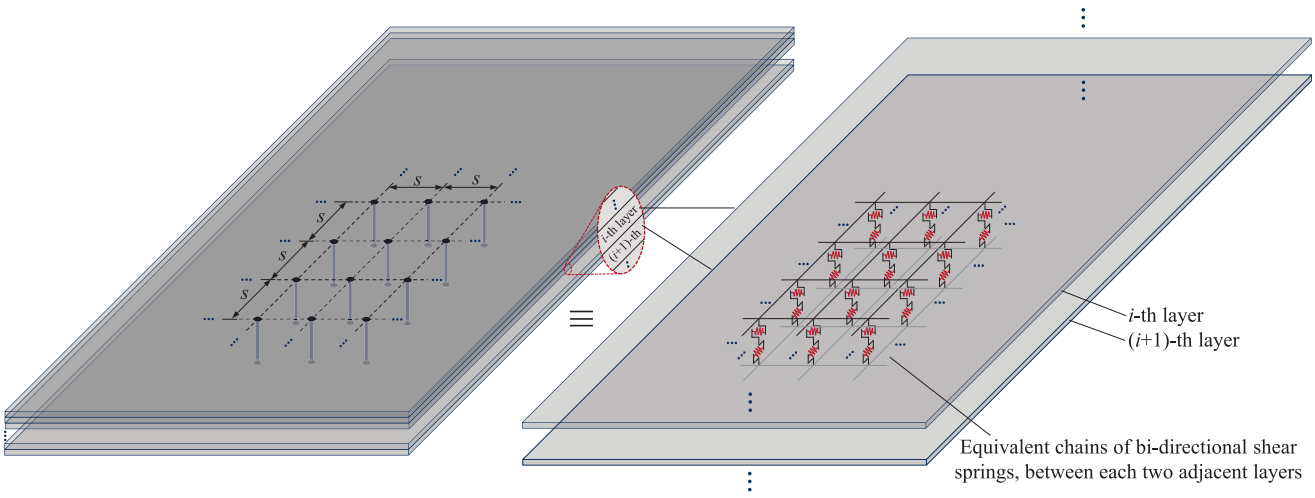

Fig. 3. The model's kinematics of deformations and the internal force and stress resultant assumptions.

between the directions due to the orthotropy in the constituent materials and adhesive bonding effects, different geometric patterns or non-identical spacing of the mechanical connectors in the two planar directions, etc.

Aside from the experimental approaches outlined, a number of simple formulae can be theoretically deduced to predict the interlayer modulus for different cases. The interlayer interaction moduli for the case of layered plates bonded through relatively soft adhesives can be estimated based on extending the conventional approach in [95] for laminated beams. Assuming pure shear deformation for relatively soft adhesive films at the interfaces of plate layers, the interlayer shear interaction modulus can be estimated, using Eq. (6), as $k \approx G_{\text{adh}}/h_{\text{adh}}$; in which G_{adh} and h_{adh} are, respectively, the shear modulus of the soft adhesive material and the adhesive film thickness. The aforementioned

Table 1
Comparison of dimensionless critical buckling loads for rectangular plates under mono-axial compression based on the 3-D elasticity, Reddy's higher-order shear deformation theory (HSDT), the classical plate theory (CPT), and a special case of the present LPCPT, provided for various values of the total thickness-to-length ratio, h_{Tot}/b, and the plate aspect ratio $\eta = a/b$. The percentage discrepancy provided in front of each value [%] is calculated with reference to the 3-D elasticity. The provided numerical results based on the present model are computed for the two special cases: (*i*) setting the interlayer modulus to be equivalent to the transverse shear strains $\overline{k} = \overline{k}^{*}$, and the number of constituting layers approaches infinity, while the total thickness-to-length ratio is kept fixed ($nh = \text{const.} = h_{\text{Tot}}$); (*ii*) assuming the material transverse shear-rigidity via tending the interlayer interaction modulus to infinity (i.e., interfacial perfect-bonding and full-composite interaction).

h_{Tot}/b	Method	$N_{\text{cr}}b^2/(\pi^2 D)^{**}$					
		$\eta = 0.2$	$\eta = 0.4$	$\eta = 0.8$	$\eta = 1.0$	$\eta = 1.2$	$\eta = 1.4$
0.5	3-D Elasticity [97]	–	–	–	1.6598	–	–
	Present ($\overline{k} = \overline{k}^{*}$, $n\to\infty$)	1.5088	1.4230	1.5149	1.6740 [0.8 %]	1.8970	2.1779
	HSDT† [98]	1.6851	1.4455	1.5179	1.6759 [1.0 %]	1.8984	2.1791
	HSDT† [94]	–	1.4455	1.5179	1.6759 [1.0 %]	–	2.1792
0.2	3-D Elasticity [97]	–	–	–	3.1527	–	–
	Present ($\overline{k} = \overline{k}^{*}$, $n\to\infty$)	7.0143	4.6452	3.2626	3.2653 [3.5 %]	3.4723	3.8207
	HSDT† [98]	7.0529	4.6466	3.2626	3.2653 [3.5 %]	3.4722	3.8206
	HSDT† [94]	–	4.6466	3.2627	3.2653 [3.5 %]	–	3.8207
0.1	3-D Elasticity [97]	–	–	–	3.7408	–	–
	Present ($\overline{k} = \overline{k}^{*}$, $n\to\infty$)	15.655	6.9853	3.9195	3.7866 [1.2 %]	3.9460	4.2877
	HSDT† [98]	15.658	6.9853	3.9195	3.7865 [1.2 %]	3.9459	4.2876
	HSDT† [94]	–	6.9853	3.9195	3.7866 [1.2 %]	–	4.2876
0.05	3-D Elasticity [97]	–	–	–	3.928	–	–
	Present ($\overline{k} = \overline{k}^{*}$, $n\to\infty$)	22.859	8.0013	4.1279	3.9444 [0.4 %]	4.0856	4.4231
	HSDT† [98]	22.859	8.0012	4.1279	3.9443 [0.4 %]	4.0856	4.4231
	HSDT† [94]	–	8.0012	4.1279	3.9443 [0.4 %]	–	4.4231
0.02	3-D Elasticity [97]	–	–	–	–	–	–
	Present ($\overline{k} = \overline{k}^{*}$, $n\to\infty$)	26.270	8.3418	4.1904	3.9910 [–]	4.1266	4.4626
	HSDT† [98]	26.270	8.3417	4.1903	3.9909 [–]	4.1265	4.4625
	HSDT† [94]	–	8.3417	4.1903	3.9909 [–]	–	4.4625
0.01	3-D Elasticity [97]	–	–	–	3.9975	–	–
	Present ($\overline{k} = \overline{k}^{*}$, $n\to\infty$)	26.843	8.3928	4.1995	3.9977 [0.0 %]	4.1325	4.4683
	HSDT† [98]	26.843	8.3928	4.1994	3.9977 [0.0 %]	4.1324	4.4682
	HSDT† [94]	–	8.3928	4.1994	3.9977 [0.0 %]	–	4.4682
–	CPT [98]	27.040	8.4100	4.202	4.0000	4.134	4.470
	Present ($n\to\infty$)	27.040	8.4100	4.2025	4.0000	4.1344	4.4702

* Equivalent $\overline{k}$ value for the interlayer modulus of $k^{*} = G_{\ell}/h_{\ell}$.
** D is set for comparison to the compatible parameter: D_{∞}.
† Reddy's higher-order shear deformation theory.

formula can be accommodated with a correction factor, taking into account the effect of geometrical uncertainties and imperfections of the adhesive layer [34].

In the case of partial composite behaviour in laminated plates and panels where layers are connected via discrete mechanical connectors such as bolts, screws, dowels, studs, or rivets, each fastener can be considered as a member of a chain of bi-directional shear springs between adjacent layers. Each connector from the network of connectors acts for the shear interaction over their spacing in each direction, as illustrated in Fig. 3. Referring to Eq. (6) in correlation with the definition of fasteners stiffness in layered elements, the interlayer interaction modulus can be obtained from $k = K_{\text{ser}}/s^2$ or $k = K_{\text{u}}/s^2$ where K_{ser} and K_{u} represent the shear stiffness of a fastener in layered elements, respectively, in the serviceability limit state (SLS) and the ultimate limit states (ULS); see e.g., [96] for the laminated timber elements according to the Eurocode 5. Moreover, the parameter s represents the fasteners spacing, as shown in Fig. 3. It should be pointed out that s^2 should be replaced by $s_1 s_2$ in case that the fasteners spacing is different in the two planar directions of a laminated plate.

It should also be noted that this study has focused on the developed imperfect partial-composite models and their exact solution techniques for the buckling and vibration behaviour of laminated plates. Therefore, any further details on the methods of determining the interlayer interaction moduli fall beyond the scope of the present work.

4. Numerical results and discussion

In this section, numerical results and discussion are presented based on the introduced model and the presented exact analytical solution schemes for the buckling and free vibrations of n-layer laminated partial composite plates. A computational code is developed using Maple software to extract the numerical results. A comparative study is conducted to verify the validity and efficiency of the model and the associated solution technique. Furthermore, a comprehensive set of benchmark results has been presented in a generalised dimensionless format for both the critical buckling loads as well as the natural frequencies of partial-composite plates. For the sake of generality and convenience, the results are presented in terms of the following dimensionless parameters:

$$\begin{aligned}
&\overline{N}_{\text{cr}} = N_{\text{cr}} a^2/D_\infty \\
&\overline{\omega} = \omega a^2 \sqrt{\rho_\ell h_{\text{Tot}}/D_\infty} \\
&\overline{k} = \frac{a^2 k}{n E_\ell h_{\text{Tot}}} \\
&\overline{h} = h_{\text{Tot}}/a \\
&\eta = a/b
\end{aligned} \tag{57}$$

where $\overline{N}_{\text{cr}}$ and $\overline{\omega}$ are the dimensionless critical buckling load and frequency parameters, respectively, $\overline{k}$ is the dimensionless interlayer interaction modulus, and $\overline{h}$ and η are the total thickness-to-length ratio and the plate aspect ratio, respectively. For the case of the buckling problem, the nondimensional parameters ξ_1 and ξ_2 represent the compressive buckling load intensity factors for the applied edge loads along the x and y directions, respectively, taken a value between zero to unity; see Eq. (42).

To show the validity, high accuracy, and reliability of the presented analytical solution approaches for the introduced model, numerical results for some special cases are compared with those reported in the literature.

Table 1 shows a comparison of the dimensionless critical buckling loads for rectangular plates under mono-axial compression based on the Reddy's higher-order shear deformation theory (HSDT) from two different sources, and special cases of the current LPCP model, presented for various values of length-to-thickness ratio and the plate aspect ratio. Moreover, some comparative results have been provided with the available data based on the 3-D elasticity as well as the classical plate theory (CPT). The percentage discrepancy provided in front of each value [%] is calculated with reference to the 3-D elasticity. The provided numerical results based on the present model are computed for the two special cases: (*i*) setting the interlayer modulus to be equivalent to the transverse shear strains, while the number of constituting layers approaches infinity; (*ii*) assuming the material transverse-shear-rigidity via tending the interlayer interaction modulus to infinity (i.e., perfectly bonded laminate).

The effect of the material's transverse shear stiffness in the structural responses has been considered by setting the interlayer shear interaction modulus as (see Eq. (6) for the definition of the interlayer shear stresses):

$$k^* = \frac{G_\ell}{h_\ell} = \frac{E_\ell}{2(1+\nu_\ell)h_\ell} \tag{58}$$

and therefore,

$$\overline{k}^* = \frac{k^* a^2}{n E_\ell h_{\text{Tot}}} = \frac{1}{2(1+\nu_\ell)\overline{h}^2} \tag{59}$$

where $\overline{h}$ is the total thickness-to-length ratio, according to Eq. (57). It can be seen from Table 1 that for all cases, including various values of plates aspect ratio as well as different values of thickness-to-length ratio, ranging from thin to thick plates, there is excellent agreement between the buckling results predicted based on a special case of the present LPCP model and those of HSDTs reported from different sources. The comparative results in Table 1 reveal that there is also an excellent agreement between the buckling load predictions from both special cases of the proposed LPCP model and those reported in the literature for thick plates, based on the three-dimensional elasticity, as well as the classical plate theory (CPT). This strong correlation is evident for all cases with various values of plate thickness-to-length ratio as well as a wide range of plate aspect ratios, confirming the high accuracy and validity of the developed LPCPT and the associated analytical solution technique. It should also be pointed out that although the HSDT-based results from both sources and the present LPCP model, under the described special case, match for all cases, their discrepancy relative to the 3-D elasticity is expected to increase as the plate thickness-to-length ratio increases. This trend is observed to hold true except for the extremely thick case of $h_{\text{Tot}}/b = 0.5$ which may be attributed to the convergence level associated with the employed numerical technique of discrete singular convolutional in obtaining the reported 3-D value in [97].

To show the validity and merit of the present method for dynamic analyses, the first five natural frequency parameters of laminated rectangular plates based on the LPCPT are tabulated in Table 2. The results are presented for laminated plates having different numbers of identical constituting layers, ranging from unity to asymptotically an infinite number of extremely thin layers, while the ratio of plates' total thickness to length is kept constant. The dimensionless interlayer interaction modulus is numerically assigned special values according to Eq. (59) for comparisons with the conventional theories. The obtained LPCPT-based vibration results are compared with the results reported in the literature for the vibration of thick solid plates based on the 3-D elasticity theory and the simplest CPT, as the lower and upper bounds of the presented LPCPT results, respectively. The results are provided for two different values of the plate's aspect ratio. It can be observed from the results of Table 2 that there is a strong correlation between the frequency parameters based on the 3-D elasticity and those obtained based on the special case of LPCPT, where the number of constituting layers tends to a large value. An excellent agreement can also be observed from the comparison of the CPT results and those of the LPCPT for comparable single-layer plates. The percentage discrepancies as low as below 1 % for each comparable case, reported in brackets in Table 2 confirm the high

Table 2
The first five natural frequencies of rectangular plates based on both the classical plate theory (CPT) and the 3-D elasticity, in comparison with those corresponding deduced from some special cases of the present LPCP model. The percentage discrepancy given for each value [%] is calculated with respect to the reference values for each case: (CPT as the reference for the single-layer $n = 1$, and 3-D elasticity for multilayers theoretically consisting of an infinite no. of extremely-thin film layers). The provided numerical results based on the present model are computed for a special case in which the interlayer interaction modulus is set to be equivalent to the transverse shear strains ($\bar{k} = \bar{k}^*$), while the number of constituting layers ranges from one to large values, tending to infinity (while the total thickness, $h_{\mathrm{Tot}} = nh_\ell$, is kept constant as the number of layers n, increases). The comparative results are available for the Poisson's ratio $\nu_\ell = 0.3$ and the overall plate thickness-to-length ratio $h_{\mathrm{Tot}}/a = 0.1$.

η	Method	No. of constituting Layers	$\omega h_{\mathrm{Tot}}\sqrt{\rho_\ell/G_\ell}$(Mode sequence) 1st	2nd	3rd	4th	5th
1	CPT [98]	–	0.0955 [1,1]**	0.2360 [1,2]	0.3732 [2,2]	0.4629 [1,3]	0.5951 [2,3]
	Present ($\bar{k} = \bar{k}^*$)	$n = 1$	0.0955 [0.0 %]†	0.2360 [0.0 %]	0.3732 [0.0 %]	0.4629 [0.0 %]	0.5951 [0.0 %]
		$n = 2$	0.0932	0.2232	0.3441	0.4206	0.5303
		$n = 5$	0.0930	0.2220	0.3409	0.4155	0.5216
		$n = 10$	0.0930	0.2220	0.3407	0.4152	0.5210
		$n = 20$	0.0930	0.2220	0.3406	0.4151	0.5208
		$n \to \infty$	0.0930 [0.2 %]††	0.2220 [1.7 %]	0.3406 [0.4 %]	0.4151 [0.5 %]	0.5208 [0.6 %]
	3-D Elasticity [99]	–	0.0932	0.2260	0.3421	0.4171	0.5239
$1/\sqrt{2}$	CPT [98]	–	0.7180 [1,1]*	1.4273 [1,2]	2.1281 [2,1]	2.5908 [1,3]	2.8207 [2,2]
	Present ($\bar{k} = \bar{k}^*$)	$n = 1$	0.7180 [0.0 %]†	1.4273 [0.0 %]	2.1281 [0.0 %]	2.5908 [0.0 %]	2.8207 [0.0 %]
		$n = 2$	0.7046	1.3774	2.0227	2.4396	2.6443
		$n = 5$	0.7036	1.3732	2.0131	2.4249	2.6267
		$n = 10$	0.7036	1.3730	2.0125	2.4240	2.6256
		$n = 20$	0.7036	1.3730	2.0124	2.4239	2.6254
		$n \to \infty$	0.7036 [0.1 %]††	1.3730 [0.2 %]	2.0124 [0.3 %]	2.4238 [0.3 %]	2.6254 [0.3 %]
	3-D Elasticity [100]	–	0.704	1.376	2.018	2.431	2.634

*Equivalent $\bar{k}$ value for the interlayer modulus of $k^* = G_\ell/h_\ell$.
**No. of vibration modes' half-waves along x and y directions.
†Percentage discrepancy with respect to CPT.
††Percentage discrepancy with respect to the 3-D Elasticity.

Table 3
Mechanical and physical properties of the aluminium sheets Al 2024-T2 in the studied multilayer panels.

Property	Young's modulus [GPa]	Shear modulus [GPa]	Poisson's ratio [-]	Density [Kg/m^3]
	70.15	27.6	0.33	2780

accuracy and reliability of the present approach and the proposed solution technique for the vibration analysis of laminated plates.

To demonstrate the validity and efficiency of the developed approach for laminated panels composed of multiple layers with different levels of interlayer interaction, a special aluminium sheet-based impact-resistant lightweight panel was modelled using the finite element analysis (FEA) for the comparative study. The panels are composed of thin layers of Aluminium 2024-T2 [101], with the layer thickness of 1 mm and an overall planar dimension of 110 × 165 mm^2.

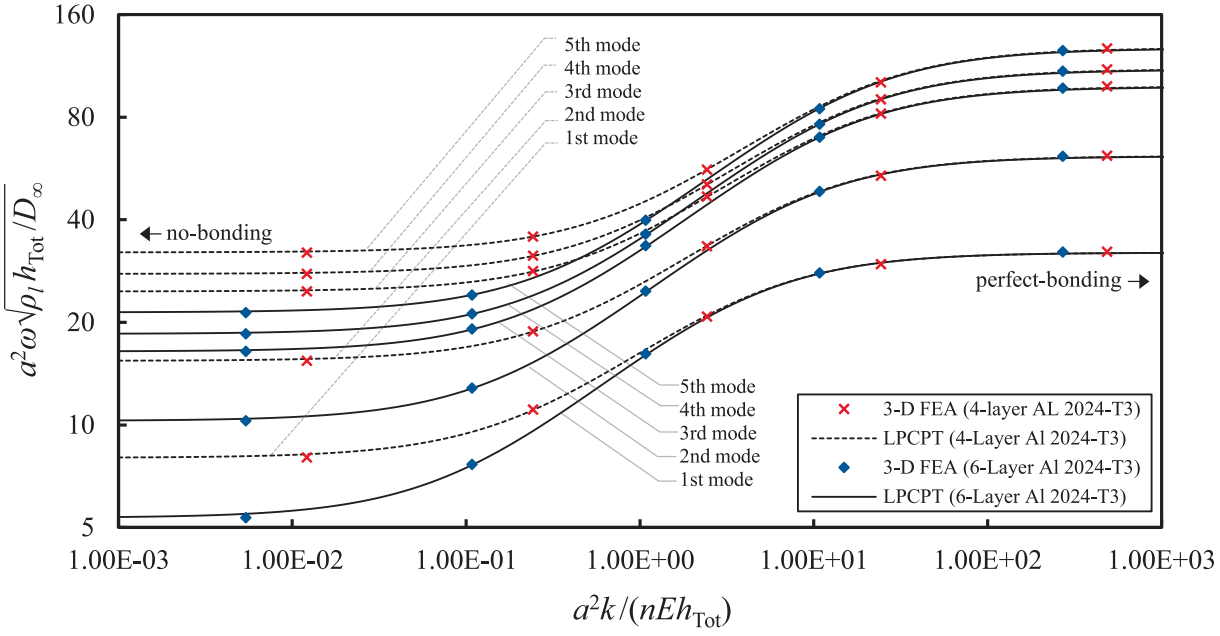

Fig. 4. Variations of the first five natural frequency parameters of the four- and six-layer Al 2024-T3 panels vs. the dimensionless interlayer interaction parameter, predicted based on the present LPCPT as well as the 3-D FE simulations.

Two different multilayer aluminium samples, composed of four and six sheets, bonded with soft adhesive films, are modelled and studied. The mechanical properties of the constituting Al 2024-T3 sheets [101] are given in Table 3.

The finite element modelling and analysis of the mentioned multilayer plate samples were carried out using the commercially available software Abaqus/CAE (Dassault Systèmes) for the free vibration analysis. Each of the bonded aluminium sheets was modelled by employing the continuum solid shell element type CSS8, an eight-node brick element, to achieve sufficiently accurate results in an efficient computational time frame. Each aluminium sheet was assigned an isotropic linear elastic section, built up with the elastic property set, as given in Table 3. The adhesive bonding films at the interfaces were modelled using the three-dimensional (3-D) solid element type C3D8R, an eight-node hexahedral/brick element with reduced integration and enhanced hourglass control, and applying quadratic geometric order to achieve accurate results. A relatively soft-shear isotropic material with flexible values of the shear modulus was assigned, corresponding to different values of the interlayer interaction modulus. The adhesive-sheet coinciding surfaces were constrained via the tie constraint of the elements' nodes. A double-sided bias-pattern fine mesh distribution was implemented for the through-depth element sizing using the structured technique, to achieve a denser mesh in the vicinity of the adhesive-sheet interfaces. This was applied to ensure that interaction effects are properly captured, gaining accurate and reliable results.

Variations of the first five natural frequency parameters versus the dimensionless interlayer interaction parameter based on the present LPCP model are depicted in Fig. 4 for the described four- and six-layer aluminium sheet panels, in comparison with the simulation results from the conducted FEA. Excellent agreement between the simulation results and the predictions based on the LPCP model at different levels of interlayer interaction is evident for both examined multilayer panels. Such a strong correlation across all vibration modes confirms the high accuracy and validity of the proposed LPCPT and its associated analytical solution technique. It can also be concluded from Fig. 4 that the extent of interlayer interaction has a more pronounced effect on the frequencies of panels composed of a greater number of constituent layers.

To visually elucidate the influence of partial interlayer interaction on the vibration modes of laminates, three-dimensional contours of the first five vibration modes of the four-layer AL 2024-T3 panel are illustrated in Fig. 5. The relative interlayer slips at different locations of the edges for the first two modes are shown.

A comprehensive set of dimensionless buckling load parameters ($\overline{N}_{cr}$) of laminated partial-composite plates is tabulated in Table 4. These results may serve as benchmark solutions for validating new solution approaches and computational techniques based on the LPCP model in the future. The results of Table 4 are general in nature and are provided for various numbers of constituting layers (n) and different levels of interlayer interaction, formulated via the nondimensional interlayer shear modulus ($\overline{k} = (a^2k)/(nEh_{Tot})$). The presented dimensionless buckling results are presented for three different compressive edge-load cases: (*i*) mono-axial along x-axis; (*ii*) mono-axial along y-axis; and (*iii*) bi-axial compression.

The results are generalised with regard to any thickness-to-length ratios, and are given for different aspect ratios (η). The graphical mode-shape contours corresponding to each buckling case, as well as their associated number of half-waves along the two planar directions, are presented in the tables.

It can be observed from the results of Table 4 that the critical buckling load parameters of the partial composite plates, regardless of the number of layers n, approach a specific value (bolded) for each case when the interlayer interaction parameter $\overline{k}$ approaches infinity (i.e., the so-called full-composite state or perfect interfacial bonding). The mentioned special values are identical to the critical load parameters of single-layer plates ($n = 1$ in the tables) based on the classical plate theory (CPT). It can also be deduced from the results of Table 4 that the effect of the interlayer interaction parameter, $\overline{k}$, is more dominant when the number of constituting layers of a plate increases. It can also be observed from the results of Table 4 that, the greater extent of interlayer interaction obviously causes a higher critical buckling load, for all plate and loading cases.

The first five frequency parameters ($\overline{\omega} = \omega a^2\sqrt{\rho_\ell h_{Tot}/D_\infty}$) of laminated partial-composite plates, as benchmark vibration results for the established LPCPT, are tabulated in Table 5 for a wide range of numbers

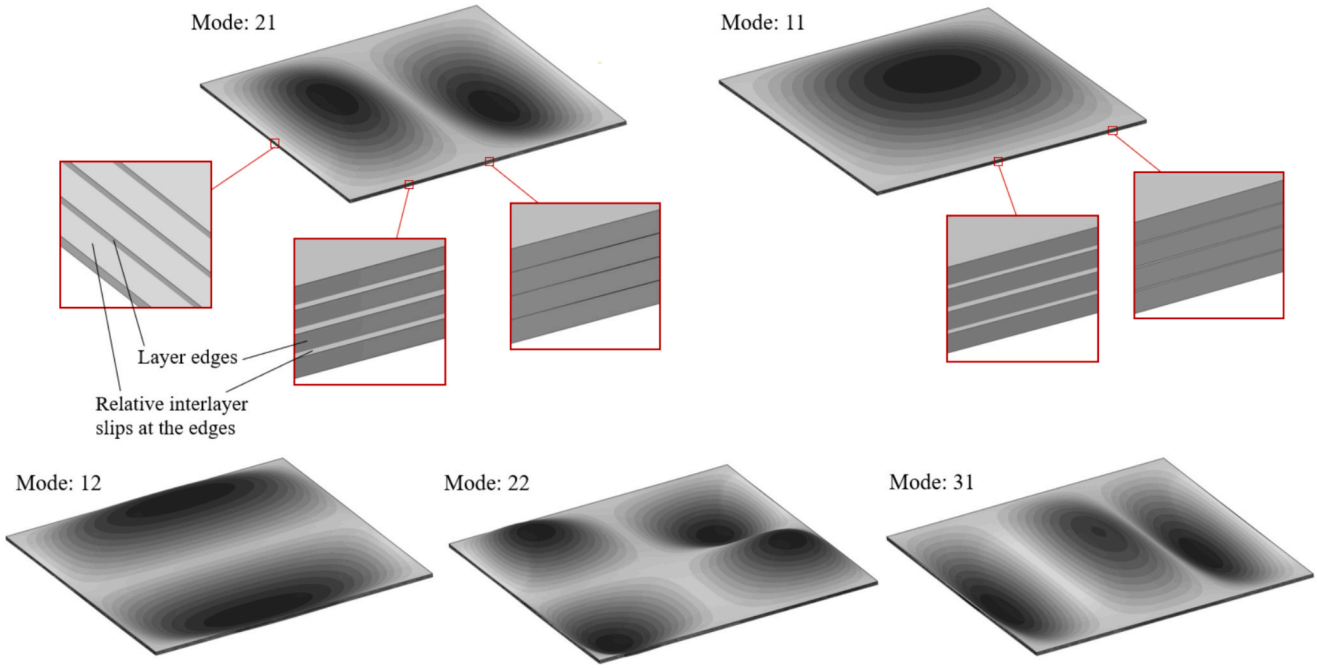

Fig. 5. Three-dimensional vibration mode-shapes of the four-layer AL 2024-T3 partial composite panel. The relative interlayer slips at different locations of the edges for the first two modes are illustrated.

Table 4

Dimensionless critical buckling loads ($\overline{N}_{cr} = a^2 N_{cr}/D_\infty$) of laminated partial-composite plates with different aspect ratios (η), for various numbers of constituting layers (n), and different levels of interlayer interaction, formulated via the nondimensional interlayer shear modulus ($\overline{k} = (a^2 k)/(nEh_{Tot})$). The presented dimensionless benchmark buckling results are general in nature and are provided for three different compressive edge-load cases: (i) mono-axial along x-axis; (ii) mono-axial along y-axis; and (iii) bi-axial compression. The results are generalised with regard to any thickness-to-length ratios. The numbers of layers (n) are varied, while the total thickness-to-length ratio is kept constant. The buckling loads, for the case $\overline{k}\to 0$, is reduced by the factor of $1/n^2$ compared to a corresponding perfectly bonded ideal case, as in the beam-case shown in [34].

(ξ_1, ξ_2)	$\eta = \frac{a}{b}$	No. of Layers (n)	$\overline{N}_{cr} = a^2 N_{cr}/D_\infty$									
			$\overline{k}\to 0$	$\overline{k} = 10^{-4}$	$\overline{k} = 10^{-2}$	$\overline{k} = 10^{-1}$	$\overline{k} = 1.0$	$\overline{k} = 10$	$\overline{k} = 10^{2}$	$\overline{k} = 10^{4}$	$\overline{k} = 10^{6}$	$\overline{k}\to\infty$
Case *i*: (1,0)	1.0(cr. buckling mode:1,1)	1	**39.4784**	**39.4784**	**39.4784**	**39.4784**	**39.4784**	**39.4784**	**39.4784**	**39.4784**	**39.4784**	**39.4784**
Mono-axial along *x*-axis		2	9.8696	9.8707	9.9784	10.9228	17.8473	33.1627	38.6968	39.4704	39.4783	**39.4784**
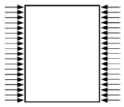		5	1.5791	1.5809	1.7529	3.2352	13.2998	32.5098	38.6424	39.4699	39.4783	**39.4784**
		10	0.3948	0.3967	0.5894	2.2105	12.7938	32.4672	38.6407	39.4699	39.4783	**39.4784**
		20	0.0987	0.1008	0.3027	1.9667	12.6761	32.4586	38.6405	39.4699	39.4783	**39.4784**
		50	0.0158	0.0179	0.2238	1.9000	12.6439	32.4564	38.6405	39.4699	39.4783	**39.4784**
		100	0.0039	0.0061	0.2127	1.8906	12.6393	32.4561	38.6405	39.4699	39.4783	**39.4784**
		1000	<0.0001	0.0022	0.2091	1.8875	12.6378	32.4560	38.6405	39.4699	39.4783	**39.4784**
		→∞	0	0.0022	0.2090	1.8874	12.6377	32.4560	38.6405	39.4699	39.4783	**39.4784**
	2/3(cr. buckling mode:1,1)	1	**20.5921**	**20.5921**	**20.5921**	**20.5921**	**20.5921**	**20.5921**	**20.5921**	**20.5921**	**20.5921**	**20.5921**
		2	5.1480	5.1488	5.2265	5.8984	10.3687	18.0630	20.2955	20.5891	20.5921	**20.5921**
		5	0.8237	0.8249	0.9489	1.9973	8.3784	17.8248	20.2752	20.5889	20.5921	**20.5921**
		10	0.2059	0.2073	0.3460	1.4859	8.1666	17.8110	20.2746	20.5889	20.5921	**20.5921**
		20	0.0515	0.0530	0.1980	1.3647	8.1177	17.8083	20.2746	20.5889	20.5921	**20.5921**
		50	0.0082	0.0098	0.1574	1.3316	8.1043	17.8076	20.2746	20.5889	20.5921	**20.5921**
		100	0.0021	0.0036	0.1517	1.3269	8.1024	17.8076	20.2746	20.5889	20.5921	**20.5921**
		1000	<0.0001	0.0016	0.1498	1.3253	8.1018	17.8075	20.2746	20.5889	20.5921	**20.5921**
		→∞	0	0.0016	0.1498	1.3253	8.1018	17.8075	20.2746	20.5889	20.5921	**20.5921**
	0.5(cr. buckling mode:1,1)	1	**15.4213**	**15.4213**	**15.4213**	**15.4213**	**15.4213**	**15.4213**	**15.4213**	**15.4213**	**15.4213**	**15.4213**
		2	3.8553	3.8560	3.9232	4.4998	8.1475	13.7453	15.2285	15.4193	15.4212	**15.4213**
		5	0.6169	0.6179	0.7251	1.6220	6.7846	13.5932	15.2154	15.4192	15.4212	**15.4213**
		10	0.1542	0.1554	0.2752	1.2479	6.6429	13.5848	15.2151	15.4192	15.4212	**15.4213**
		20	0.0386	0.0398	0.1650	1.1594	6.6103	13.5832	15.2150	15.4192	15.4212	**15.4213**
		50	0.0062	0.0075	0.1348	1.1351	6.6014	13.5828	15.2150	15.4192	15.4212	**15.4213**
		100	0.0015	0.0029	0.1305	1.1317	6.6001	13.5828	15.2150	15.4192	15.4212	**15.4213**
		1000	<0.0001	0.0014	0.1291	1.1306	6.5997	13.5828	15.2150	15.4192	15.4212	**15.4213**
		→∞	0	0.0014	0.1291	1.1305	6.5997	13.5828	15.2150	15.4192	15.4212	**15.4213**
	0.4(cr. buckling mode:1,1)	1	**13.2805**	**13.2805**	**13.2805**	**13.2805**	**13.2805**	**13.2805**	**13.2805**	**13.2805**	**13.2805**	**13.2805**
		2	3.3201	3.3208	3.3831	3.9156	7.1918	11.9270	13.1263	13.2790	13.2805	**13.2805**
		5	0.5312	0.5322	0.6316	1.4586	6.0744	11.8064	13.1159	13.2789	13.2805	**13.2805**
		10	0.1328	0.1339	0.2449	1.1406	5.9596	11.7999	13.1156	13.2789	13.2805	**13.2805**
		20	0.0332	0.0344	0.1503	1.0653	5.9333	11.7987	13.1156	13.2789	13.2805	**13.2805**
		50	0.0053	0.0066	0.1244	1.0448	5.9261	11.7984	13.1156	13.2789	13.2805	**13.2805**
		100	0.0013	0.0026	0.1207	1.0418	5.9251	11.7984	13.1156	13.2789	13.2805	**13.2805**
		1000	<0.0001	0.0013	0.1195	1.0409	5.9247	11.7984	13.1156	13.2789	13.2805	**13.2805**
		→∞	0	0.0013	0.1195	1.0409	5.9247	11.7984	13.1156	13.2789	13.2805	**13.2805**

(ξ_1, ξ_2)	$\eta = \frac{a}{b}$	No. of Layers (n)	$\overline{N}_{cr} = a^2 N_{cr}/D_\infty$									
			$\overline{k}\to 0$	$\overline{k} = 10^{-4}$	$\overline{k} = 10^{-2}$	$\overline{k} = 10^{-1}$	$\overline{k} = 1.0$	$\overline{k} = 10$	$\overline{k} = 10^{2}$	$\overline{k} = 10^{4}$	$\overline{k} = 10^{6}$	$\overline{k}\to\infty$
Case *ii*: (0,1)	1.0(cr. buckling mode:1,1)	1	**39.4784**	**39.4784**	**39.4784**	**39.4784**	**39.4784**	**39.4784**	**39.4784**	**39.4784**	**39.4784**	**39.4784**
Mono-axial along *y*-axis		2	9.8696	9.8707	9.9784	10.9228	17.8473	33.1627	38.6968	39.4704	39.4783	**39.4784**
		5	1.5791	1.5809	1.7529	3.2352	13.2998	32.5098	38.6424	39.4699	39.4783	**39.4784**
		10	0.3948	0.3967	0.5894	2.2105	12.7938	32.4672	38.6407	39.4699	39.4783	**39.4784**
		20	0.0987	0.1008	0.3027	1.9667	12.6761	32.4586	38.6405	39.4699	39.4783	**39.4784**
		50	0.0158	0.0179	0.2238	1.9000	12.6439	32.4564	38.6405	39.4699	39.4783	**39.4784**
		100	0.0039	0.0061	0.2127	1.8906	12.6393	32.4561	38.6405	39.4699	39.4783	**39.4784**
		1000	<0.0001	0.0022	0.2091	1.8875	12.6378	32.4560	38.6405	39.4699	39.4783	**39.4784**
		→∞	0	0.0022	0.2090	1.8874	12.6377	32.4560	38.6405	39.4699	39.4783	**39.4784**
	2/3(cr. buckling mode:1,2)	1	**42.8368**	**42.8368**	**42.8368**	**42.8368**	**42.8368**	**42.8368**	**42.8368**	**42.8368**	**42.8368**	**42.8368**
	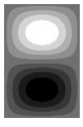	2	10.7092	10.7101	10.7943	11.5403	17.4504	34.0478	41.6708	42.8247	42.8367	**42.8368**
		5	1.7135	1.7148	1.8494	3.0259	11.7582	33.0392	41.5877	42.8239	42.8367	**42.8368**
		10	0.4284	0.4299	0.5808	1.8743	11.1005	32.9658	41.5849	42.8239	42.8367	**42.8368**
		20	0.1071	0.1087	0.2672	1.5990	10.9467	32.9505	41.5845	42.8239	42.8367	**42.8368**
		50	0.0171	0.0188	0.1807	1.5238	10.9045	32.9465	41.5845	42.8239	42.8367	**42.8368**
		100	0.0043	0.0060	0.1685	1.5132	10.8985	32.9459	41.5845	42.8239	42.8367	**42.8368**
		1000	<0.0001	0.0017	0.1644	1.5097	10.8965	32.9457	41.5845	42.8239	42.8367	**42.8368**
		→∞	0	0.0017	0.1644	1.5096	10.8965	32.9457	41.5845	42.8239	42.8367	**42.8368**
	0.5(cr. buckling mode:1,2)	1	**39.4784**	**39.4784**	**39.4784**	**39.4784**	**39.4784**	**39.4784**	**39.4784**	**39.4784**	**39.4784**	**39.4784**
	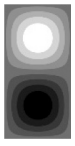	2	9.8696	9.8707	9.9784	10.9228	17.8473	33.1627	38.6968	39.4704	39.4783	**39.4784**
		5	1.5791	1.5809	1.7529	3.2352	13.2998	32.5098	38.6424	39.4699	39.4783	**39.4784**
		10	0.3948	0.3967	0.5894	2.2105	12.7938	32.4672	38.6407	39.4699	39.4783	**39.4784**
		20	0.0987	0.1008	0.3027	1.9667	12.6761	32.4586	38.6405	39.4699	39.4783	**39.4784**
		50	0.0158	0.0179	0.2238	1.9000	12.6439	32.4564	38.6405	39.4699	39.4783	**39.4784**
		100	0.0039	0.0061	0.2127	1.8906	12.6393	32.4561	38.6405	39.4699	39.4783	**39.4784**
		1000	<0.0001	0.0022	0.2091	1.8875	12.6378	32.4560	38.6405	39.4699	39.4783	**39.4784**
		→∞	0	0.0022	0.2090	1.8874	12.6377	32.4560	38.6405	39.4699	39.4783	**39.4784**

(*continued on next page*)

Table 4 (*continued*)

(ξ_1,ξ_2)	$\eta=\frac{a}{b}$	No. of Layers (n)	$\overline{N}_{cr}=a^2N_{cr}/D_\infty$									
			$\overline{k}\to0$	$\overline{k}=10^{-4}$	$\overline{k}=10^{-2}$	$\overline{k}=10^{-1}$	$\overline{k}=1.0$	$\overline{k}=10$	$\overline{k}=10^{2}$	$\overline{k}=10^{4}$	$\overline{k}=10^{6}$	$\overline{k}\to\infty$
	0.4(cr. buckling mode:1,3) 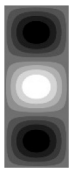	1	**40.8053**	**40.8053**	**40.8053**	**40.8053**	**40.8053**	**40.8053**	**40.8053**	**40.8053**	**40.8053**	**40.8053**
		2	10.2013	10.2023	10.2936	11.0994	17.3054	33.1981	39.8254	40.7952	40.8052	**40.8053**
		5	1.6322	1.6337	1.7795	3.0482	12.1606	32.3613	39.7562	40.7946	40.8052	**40.8053**
		10	0.4081	0.4097	0.5732	1.9652	11.5745	32.3029	39.7540	40.7945	40.8052	**40.8053**
		20	0.1020	0.1038	0.2753	1.7068	11.4376	32.2909	39.7537	40.7945	40.8052	**40.8053**
		50	0.0163	0.0181	0.1933	1.6362	11.4001	32.2877	39.7536	40.7945	40.8052	**40.8053**
		100	0.0041	0.0059	0.1817	1.6262	11.3948	32.2873	39.7536	40.7945	40.8052	**40.8053**
		1000	<0.0001	0.0019	0.1779	1.6229	11.3930	32.2872	39.7536	40.7945	40.8052	**40.8053**
		→∞	0	0.0018	0.1778	0.1628	11.3930	32.2872	39.7536	40.7945	40.8052	**40.8053**
(ξ_1,ξ_2)	$\eta=\frac{a}{b}$	No. of Layers (n)	$\overline{N}_{cr}=a^2N_{cr}/D_\infty$									
			$\overline{k}\to0$	$\overline{k}=10^{-4}$	$\overline{k}=10^{-2}$	$\overline{k}=10^{-1}$	$\overline{k}=1.0$	$\overline{k}=10$	$\overline{k}=10^{2}$	$\overline{k}=10^{4}$	$\overline{k}=10^{6}$	$\overline{k}\to\infty$
Case *iii*: (1,1)Bi-axial compression 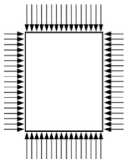	1.0(cr. buckling mode:1,1) 	1	**19.7392**	**19.7392**	**19.7392**	**19.7392**	**19.7392**	**19.7392**	**19.7392**	**19.7392**	**19.7392**	**19.7392**
		2	4.9348	4.9353	4.9892	5.4614	8.9237	16.5813	19.3484	19.7352	19.7392	**19.7392**
		5	0.7896	0.7904	0.8764	1.6176	6.6499	16.2549	19.3212	19.7349	19.7392	**19.7392**
		10	0.1974	0.1984	0.2947	1.1052	6.3969	16.2336	19.3203	19.7349	19.7392	**19.7392**
		20	0.0493	0.0504	0.1514	0.9833	6.3381	16.2293	19.3203	19.7349	19.7392	**19.7392**
		50	0.0079	0.0090	0.1119	0.9500	6.3219	16.2282	19.3202	19.7349	19.7392	**19.7392**
		100	0.0020	0.0031	0.1064	0.9453	6.3196	16.2281	19.3202	19.7349	19.7392	**19.7392**
		1000	<0.0001	0.0011	0.1045	0.9437	6.3189	16.2280	19.3202	19.7349	19.7392	**19.7392**
		→∞	0	0.0011	0.1045	0.9437	6.3189	16.2280	19.3202	19.7349	19.7392	**19.7392**
	2/3(cr. buckling mode:1,1) 	1	**14.2561**	**14.2561**	**14.2561**	**14.2561**	**14.2561**	**14.2561**	**14.2561**	**14.2561**	**14.2561**	**14.2561**
		2	3.564	3.5646	3.6183	4.0835	7.1783	12.5052	14.0507	14.254	14.2561	**14.2561**
		5	0.5702	0.5711	0.6569	1.3827	5.8004	12.3402	14.0367	14.2539	14.2561	**14.2561**
		10	0.1426	0.1435	0.2395	1.0287	5.6538	12.3307	14.0363	14.2539	14.2561	**14.2561**
		20	0.0356	0.0367	0.1371	0.9448	5.6200	12.3288	14.0363	14.2539	14.2561	**14.2561**
		50	0.0057	0.0068	0.109	0.9219	5.6107	12.3284	14.0362	14.2539	14.2561	**14.2561**
		100	0.0014	0.0025	0.105	0.9186	5.6094	12.3283	14.0362	14.2539	14.2561	**14.2561**
		1000	<0.0001	0.0011	0.1037	0.9175	5.6090	12.3283	14.0362	14.2539	14.2561	**14.2561**
		→∞	0	0.0011	0.1037	0.9175	5.6090	12.3283	14.0362	14.2539	14.2561	**14.2561**
	0.5(cr. buckling mode:1,1) 	1	**12.3370**	**12.3370**	**12.3370**	**12.3370**	**12.3370**	**12.3370**	**12.3370**	**12.3370**	**12.3370**	**12.3370**
		2	3.0843	3.0848	3.1385	3.5998	6.5180	10.9962	12.1828	12.3354	12.3370	**12.3370**
		5	0.4935	0.4944	0.5800	1.2976	5.4277	10.8745	12.1724	12.3353	12.3370	**12.3370**
		10	0.1234	0.1244	0.2201	0.9983	5.3143	10.8678	12.1720	12.3353	12.3370	**12.3370**
		20	0.0308	0.0319	0.1320	0.9275	5.2882	10.8666	12.1720	12.3353	12.3370	**12.3370**
		50	0.0049	0.0060	0.1078	0.9081	5.2811	10.8663	12.1720	12.3353	12.3370	**12.3370**
		100	0.0012	0.0023	0.1044	0.9053	5.2801	10.8662	12.1720	12.3353	12.3370	**12.3370**
		1000	<0.0001	0.0011	0.1033	0.9044	5.2797	10.8662	12.1720	12.3353	12.3370	**12.3370**
		→∞	0	0.0011	0.1033	0.9044	5.2797	10.8662	12.1720	12.3353	12.3370	**12.3370**
	0.4(cr. buckling mode:1,1) 	1	**11.4487**	**11.4487**	**11.4487**	**11.4487**	**11.4487**	**11.4487**	**11.4487**	**11.4487**	**11.4487**	**11.4487**
		2	2.8622	2.8627	2.9164	3.3755	6.1998	10.2819	11.3158	11.4474	11.4487	**11.4487**
		5	0.4579	0.4588	0.5445	1.2574	5.2366	10.1779	11.3068	11.4473	11.4487	**11.4487**
		10	0.1145	0.1155	0.2112	0.9833	5.1376	10.1723	11.3065	11.4473	11.4487	**11.4487**
		20	0.0286	0.0297	0.1296	0.9184	5.1149	10.1713	11.3065	11.4473	11.4487	**11.4487**
		50	0.0046	0.0056	0.1072	0.9007	5.1087	10.1711	11.3065	11.4473	11.4487	**11.4487**
		100	0.0011	0.0022	0.1041	0.8981	5.1078	10.1710	11.3065	11.4473	11.4487	**11.4487**
		1000	<0.0001	0.0011	0.1031	0.8973	5.1075	10.1710	11.3065	11.4473	11.4487	**11.4487**
		→∞	0	0.0011	0.1030	0.8973	5.1075	10.1710	11.3065	11.4473	11.4487	**11.4487**

of identical constituent layers in the plates, while the total thickness is kept constant. The results also cover a wide ranges of interlayer interaction level, and are provided for different values of plate aspect ratio (η), while the total thickness-to-length ratio of $\overline{h}_{Tot}=0.1$ is chosen corresponding to moderately-thick range of plate thickness. The number of vibration half-waves in each direction, along with the contours of vibration mode-shapes, is provided in the tables for each case.

It can be concluded from Table 5 that increasing the extent of interlayer interaction will cause an increase in the frequency parameters of the layered plates. However, that influence, similar to the buckling problem, is more pronounced when the number of constituting layers increases. As a special case of the present LPCP model, the frequency parameters of plates with different numbers of identical constituting layers approach a unique value corresponding to that of a single-layer based on the CPT, when the interlayer interaction parameter approaches infinity (bolded data in Table 5).

To evaluate the validity and performance of the proposed LPCPT for laminated partial composite plates with non-identical layers, the numerical vibration results for cross-ply laminated partial-composite plates with the stacking sequence (0/90/90/0) are reported in Table 6, based on the direct solution approach described in Subsection 3.2. A wide range of values in logarithmic scale is considered for the interlayer interaction modulus in dimensionless form, covering the full range from the lower-bound of the non-composite case (zero shear interaction) to the upper-bound corresponding to the fully composite case (perfect-bonding). Each ply is assumed to be orthotropic with two different modulus ratios: $E_{\|}/E_{\perp}=$ 10 and 20 ($G_{12}=0.5E_{\perp}$ and $\nu_{12}=0.25$). All plies have equal thickness, with a total thickness-to-length ratio of $\overline{h}_{Tot}=0.1$.

The frequency results accounting for the rotary inertia effects (arising from the in-plane translational-inertia contributions of all layers in a partial interaction) are presented in the table in comparison with those obtained when the mentioned effects are neglected. For each reported frequency, the corresponding vibration mode is indicated as a superscript denoting the number of half-waves in each orthogonal planar direction. For instance, a 23-mode represents two half-waves in the x - and three is in the y - direction.

It can be observed from Table 6 that, in the limiting special case of

Table 5

First five dimensionless frequencies ($\overline{\omega} = \omega a^2\sqrt{\rho_\ell h_{\mathrm{Tot}}/D_\infty}$) of laminated partial-composite plates with different aspect ratios (η), for various numbers of constituting layers (n) while the total thickness is kept constant. The results are presented for different levels of interlayer interaction, formulated via the nondimensional interlayer shear modulus ($\overline{k} = (a^2k)/(nEh_{\mathrm{Tot}})$). The given dimensionless benchmark vibration results are general in nature and are provided for the total thickness-to-length ratio $\overline{h}_{\mathrm{Tot}} = 0.1$. The number of half-waves along the two planar directions for each vibration mode-shape is provided. The numbers of layers (n) are varied, while the total thickness-to-length ratio is kept constant.

$\eta = \frac{a}{b}$	Mode sequence	No. of Layers (n)	$\overline{\omega} = \omega a^2\sqrt{\rho_\ell h_{\mathrm{Tot}}/D_\infty}$ $\overline{k}\to 0$	$\overline{k} = 10^{-4}$	$\overline{k} = 10^{-2}$	$\overline{k} = 10^{-1}$	$\overline{k} = 1.0$	$\overline{k} = 10$	$\overline{k} = 10^{2}$	$\overline{k} = 10^{4}$	$\overline{k} = 10^{6}$	$\overline{k}\to\infty$
1.0	1st(mode: 1,1)	1	**19.5788**	**19.5788**	**19.5788**	**19.5788**	**19.5788**	**19.5788**	**19.5788**	**19.5788**	**19.5788**	**19.5788**
		2	9.8494	9.8499	9.9035	10.3615	13.2389	17.9860	19.3901	19.5769	19.5788	**19.5788**
		5	3.9465	3.9487	4.1580	5.6487	11.4444	17.8130	19.3769	19.5768	19.5788	**19.5788**
		10	1.9738	1.9787	2.4117	4.6703	11.2266	17.8017	19.3765	19.5768	19.5788	**19.5788**
		100	0.1974	0.2455	1.4489	4.3195	11.1591	17.7988	19.3765	19.5768	19.5788	**19.5788**
		1000	0.0197	0.1478	1.4364	4.3159	11.1585	17.7988	19.3765	19.5768	19.5788	**19.5788**
		$\to\infty$	0	0.1465	1.4363	4.3159	11.1585	17.7988	19.3765	19.5768	19.5788	**19.5788**
	2nd(mode: 1,2)	1	**48.3636**	**48.3636**	**48.3636**	**48.3636**	**48.3636**	**48.3636**	**48.3636**	**48.3636**	**48.3636**	**48.3636**
		2	24.5481	24.5487	24.6023	25.0777	28.8894	40.7658	47.2829	48.3523	48.3635	**48.3636**
		5	9.8615	9.8637	10.0769	11.8041	21.3011	39.5686	47.1998	48.3515	48.3635	**48.3636**
		10	4.9338	4.9387	5.4010	8.4324	20.1710	39.4642	47.1965	48.3515	48.3635	**48.3636**
		100	0.4935	0.5448	2.3402	7.0335	19.8084	39.4342	47.1959	48.3515	48.3635	**48.3636**
		1000	0.0493	0.2370	2.2901	7.0185	19.8048	39.4339	47.1959	48.3515	48.3635	**48.3636**
		$\to\infty$	0	0.2318	2.2896	7.0184	19.8048	39.4339	47.1959	48.3515	48.3635	**48.3636**
	3rd(mode: 2,1)	1	**48.3636**	**48.3636**	**48.3636**	**48.3636**	**48.3636**	**48.3636**	**48.3636**	**48.3636**	**48.3636**	**48.3636**
		2	24.5481	24.5487	24.6023	25.0777	28.8894	40.7658	47.2829	48.3523	48.3635	**48.3636**
		5	9.8615	9.8637	10.0769	11.8041	21.3011	39.5686	47.1998	48.3515	48.3635	**48.3636**
		10	4.9338	4.9387	5.4010	8.4324	20.1710	39.4642	47.1965	48.3515	48.3635	**48.3636**
		100	0.4935	0.5448	2.3402	7.0335	19.8084	39.4342	47.1959	48.3515	48.3635	**48.3636**
		1000	0.0493	0.2370	2.2901	7.0185	19.8048	39.4339	47.1959	48.3515	48.3635	**48.3636**
		$\to\infty$	0	0.2318	2.2896	7.0184	19.8048	39.4339	47.1959	48.3515	48.3635	**48.3636**
	4th(mode: 2,2)	1	**76.4808**	**76.4808**	**76.4808**	**76.4808**	**76.4808**	**76.4808**	**76.4808**	**76.4808**	**76.4808**	**76.4808**
		2	39.1577	39.1582	39.2117	39.6906	43.8289	60.8098	73.9324	76.4534	76.4805	**76.4808**
		5	15.7706	15.7728	15.9869	17.7916	29.2547	57.7403	73.7194	76.4517	76.4805	**76.4808**
		10	7.8931	7.8980	8.3687	11.7494	26.8192	57.4372	73.7096	76.4516	76.4805	**76.4808**
		100	0.7896	0.8419	3.0069	8.9958	26.0167	57.3472	73.7075	76.4516	76.4805	**76.4808**
		1000	0.0790	0.3038	2.9057	8.9649	26.0088	57.3463	73.7075	76.4516	76.4805	**76.4808**
		$\to\infty$	0	0.2933	2.9046	8.9646	26.0087	57.3463	73.7075	76.4516	76.4805	**76.4808**
	5th(mode: 1,3)	1	**94.8717**	**94.8717**	**94.8717**	**94.8717**	**94.8717**	**94.8717**	**94.8717**	**94.8717**	**94.8717**	**94.8717**
	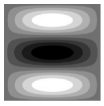	2	48.8484	48.8489	48.9024	49.3819	53.6384	73.2458	91.0924	94.8305	94.8713	**94.8717**
		5	19.7068	19.7090	19.9234	21.7560	34.1188	68.5373	90.7603	94.8279	94.8712	**94.8717**
		10	9.8656	9.8705	10.3441	13.8714	30.6648	68.0460	90.7438	94.8278	94.8712	**94.8717**
		100	0.9870	1.0396	3.3938	10.1051	29.5079	67.8984	90.7401	94.8278	94.8712	**94.8717**
		1000	0.0987	0.3425	3.2527	10.0617	29.4964	67.8969	90.7401	94.8278	94.8712	**94.8717**
		$\to\infty$	0	0.3280	3.2513	10.0612	29.4963	67.8969	90.7401	94.8278	94.8712	**94.8717**
$\eta = \frac{a}{b}$	Mode sequence	No. of Layers (n)	$\overline{\omega} = \omega a^2\sqrt{\rho_\ell h_{\mathrm{Tot}}/D_\infty}$ $\overline{k}\to 0$	$\overline{k} = 10^{-4}$	$\overline{k} = 10^{-2}$	$\overline{k} = 10^{-1}$	$\overline{k} = 1.0$	$\overline{k} = 10$	$\overline{k} = 10^{2}$	$\overline{k} = 10^{4}$	$\overline{k} = 10^{6}$	$\overline{k}\to\infty$
2/3	1st(mode: 1,1)	1	**14.1722**	**14.1722**	**14.1722**	**14.1722**	**14.1722**	**14.1722**	**14.1722**	**14.1722**	**14.1722**	**14.1722**
		2	7.0861	7.1180	7.17152	7.61847	10.0959	13.2909	14.0721	14.1711	14.1722	**14.1722**
		5	2.8344	2.8527	3.05951	4.43868	9.0837	13.2048	14.0652	14.1711	14.1721	**14.1722**
		10	1.4172	1.4304	1.84778	3.82921	8.9691	13.1998	14.0650	14.1711	14.1721	**14.1722**
		100	0.1417	0.1890	1.22348	3.61865	8.9341	13.1986	14.0650	14.1711	14.1721	**14.1722**
		1000	0.0142	0.1253	1.21585	3.61653	8.9337	13.1986	14.0650	14.1711	14.1721	**14.1722**
		$\to\infty$	0	0.1245	1.21577	3.61651	8.9337	13.1986	14.0650	14.1711	14.1721	**14.1722**
	2nd(mode: 1,2)	1	**27.1077**	**27.1077**	**27.1077**	**27.1077**	**27.1077**	**27.1077**	**27.1077**	**27.1077**	**27.1077**	**27.1077**
	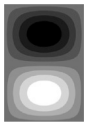	2	13.6688	13.6693	13.7230	14.1892	17.4418	24.2629	26.7520	27.1040	27.1076	**27.1077**
		5	5.4806	5.4828	5.6939	7.2830	14.3472	23.9138	26.7265	27.1038	27.1076	**27.1077**
		10	2.7412	2.7462	3.1920	5.7339	13.9438	23.8883	26.7256	27.1038	27.1076	**27.1077**
		100	0.2742	0.3237	1.7193	5.1526	13.8175	23.8814	26.7255	27.1038	27.1076	**27.1077**
		1000	0.0274	0.1749	1.6986	5.1466	13.8162	23.8813	26.7255	27.1038	27.1076	**27.1077**
		$\to\infty$	0	0.1727	1.6984	5.1465	13.8162	23.8813	26.7255	27.1038	27.1076	**27.1077**
	3rd(mode: 2,1)	1	**43.0845**	**43.0845**	**43.0845**	**43.0845**	**43.0845**	**43.0845**	**43.0845**	**43.0845**	**43.0845**	**43.0845**
	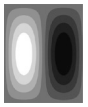	2	21.8329	21.8335	21.8871	22.3611	26.0739	36.8043	42.2171	43.0755	43.0844	**43.0845**
		5	8.7666	8.7688	8.9816	10.6850	19.6858	35.8654	42.1514	43.0749	43.0844	**43.0845**
		10	4.3857	4.3906	4.8502	7.7871	18.7602	35.7863	42.1489	43.0749	43.0844	**43.0845**
		100	0.4386	0.4897	2.1992	6.6107	18.7602	35.7637	42.1485	43.0749	43.0844	**43.0845**
		1000	0.0439	0.2229	2.1573	6.5982	18.4620	35.7635	42.1485	43.0749	43.0844	**43.0845**
		$\to\infty$	0	0.2185	2.1569	6.5981	18.4620	35.7635	42.1485	43.0749	43.0844	**43.0845**
	4th(mode: 1,3)	1	**48.3636**	**48.3636**	**48.3636**	**48.3636**	**48.3636**	**48.3636**	**48.3636**	**48.3636**	**48.3636**	**48.3636**
	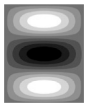	2	24.5481	24.5487	24.6023	25.0777	28.8894	40.7658	47.2829	48.3523	48.3635	**48.3636**
		5	9.8615	9.8637	10.077	11.8041	21.3011	39.5686	47.1998	48.3515	48.3635	**48.3636**
		10	4.9338	4.9387	5.4010	8.4324	20.1710	39.4642	47.1965	48.3515	48.3635	**48.3636**
		100	0.4935	0.5448	2.3402	7.0335	19.8084	39.4342	47.1959	48.3515	48.3635	**48.3636**
		1000	0.0493	0.2370	2.2902	7.0185	19.8048	39.4339	47.1959	48.3515	48.3635	**48.3636**
		$\to\infty$	0	0.2318	2.2896	7.0184	19.8048	39.4339	47.1959	48.3515	48.3635	**48.3636**

(*continued on next page*)

Table 5 (*continued*)

$\eta = \frac{a}{b}$	Mode sequence	No. of Layers (n)	$\overline{\omega} = \omega a^2\sqrt{\rho_\ell h_{\mathrm{Tot}}/D_\infty}$ $\overline{k}\to 0$	$\overline{k}=10^{-4}$	$\overline{k}=10^{-2}$	$\overline{k}=10^{-1}$	$\overline{k}=1.0$	$\overline{k}=10$	$\overline{k}=10^{2}$	$\overline{k}=10^{4}$	$\overline{k}=10^{6}$	$\overline{k}\to\infty$
	5th(mode: 2,2) 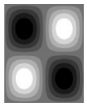	1	**55.7159**	**55.7159**	**55.7159**	**55.7159**	**55.7159**	**55.7159**	**55.7159**	**55.7159**	**55.7159**	**55.7159**
		2	28.3443	28.3449	28.3985	28.8752	32.7989	46.1629	54.3040	55.7010	55.7158	**55.7159**
		5	11.3941	11.3962	11.6098	13.3637	23.4705	44.5552	54.1929	55.7000	55.7158	**55.7159**
		10	5.7011	5.7060	6.1713	9.3153	22.0323	44.4093	54.1882	55.7000	55.7158	**55.7159**
		100	0.5702	0.6219	2.5265	7.5881	21.5676	44.3669	54.1874	55.7000	55.7158	**55.7159**
		1000	0.0570	0.2556	2.4643	7.5694	21.5630	44.3665	54.1874	55.7000	55.7158	**55.7159**
		→∞	0	0.2492	2.4637	7.5692	21.5629	44.3665	54.1874	55.7000	55.7158	**55.7159**
$\eta = \frac{a}{b}$	Mode sequence	No. of Layers (n)	$\overline{\omega} = \omega a^2\sqrt{\rho_\ell h_{\mathrm{Tot}}/D_\infty}$ $\overline{k}\to 0$	$\overline{k}=10^{-4}$	$\overline{k}=10^{-2}$	$\overline{k}=10^{-1}$	$\overline{k}=1.0$	$\overline{k}=10$	$\overline{k}=10^{2}$	$\overline{k}=10^{4}$	$\overline{k}=10^{6}$	$\overline{k}\to\infty$
0.4	1st(mode: 1,1) 	1	**11.3945**	**11.3945**	**11.3945**	**11.3945**	**11.3945**	**11.3945**	**11.3945**	**11.3945**	**11.3945**	**11.3945**
		2	5.7176	5.7181	5.7715	6.2091	8.4104	10.8079	11.3294	11.3939	11.3945	**11.3945**
		5	2.2893	2.2915	2.4962	3.7933	7.7346	10.7541	11.3250	11.3938	11.3945	**11.3945**
		10	1.1448	1.1497	1.5547	3.3549	7.6618	10.7512	11.3248	11.3938	11.3945	**11.3945**
		100	0.1145	0.1596	1.0917	3.2065	7.6397	10.7505	11.3248	11.3938	11.3945	**11.3945**
		1000	0.0114	0.1121	1.0862	3.2050	7.6395	10.7505	11.3248	11.3938	11.3945	**11.3945**
		→∞	0	0.1115	1.0861	3.2050	7.6395	10.7505	11.3248	11.3938	11.3945	**11.3945**
	2nd(mode: 1,2) 	1	**16.0781**	**16.0781**	**16.0781**	**16.0781**	**16.0781**	**16.0781**	**16.0781**	**16.0781**	**16.0781**	**16.0781**
		2	8.0795	8.0800	8.1335	8.5852	11.2209	14.9658	15.9498	16.0768	16.0781	**16.0781**
		5	3.2364	3.2385	3.4464	4.8706	9.9504	14.8528	15.9410	16.0767	16.0781	**16.0781**
		10	1.6185	1.6234	2.0473	4.1359	9.8025	14.8459	15.9407	16.0767	16.0781	**16.0781**
		100	0.1619	0.2090	1.3069	3.8787	9.7571	14.8442	15.9407	16.0767	16.0781	**16.0781**
		1000	0.0162	0.1336	1.2977	3.8761	9.7567	14.8442	15.9407	16.0767	16.0781	**16.0781**
		→∞	0	0.1326	1.2976	3.8760	9.7567	14.8442	15.9407	16.0767	16.0781	**16.0781**
	3rd(mode: 1,3) 	1	**23.8438**	**23.8438**	**23.8438**	**23.8438**	**23.8438**	**23.8438**	**23.8438**	**23.8438**	**23.8438**	**23.8438**
		2	12.0108	12.0114	12.0650	12.5282	15.6372	21.5757	23.5666	23.8409	23.8437	**23.8438**
		5	4.8144	4.8166	5.0270	6.5791	13.1318	21.3110	23.5469	23.8407	23.8437	**23.8438**
		10	2.4079	2.4128	2.8540	5.2842	12.8143	21.2924	23.5463	23.8407	23.8437	**23.8438**
		100	0.2408	0.2898	1.6069	4.8073	12.7153	21.2875	23.5462	23.8407	23.8437	**23.8438**
		1000	0.0241	0.1636	1.5900	4.8024	12.7143	21.2875	23.5462	23.8407	23.8437	**23.8438**
		→∞	0	0.1618	1.5898	4.8024	12.7143	21.2875	23.5462	23.8407	23.8437	**23.8438**
	4th(mode: 1,4) 	1	**34.6324**	**34.6324**	**34.6324**	**34.6324**	**34.6324**	**34.6324**	**34.6324**	**34.6324**	**34.6324**	**34.6324**
		2	17.5040	17.5045	17.5582	18.0290	21.5371	30.2850	34.0615	34.6265	34.6324	**34.6324**
		5	7.0230	7.0252	7.2373	8.8907	16.9649	29.6945	34.0195	34.6261	34.6324	**34.6324**
		10	3.5131	3.5180	3.9717	6.7249	16.3352	29.6479	34.0180	34.6261	34.6324	**34.6324**
		100	0.3514	0.4018	1.9573	5.8793	16.1361	29.6349	34.0177	34.6261	34.6324	**34.6324**
		1000	0.0351	0.1987	1.9273	5.8705	16.1341	29.6348	34.0177	34.6261	34.6324	**34.6324**
		→∞	0	0.1956	1.9270	5.8704	16.1341	29.6348	34.0177	34.6261	34.6324	**34.6324**
	5th(mode: 2,1) 	1	**40.3727**	**40.3727**	**40.3727**	**40.3727**	**40.3727**	**40.3727**	**40.3727**	**40.3727**	**40.3727**	**40.3727**
		2	20.4415	20.4421	20.4957	20.9689	24.6232	34.7379	39.6065	40.3647	40.3726	**40.3727**
		5	8.2059	8.2081	8.4207	10.1099	18.8330	33.9196	39.5491	40.3642	40.3726	**40.3727**
		10	4.1051	4.1100	4.5679	7.4507	18.0068	33.8519	39.5469	40.3642	40.3726	**40.3727**
		100	0.4106	0.4615	2.1240	6.3841	17.7439	33.8327	39.5465	40.3642	40.3726	**40.3727**
		1000	0.0411	0.2154	2.0861	6.3728	17.7413	33.8325	39.5465	40.3642	40.3726	**40.3727**
		→∞	0	0.2114	2.0857	6.3727	17.7413	33.8325	39.5465	40.3642	40.3726	**40.3727**

the LPCPT in which the interlayer interaction modulus approaches infinity, and the influence of the rotary inertia is excluded, the predicted dimensionless frequencies show excellent agreement with those reported in [102] based on the classical laminated plate theory (CLPT). As expected, the natural frequencies of the laminated plate decrease with a decrease in the interlayer interaction modulus. Moreover, the influence of the rotary inertia becomes more pronounced as the interlayer interaction modulus increases. It can be deduced that there is a "partial rotary inertia" effect arising from the in-plane translational-inertia contributions of all the layers when the shear interaction at the interfaces is not perfect. It is also evident from Table 6 that the additional flexibility in the displacements of a laminate associated with the rotary motions in the vibration reduces the natural frequencies of the laminates.

The results of Table 6 reveal that not only variations of orthotropic material properties of constituting layers, but also the extent of shear interaction at the interfaces of a laminate can significantly affect the vibration mode sequence, leading to vibration mode shifting. To gain a clearer understanding and insight into these effects and how the interlayer slip modulus influences the vibration mode sequences, the shifts in the modes due to variations in the interlayer shear interaction modulus are exhibited via upward and downward arrows relative to the perfectly bonded (full-composite) case. Each arrow indicates one instance of mode shifting compared with an identical laminate case but with the corresponding idealised case based on the classical laminated theory (CLPT). For instance, two arrows next to a frequency signifies that the associated vibration mode has shifted twice as a result of the specified level of interlayer interaction.

5. Conclusions

This paper has introduced a new class of layered plate theory that incorporates the effects of partial-interaction imperfection at the constituting layers' interfaces. The proposed Laminated Partial-Composite Plate Theory (LPCPT), as an extension of the simplest classical laminated plate theory (CLPT), includes the interlayer interaction effects in the form of out-of-plane shear stresses based on a shear spring model in terms of the relative displacements/slips at the interfaces. Exact analytical solution schemes were introduced for the free vibrations and buckling of laminated partial composite plates with identical orthotropic layers under different compressive in-plane loading, to show the merit and reliability of the proposed LPCPT. The introduced analytical solutions were shown to be general and flexible with regard to

Table 6

Dimensionless frequencies ($\overline{\omega} = \omega(b^2/\pi^2)\sqrt{\rho h_{\mathrm{Tot}}/D_{22}^{(\infty)}}$) of cross-ply laminated partial-composite plates with stacking sequence (0/90/90/0) for different levels of the interlayer partial interaction modulus. Each ply is orthotropic with two different modulus ratios: $E_{\|}/E_{\perp} = 10$ and 20 ($G_{12} = 0.5E_{\perp}$ and $\nu_{12} = 0.25$). All plies are of equal thickness, with a total thickness-to-length ratio $\overline{h}_{\mathrm{Tot}} = 0.1$. The frequency results accounting for the rotary inertia effects (arising from the in-plane translational-inertia contributions of each layer) are presented in comparison with those obtained when those effects are neglected. The number of half-waves along the two planar directions for each vibration mode is provided. Mode shifting due to the changes in the interlayer interaction level is indicated for each case with arrows, with reference to the perfectly bonded (full-composite) cases.

$(E_{\|}/E_{\perp})^{*}$	Mode sequence	Rotary Inertia Effects	$\overline{\omega} = (\omega a^2/h_{\mathrm{Tot}})\sqrt{\rho_{\ell}/E_{\perp}^{*}}$										
			$\overline{k}\to 0$	$\overline{k} = 10^{-4}$	$\overline{k} = 10^{-2}$	$\overline{k} = 10^{-1}$	$\overline{k} = 1.0$	$\overline{k} = 10$	$\overline{k} = 10^{2}$	$\overline{k} = 10^{4}$	$\overline{k} = 10^{6}$	$\overline{k}\to\infty$	CLPT† [102]
10	1st	Included	0.6295^{11}	0.6295^{11}	0.6312^{11}	0.6461^{11}	0.7701^{11}	1.3325^{11}	2.1732^{11}	2.4947^{11}	2.4988^{11}	2.4989^{11}	–
		Neglected	0.6298^{11}	0.6299^{11}	0.6315^{11}	0.6464^{11}	0.7706^{11}	1.3347^{11}	2.1849^{11}	2.5150^{11}	2.5193^{11}	2.5193^{11}	2.519^{11}
	2nd	Included	1.7421^{12}	1.7421^{12}	$1.7436^{21}\uparrow\uparrow$	$1.7572^{21}\uparrow\uparrow$	$1.8858^{21}\uparrow\uparrow$	$2.7727^{21}\uparrow\uparrow$	4.4374^{12}	4.8810^{12}	4.8863^{12}	4.8864^{12}	–
		Neglected	1.7443^{12}	1.7443^{12}	$1.7458^{21}\uparrow\uparrow$	$1.7595^{21}\uparrow\uparrow$	$1.8883^{21}\uparrow\uparrow$	$2.7780^{21}\uparrow\uparrow$	4.5018^{12}	4.9799^{12}	4.9858^{12}	4.9859^{12}	4.986^{12}
	3rd	Included	$1.7421^{21}\uparrow$	$1.7421^{21}\uparrow$	$1.7451^{12}\downarrow$	$1.7721^{12}\downarrow$	$2.0022^{12}\downarrow$	$3.0503^{12}\downarrow$	$5.5430^{21}\uparrow$	$8.2896^{21}\uparrow$	$8.3446^{21}\uparrow$	9.4041^{13}	–
		Neglected	$1.7443^{21}\uparrow$	$1.7443^{21}\uparrow$	$1.7474^{12}\downarrow$	$1.7743^{12}\downarrow$	$2.0051^{12}\downarrow$	$3.0636^{12}\downarrow$	$5.5773^{21}\uparrow$	$8.4544^{21}\uparrow$	$8.5144^{21}\uparrow$	9.7832^{13}	9.783^{13}
	4th	Included	$2.5142^{22}\uparrow$	$2.5142^{22}\uparrow$	$2.5175^{22}\uparrow$	$2.5476^{22}\uparrow$	$2.8192^{22}\uparrow$	$4.3776^{22}\uparrow$	$7.7536^{22}\uparrow$	$9.3912^{13}\downarrow$	$9.4040^{13}\downarrow$	8.3452^{21}	–
		Neglected	$2.5193^{22}\uparrow$	$2.5194^{22}\uparrow$	$2.5227^{22}\uparrow$	$2.5528^{22}\uparrow$	$2.8252^{22}\uparrow$	$4.3967^{22}\uparrow$	$7.8810^{22}\uparrow$	$9.7679^{13}\downarrow$	$9.7831^{13}\downarrow$	8.5150^{21}	8.515^{21}
	5th	Included	$3.7218^{13}\downarrow\downarrow$	$3.7219^{13}\downarrow\downarrow$	$3.7261^{13}\downarrow\downarrow$	$3.7640^{13}\downarrow\downarrow$	$4.1000^{13}\downarrow\downarrow$	$5.7923^{13}\downarrow\downarrow$	$8.3921^{13}\downarrow\downarrow$	9.7311^{22}	9.7610^{22}	9.7613^{22}	–
		Neglected	$3.7314^{13}\downarrow\downarrow$	$3.7314^{13}\downarrow\downarrow$	$7.7357^{13}\downarrow\downarrow$	$3.7737^{13}\downarrow\downarrow$	$4.1112^{13}\downarrow\downarrow$	$5.8361^{13}\downarrow\downarrow$	$8.6193^{13}\downarrow\downarrow$	10.0429^{22}	10.0770^{22}	10.077^{22}	10.077^{22}
20	1st	Included	0.6593^{11}	0.6593^{11}	0.6603^{11}	0.6693^{11}	0.7478^{11}	1.1669^{11}	2.0698^{11}	2.6086^{11}	2.6169^{11}	2.6170^{11}	–
		Neglected	0.6596^{11}	0.6596^{11}	0.6606^{11}	0.6696^{11}	0.7482^{11}	1.1687^{11}	2.0792^{11}	2.6297^{11}	2.6383^{11}	2.6384^{11}	2.638^{11}
	2nd	Included	1.8658^{12}	$1.8658^{21}\uparrow$	$1.8667^{21}\uparrow$	$1.8748^{21}\uparrow$	$1.9522^{21}\uparrow$	$2.5472^{21}\uparrow$	4.1460^{12}	4.8098^{12}	4.8189^{12}	4.8190^{12}	–
		Neglected	1.8682^{12}	$1.8682^{21}\uparrow$	$1.8691^{21}\uparrow$	$1.8772^{21}\uparrow$	$1.9548^{21}\uparrow$	$2.5519^{21}\uparrow$	4.1996^{12}	4.9071^{12}	4.9170^{12}	4.9171^{12}	4.917^{12}
	4th	Included	1.8658^{21}	$1.8659^{12}\downarrow$	$1.8676^{12}\downarrow$	$1.8836^{12}\downarrow$	$2.0240^{12}\downarrow$	$2.7546^{12}\downarrow$	4.9864^{21}	9.0482^{21}	9.1669^{21}	9.1681^{21}	–
		Neglected	1.8682^{21}	$1.8682^{12}\downarrow$	$1.8700^{12}\downarrow$	$1.8860^{12}\downarrow$	$2.0269^{12}\downarrow$	$2.7660^{12}\downarrow$	5.0101^{21}	9.2244^{21}	9.3534^{21}	9.3547^{21}	9.354^{21}
	3rd	Included	$2.6330^{22}\uparrow$	$2.6330^{22}\uparrow$	$2.6350^{22}\uparrow$	$2.6532^{22}\uparrow$	$2.8214^{22}\uparrow$	$3.9051^{22}\uparrow$	$7.1083^{22}\uparrow$	9.2407^{13}	9.2634^{13}	9.2636^{13}	–
		Neglected	$2.6384^{22}\uparrow$	$2.6384^{22}\uparrow$	$2.6404^{22}\uparrow$	$2.6586^{22}\uparrow$	$2.8275^{22}\uparrow$	$3.9217^{22}\uparrow$	$7.2046^{22}\uparrow$	9.6104^{13}	9.6368^{13}	9.6370^{13}	9.637^{13}
	5th	Included	$4.0344^{13}\downarrow$	$4.0344^{13}\downarrow$	$4.0369^{13}\downarrow$	$4.0590^{13}\downarrow$	$4.2594^{13}\downarrow$	$5.3754^{13}\downarrow$	$7.7718^{13}\downarrow$	10.162^{22}	10.2220^{22}	10.223^{22}	–
		Neglected	$4.0448^{13}\downarrow$	$4.0448^{13}\downarrow$	$4.0473^{13}\downarrow$	$4.0695^{13}\downarrow$	$4.2711^{13}\downarrow$	$5.4148^{13}\downarrow$	$7.9599^{13}\downarrow$	10.485^{22}	10.5529^{22}	10.554^{22}	10.554^{22}

*$E_{\|}$ and $E_{\perp}$ are the on-axis and off-axis moduli of elasticity, respectively.
†Classical Laminated Plate Theory (CLPT).

the number of constituting layers, unlike any other studies in the literature. Laminated plates with non-identical layers were also treated via direct analytical solution alternatives for laminated plates with a specified number of constituent layers based on the proposed LPCPT. It was shown that, for a special case of the present LPCP mode, there is an excellent agreement between the predicted critical buckling loads, as well as the predicted vibration frequencies, and those reported in the literature for thick plates based on both the three-dimensional elasticity and Reddy's higher-order shear deformation theory (HSDT). It was demonstrated how the critical buckling loads and the natural vibration frequencies are degraded from those predicted based on classical plate theory with perfect-bonding ideal assumptions, considering different extents of interlayer partial interaction. It was concluded that the influence of the interlayer interaction parameter on the critical buckling loads and the natural vibration frequencies is more pronounced when the number of constituting layers increases. It was also concluded that not only variations of orthotropic material properties of constituent layers, but also the extent of shear interaction at the interfaces of a laminate can significantly affect the vibration mode sequence, leading to vibration mode shifting.

The introduced Laminated Partial-Composite Plate Theory (LPCPT) provides a foundational framework for a potential series of refined extensions based on different shear-deformable kinematic models (ranging from Mindlin-Reissner to higher-order models) for internal transverse shear deformations at each layer. Moreover, the LPCPT may provide a framework for future developments of laminated partial-composite shell theories based on different kinematic models. The class of LPCPT and its extensions may also be employed for other types of constituent materials (e.g., functionally-graded materials (FGMs)), different boundary conditions and loading scenarios, and applied to a wide variety of static and dynamic problems in the future.

CRediT authorship contribution statement

S.R. Atashipour: Writing – review & editing, Writing – original draft, Visualization, Validation, Supervision, Software, Resources, Project administration, Methodology, Investigation, Funding acquisition, Formal analysis, Data curation, Conceptualization. **N. Challamel:** Writing – review & editing, Project administration, Methodology, Investigation, Funding acquisition, Conceptualization. **P.D. Folkow:** Writing – review & editing, Project administration, Methodology, Investigation, Funding acquisition, Conceptualization. **U.A. Girhammar:** Writing – review & editing, Project administration, Methodology, Investigation, Funding acquisition, Conceptualization.

Declaration of competing interest

The authors declare that they have no known competing financial interests or personal relationships that could have appeared to influence the work reported in this paper.

Appendix A

Details on the proposed solution (29) for the displacement components for the buckling of laminated composite plates based on the established LPCP model are presented here.

To exactly satisfy the boundary conditions (28a),b) with regard to the applied compressive edge load terms, while having it mathematically possible to fulfil the set of governing equations (21a)-g), the first few terms of a truncated polynomial series with unknown coefficients may be superimposed to the standard Navier-type solution. We examine a possible solution where the highest order of the mentioned truncated polynomial series is lower than the highest order of the partial derivatives of the in-plane displacement components (i.e., 2nd order), as follows

$$\begin{cases} u_{0,i} = C_{0,i}^{(u)} + C_{1,i}^{(u)} x + U_{0,i}\cos(\alpha_{m1}x)\sin(\beta_{m2}y), & i \in \{1,2,...,n\} \\ v_{0,i} = C_{0,i}^{(v)} + C_{1,i}^{(v)} y + V_{0,i}\sin(\alpha_{m1}x)\cos(\beta_{m2}y), & i \in \{1,2,...,n\} \\ w = W_0 \sin(\alpha_{m1}x)\sin(\beta_{m2}y) \end{cases} \tag{A-1}$$

where $C_{0,i}^{(u)}$, $C_{1,i}^{(u)}$, $C_{0,i}^{(v)}$, and $C_{1,i}^{(v)}$ are some unknown coefficients to be determined. It can be demonstrated that all terms related to the considered truncated polynomials vanish upon substitution of Eq. (A-1) into the set of governing equations (21a)-g) under the assumption of identical constituting layers of a laminate. Using the definition of the stress resultants by Eqs. (18) and (19), and the in-plane load distribution assumption (32a,b), the boundary conditions (28a),b) can be rewritten as,at $x = 0, a$:

$$\begin{cases} w = 0 \\ \partial^2 w/\partial x^2 = 0 \end{cases}$$

$$\begin{cases} A_{11,i}\dfrac{\partial u_{0,i}}{\partial x} + A_{12,i}\dfrac{\partial v_{0,i}}{\partial y} = -\widehat{N}_{x,i}, & i \in \{1,2,...,n\} \\ v_{0,i} = 0, & i \in \{1,2,...,n\} \end{cases}$$

and at y $= 0, b$:

$$\begin{cases} w = 0 \\ \partial^2 w/\partial y^2 = 0 \end{cases}$$

$$\begin{cases} A_{12,i}\dfrac{\partial u_{0,i}}{\partial x} + A_{22,i}\dfrac{\partial v_{0,i}}{\partial y} = -\widehat{N}_{y,i}, & i \in \{1,2,...,n\} \\ u_{0,i} = 0, & i \in \{1,2,...,n\} \end{cases}$$

The displacement components expressed by Eq. (A-1) inherently satisfy the boundary conditions defined by Eqs. (A-2a) and (A-3a). Upon substituting Eq. (A-1) into the first of the boundary equations (A-2b) and (A-3b), it follows that these conditions hold if:

$$\begin{aligned} A_{11,i}C_{1,i}^{(u)} + A_{12,i}C_{1,i}^{(v)} &= -\widehat{N}_{x,i} \\ A_{12,i}C_{1,i}^{(u)} + A_{22,i}C_{1,i}^{(v)} &= -\widehat{N}_{y,i} \end{aligned} \tag{A-4}$$

Solving the above set of algebraic equations and replacing the definition of the axial stiffnesses $A_{rs,i}$ ($r,s \in \{1,2\}$) from Eq. (12) yields:

$$C_{1,i}^{(u)} = \frac{A_{12,\ell}\widehat{N}_{y,i} - A_{22,\ell}\widehat{N}_{x,i}}{A_{11,\ell}A_{22,\ell} - A_{12,\ell}^2} = -\frac{1}{E_{x,i}h_i}\left(\widehat{N}_{x,i} - \nu_{xy,i}\widehat{N}_{y,i}\right)$$
$$C_{1,i}^{(v)} = \frac{A_{12,\ell}\widehat{N}_{x,i} - A_{11,\ell}\widehat{N}_{y,i}}{A_{11,\ell}A_{22,\ell} - A_{12,\ell}^2} = -\frac{1}{E_{y,i}h_i}\left(\widehat{N}_{y,i} - \nu_{yx,i}\widehat{N}_{x,i}\right) \tag{A-5}$$

For a plate subjected to axial compressive loading on a pair of parallel edges, the displacement conditions by the second of Eqs. (A-2b) and (A-3b) will be fulfilled at the middle of the plates' loaded parallel edges; i.e.,

$$\text{at } x = a/2 : \{u_{0,i} = 0, \quad i \in \{1,2,...,n\} \tag{A-6a}$$

$$\text{at } y = b/2 : \{v_{0,i} = 0, \quad i \in \{1,2,...,n\} \tag{A-6b}$$

Applying the conditions (A-6a,b) using Eqs. (A-1) and (A-5), the remaining unknown coefficients are determined as follows,

$$C_{0,i}^{(u)} = -C_{1,i}^{(u)}a/2$$
$$C_{0,i}^{(v)} = -C_{1,i}^{(v)}b/2 \tag{A-7}$$

and consequently,

$$\begin{cases} u_{0,i} = \dfrac{1}{E_{x,\ell}h_\ell}\left(\widehat{N}_{x,i} - \nu_{xy,\ell}\widehat{N}_{y,i}\right)(a/2 - x) + U_{0,i}\cos(\alpha_{m1}x)\sin(\beta_{m2}y), & i \in \{1,2,...,n\} \\ v_{0,i} = \dfrac{1}{E_{y,\ell}h_\ell}\left(\widehat{N}_{y,i} - \nu_{yx,\ell}\widehat{N}_{x,i}\right)(b/2 - y) + V_{0,i}\sin(\alpha_{m1}x)\cos(\beta_{m2}y), & i \in \{1,2,...,n\} \\ w = W_0\sin(\alpha_{m1}x)\sin(\beta_{m2}y) \end{cases} \tag{A-8}$$

Appendix B

Details on the solution for the set of difference equations (31a),b) are presented here. We apply a change of variable for the coefficients of the set of in-plane displacement components $U_{0,i}$ and $V_{0,i}$, $i \in \{1,2,...,N\}$ in Eqs. (31a),b) in the form:

$$\begin{cases} U_{0,i} = c_u\lambda^i, \\ V_{0,i} = c_v\lambda^i, \end{cases} \quad i \in \{1,2,...,N\} \tag{B-1}$$

Substituting Eq. (B-1) into the set of difference Eqs. (31a),b), they can be expressed as

$$\begin{bmatrix} \lambda^2 - \left(c_{11,\ell}^{m12}/k + 2\right)\lambda + 1 & -\left(c_{12,\ell}^{m12}/k\right)\lambda \\ -\left(c_{12,\ell}^{m12}/k\right)\lambda & \lambda^2 - \left(c_{22,\ell}^{m12}/k + 2\right)\lambda + 1 \end{bmatrix} \begin{Bmatrix} c_u \\ c_v \end{Bmatrix} = \begin{Bmatrix} 0 \\ 0 \end{Bmatrix} \tag{B-2}$$

in which

$$c_{11,\ell}^{m12} = \alpha_{m1}^2 A_{11,\ell} + \beta_{m2}^2 A_{66,\ell}$$
$$c_{22,\ell}^{m12} = \alpha_{m1}^2 A_{66,\ell} + \beta_{m2}^2 A_{22,\ell}$$
$$c_{12,\ell}^{m12} = \alpha_{m1}\beta_{m2}(A_{12,\ell} + A_{66,\ell}) \tag{B-3}$$

The unknown parameter λ in Eqs. (B-1) can be determined as roots of a characteristic equations, obtained from applying a non-trivial solution to Eq. (B-2). Consequently, the characteristic equation can be expressed as

$$\lambda^4 - \frac{1}{k}\left(c_{11,\ell}^{m12} + c_{22,\ell}^{m12} + 4k\right)\lambda^3 + \frac{1}{k^2}\left[c_{11,\ell}^{m12}c_{22,\ell}^{m12} + 2k\left(c_{11,\ell}^{m12} + c_{22,\ell}^{m12}\right) - \left(c_{12,\ell}^{m12}\right)^2 + 4k^2\right]\lambda^2 - \frac{1}{k}\left(c_{11,\ell}^{m12} + c_{22,\ell}^{m12} + 4k\right)\lambda + 1 = 0 \tag{B-4}$$

The polynomial Eq. (B-4), upon factorization, may be represented in the following form

$$\left(\lambda^2 - 2\Upsilon_1\lambda + 1\right)\left(\lambda^2 - 2\Upsilon_2\lambda + 1\right) = 0 \tag{B-5}$$

where

$$\begin{Bmatrix} \Upsilon_1 \\ \Upsilon_2 \end{Bmatrix} = 1 + \frac{1}{4k}\left(c_{11,\ell}^{m12} + c_{22,\ell}^{m12} \mp \sqrt{\left(c_{11,\ell}^{m12} - c_{22,\ell}^{m12}\right)^2 + 4\left(c_{12,\ell}^{m12}\right)^2}\right) \tag{B-6}$$

Assuming any of the Υ coefficients in Eq. (B-5) in a change of variables to be equivalent to $\cosh\theta$, the following polynomial equation can be deduced:

$$\lambda^2 - 2(\cosh\theta)\lambda + 1 = 0 \tag{B-7}$$

which yields

$$\lambda_{1,2} = \cosh\theta \pm \sqrt{\cosh^2\theta - 1} = \cosh\theta \pm \sinh\theta \tag{B-8}$$

Substituting Eq. (B-8) into Eq. (B-1) yields

$$\begin{cases} U_{0,i} = c_{1U}\mathrm{e}^{i\theta} + c_{2U}\lambda^{-i\theta}, \\ V_{0,i} = c_{1V}\mathrm{e}^{i\theta} + c_{1V}\lambda^{-i\theta}, \qquad i \in \{1, 2, ..., N\} \end{cases} \tag{B-9}$$

or equivalently:

$$\begin{cases} U_{0,i} = \chi_{1U}\cosh i\theta + \chi_{2U}\sinh i\theta, \\ V_{0,i} = \chi_{1V}\cosh i\theta + \chi_{2V}\sinh i\theta, \quad i \in \{1, 2, 3, ..., n\} \end{cases} \tag{B-10}$$

Appendix C

The critical buckling loads of the laminated partial-composite plate are extracted from the following determinant equations:

$$\begin{vmatrix} (c_{11}^{m12}+k)\cosh\theta - k\cosh 2\theta & (c_{11}^{m12}+k)\sinh\theta - k\sinh 2\theta & c_{12}^{m12}\cosh\theta & c_{12}^{m12}\sinh\theta & -\alpha_{m1}h_\ell k \\ c_{12}^{m12}\cosh\theta & c_{12}^{m12}\sinh\theta & (c_{22}^{m12}+k)\cosh\theta - k\cosh 2\theta & (c_{22}^{m12}+k)\sinh\theta - k\sinh 2\theta & -\beta_{m2}h_\ell k \\ (c_{11}^{m12}+k)\cosh n\theta & & & & \\ \quad -k\cosh[(n-1)\theta] & (c_{11}^{m12}+k)\sinh n\theta - k\sinh[(n-1)\theta] & c_{12}^{m12}\cosh n\theta & c_{12}^{m12}\sinh n\theta & \alpha_{m1}h_\ell k \\ c_{12}^{m12}\cosh n\theta & c_{12}^{m12}\sinh n\theta & (c_{22}^{m12}+k)\cosh n\theta - k\cosh[(n-1)\theta] & (c_{22}^{m12}+k)\sinh n\theta - k\sinh[(n-1)\theta] & \beta_{m2}h_\ell k \\ \alpha_{m1}(\cosh n\theta - \cosh\theta) & \alpha_{m1}(\sinh n\theta - \sinh\theta) & \beta_{m2}(\cosh n\theta - \cosh\theta) & \beta_{m2}(\sinh n\theta - \sinh\theta) & c_{33}^{m12} - \dfrac{\alpha_{m1}^2\xi_1 + \beta_{m2}^2\xi_2}{h_\ell k}\widehat{N}_{cr} \end{vmatrix} = 0 \tag{C-1}$$

in which ξ_1 and ξ_2 are the critical load coefficients, applied in x- and y-directions, respectively, corresponding to bi-directional compressive edge loads; i.e.,

$$\begin{aligned} \widehat{N}_{x,Tot.} &= \xi_1\widehat{N}_{cr} \\ \widehat{N}_{y,Tot.} &= \xi_2\widehat{N}_{cr} \end{aligned} \tag{C-2}$$

Obviously, for a mono-axial load case, it is set $\xi_1 = 0$ or $\xi_2 = 0$. Also, the coefficient c_{33mn} in Eq. (C-1) is defined as

$$c_{33} = \frac{1}{h_\ell k}\left[\alpha_{m1}^4 D_{11}^{(0)} + 2\alpha_{m1}^2\beta_{m2}^2(D_{12}^{(0)} + 2D_{66}^{(0)}) + \beta_{m2}^4 D_{22}^{(0)}\right] + (n-1)\gamma_{m12}^2 h_\ell \tag{C-3}$$

Appendix D

The systems of equations for simply-supported laminated orthotropic plates composed of n non-identical layers are expressed as follows,

– For the buckling of laminated partial composite plates:

$$(\alpha_{m1}^2 A_{11,1} + \beta_{m2}^2 A_{66,1} + k)U_{0,1} - kU_{0,2} + \alpha_{m1}\beta_{m2}(A_{12,1} + A_{66,1})V_{0,1} - \alpha_{m1}hkW = 0$$

$$\alpha_{m1}\beta_{m2}(A_{12,1} + A_{66,1})U_{0,1} + (\alpha_{m1}^2 A_{66,1} + \beta_{m2}^2 A_{22,1} + k)V_{0,1} - kV_{0,2} - \beta_{m2}hkW = 0$$

$$\begin{cases} -kU_{0,i-1} + (\alpha_{m1}^2 A_{11,i} + \beta_{m2}^2 A_{66,i} + 2k)U_{0,i} - kU_{0,i+1} + \alpha_{m1}\beta_{m2}(A_{12,i} + A_{66,i})V_{0,i} = 0, \\ (i = 2, 3, ..., n-1) \end{cases}$$

$$\begin{cases} \alpha_{m1}\beta_{m2}(A_{12,i} + A_{66,i})U_{0,i} - kV_{0,i-1} + (\alpha_{m1}^2 A_{66,i} + \beta_{m2}^2 A_{22,i} + 2k)V_{0,i} - kV_{0,i+1} = 0, \\ (i = 2, 3, ..., n-1) \end{cases}$$

$$-kU_{0,n-1} + (\alpha_{m1}^2 A_{11,n} + \beta_{m2}^2 A_{66,n} + k)U_{0,n} + \alpha_{m1}\beta_{m2}(A_{12,n} + A_{66,n})V_{0,n} + \alpha_{m1}hkW = 0$$

$$\alpha_{m1}\beta_{m2}(A_{12,n} + A_{66,n})U_{0,n} - kV_{0,n-1} + (\alpha_{m1}^2 A_{66,n} + \beta_{m2}^2 A_{22,n} + k)V_{0,n} + \beta_{m2}hkW = 0$$

$$\left[\alpha_{m1}^4 D_{11}^{(0)} + 2\alpha_{m1}^2\beta_{m2}^2(D_{12}^{(0)} + 2D_{66}^{(0)}) + \beta_{m2}^4 D_{22}^{(0)} + (n-1)(\alpha_{m1}^2 + \beta_{m2}^2)h^2k + (\alpha_{m1}^2\xi_1 + \beta_{m2}^2\xi_2)\widehat{N}_{cr}\right]W$$
$$+\alpha_{m1}hk\left(U_{0,n} - U_{0,1}\right) + \beta_{m2}hk\left(V_{0,n} - V_{0,1}\right) = 0$$

– For the vibration of laminated partial composite plates:

$$\left(\alpha_{m1}^2 A_{11,1} + \beta_{m2}^2 A_{66,1} + k - \omega^2 I_{0,1}\right)\widetilde{U}_{0,1m_1m_2} - k\widetilde{U}_{0,2m_1m_2} + \alpha_{m1}\beta_{m2}(A_{12,1} + A_{66,1})\widetilde{V}_{0,1m_1m_2} - \alpha_{m1}hk\widetilde{W}_{0,m_1m_2} = 0$$

$$\alpha_{m1}\beta_{m2}(A_{12,1} + A_{66,1})\widetilde{U}_{0,1m_1m_2} + (\alpha_{m1}^2 A_{66,1} + \beta_{m2}^2 A_{22,1} + k - \omega^2 I_{0,1})\widetilde{V}_{0,1m_1m_2} - k\widetilde{V}_{0,2m_1m_2} - \beta_{m2}hk\widetilde{W}_{0,m_1m_2} = 0$$

$$\begin{cases} -k\widetilde{U}_{0,(i-1)m_1m_2} + (\alpha_{m1}^2 A_{11,i} + \beta_{m2}^2 A_{66,i} + 2k - \omega^2 I_{0,i})\widetilde{U}_{0,im_1m_2} - k\widetilde{U}_{0,(i+1)m_1m_2} + \alpha_{m1}\beta_{m2}(A_{12,i} + A_{66,i})\widetilde{V}_{0,im_1m_2} = 0, \\ (i = 2, 3, \ldots, n-1) \end{cases}$$

$$\begin{cases} \alpha_{m1}\beta_{m2}(A_{12,i} + A_{66,i})\widetilde{U}_{0,im_1m_2} - k\widetilde{V}_{0,(i-1)m_1m_2} + (\alpha_{m1}^2 A_{66,i} + \beta_{m2}^2 A_{22,i} + 2k - \omega^2 I_{0,i})\widetilde{V}_{0,im_1m_2} - k\widetilde{V}_{0,(i+1)m_1m_2} = 0, \\ (i = 2, 3, \ldots, n-1) \end{cases}$$

$$-k\widetilde{U}_{0,(n-1)m_1m_2} + (\alpha_{m1}^2 A_{11,n} + \beta_{m2}^2 A_{66,n} + k - \omega^2 I_{0,n})\widetilde{U}_{0,nm_1m_2} + \alpha_{m1}\beta_{m2}(A_{12,n} + A_{66,n})\widetilde{V}_{0,nm_1m_2} + \alpha_{m1}hk\widetilde{W}_{0,m_1m_2} = 0$$

$$\alpha_{m1}\beta_{m2}(A_{12,n} + A_{66,n})\widetilde{U}_{0,nm_1m_2} - k\widetilde{V}_{0,(n-1)m_1m_2} + (\alpha_{m1}^2 A_{66,n} + \beta_{m2}^2 A_{22,n} + k - \omega^2 I_{0,n})\widetilde{V}_{0,nm_1m_2} + \beta_{m2}hk\widetilde{W}_{0,m_1m_2} = 0$$

$$\left\{\alpha_{m1}^4 D_{11}^{(0)} + 2\alpha_{m1}^2\beta_{m2}^2(D_{12}^{(0)} + 2D_{66}^{(0)}) + \beta_{m2}^4 D_{22}^{(0)} + (n-1)(\alpha_{m1}^2 + \beta_{m2}^2)h^2k - \omega^2\left[I_0 + (\alpha_{m1}^2 + \beta_{m2}^2)I_{2,0}\right]\right\}\widetilde{W}_{0,m_1m_2}$$
$$+\alpha_{m1}hk\left(\widetilde{U}_{0,nm_1m_2} - \widetilde{U}_{0,1m_1m_2}\right) + \beta_{m2}hk\left(\widetilde{V}_{0,nm_1m_2} - \widetilde{V}_{0,1m_1m_2}\right) = 0$$

Data availability

Data will be made available from the corresponding author on reasonable request.

References

[1] Islami DP, Muzaqih AF, Adiputra R, Prabowo AR, Firdaus N, Ehlers S, et al. Structural design parameters of laminated composites for marine applications: Milestone study and extended review on current technology and engineering. Results Eng 2024;24:103195.

[2] Sutherland L. A review of impact testing on marine composite materials: part IV–scaling, strain rate and marine-type laminates. Compos Struct 2018;200:929–38.

[3] Fiore V, Calabrese L, Scalici T, Valenza A. Evolution of the bearing failure map of pinned flax composite laminates aged in marine environment. Compos B Eng 2020;187:107864.

[4] Kharghani N, Soares CG. Experimental, numerical and analytical study of buckling of rectangular composite laminates. European Journal of Mechanics-A/Solids 2020;79:103869.

[5] Qatu M, Zannon M, Mainuddin G. Application of laminated composite materials in vehicle design: Theories and analyses of composite shells. SAE International Journal of Passenger Cars-Mechanical Systems 2013;6:1347–53.

[6] Vlase S, Gheorghe V, Marin M, Öchsner A. Study of structures made of composite materials used in automotive industry. Proceedings of the Institution of Mechanical Engineers, Part L: Journal of Materials: Design and Applications. 2021;235:2574-87.

[7] Khan F, Hossain N, Mim JJ, Rahman SM, Iqbal MJ, Billah M, et al. Advances of composite materials in automobile applications–a review. Journal of Engineering Research 2024.

[8] Zang J, Chen B, Song X-Y, Zhang Z, Zhang Y-W, Chen L-Q. Vibration of composite laminated airfoil-beam-structures of electric aircraft in hygrothermal environment: Theory formulation and experimental investigation. Compos Struct 2025;354:118781.

[9] van Hoorn N, Turteltaub S, Kassapoglou C, van den Brink W. Numerical prediction of impact damage in thick fabric composite laminates. Compos Struct 2025;353:118726.

[10] Riccio A, Di Caprio F, Tsai S, Russo A, Sellitto A. Optimization of composite aeronautical components by Re-Designing with Double-double Laminates. Aerosp Sci Technol 2024;109304.

[11] Lemos DM, Marques FD, Ferreira AJ. A review on bistable composite laminates for aerospace applications. Compos Struct 2024;329:117756.

[12] Walsh J, Kim H-I, Suhr J. Low velocity impact resistance and energy absorption of environmentally friendly expanded cork core-carbon fiber sandwich composites. Compos A Appl Sci Manuf 2017;101:290–6.

[13] Atashipour S, Al-Emrani M. A realistic model for transverse shear stiffness prediction of composite corrugated-core sandwich elements. Int J Solids Struct 2017;129:1–17.

[14] Yu J, Zhao C, Zhong W, Pan Z, Zhang P. Study on elastic buckling and seismic behavior of two-side connected stiffened shear wall with FRP-laminated steel composite plate. Constr Build Mater 2025;481:141560.

[15] Reissner E, Stavsky Y. Bending and stretching of certain types of heterogeneous aeolotropic elastic plates. J Appl Mech 1961;28:402–8.

[16] Mindlin R. Influence of rotatory inertia and shear on flexural motions of isotropic, elastic plates. J Appl Mech 1951;18:31–8.

[17] Nosier A, Yavari A, Sarkani S. A study of the edge-zone equation of Mindlin-Reissner plate theory in bending of laminated rectangular plates. Acta Mech 2001;146:227–38.

[18] Levinson M. An accurate, simple theory of the statics and dynamics of elastic plates. Mech Res Commun 1980;7:343–50.

[19] Librescu L, Khdeir A. Analysis of symmetric cross-ply laminated elastic plates using a higher-order theory: Part I—Stress and displacement. Compos Struct 1988;9:189–213.

[20] Reddy JN. A simple higher-order theory for laminated composite plates. J Appl Mech 1984;51:745–52.

[21] Touratier M. An efficient standard plate theory. Int J Eng Sci 1991;29:901–16.

[22] Karama M, Afaq K, Mistou S. Mechanical behaviour of laminated composite beam by the new multi-layered laminated composite structures model with transverse shear stress continuity. Int J Solids Struct 2003;40:1525–46.

[23] Mechab I. Etude des structures composites en utilisant les theories d'ordre eleve sous chargement thermomecanique (in French): University of Sidi Bel Abbes, 2009.

[24] Shankara C, Iyengar N. A C0element for the free vibration analysis of laminated composite plates. J Sound Vib 1996;191:721–38.

[25] Nguyen TN, Thai CH, Nguyen-Xuan H. On the general framework of high order shear deformation theories for laminated composite plate structures: a novel unified approach. Int J Mech Sci 2016;110:242–55.

[26] Chen W, Tang Z, Liao Y, Peng L. A six-variable quasi-3D isogeometric approach for free vibration of functionally graded graphene origami-enabled auxetic metamaterial plates submerged in a fluid medium. Appl Math Mech 2025;46:157–76.

[27] Carrera E. Historical review of zig-zag theories for multilayered plates and shells. Appl Mech Rev 2003;56:287–308.

[28] Carrera E, Filippi M, Zappino E. Laminated beam analysis by polynomial, trigonometric, exponential and zig-zag theories. European Journal of Mechanics-A/Solids 2013;41:58–69.

[29] Caliri Jr MF, Ferreira AJ, Tita V. A review on plate and shell theories for laminated and sandwich structures highlighting the Finite Element Method. Compos Struct 2016;156:63–77.

[30] Shu X. A generalised model of laminated composite plates with interfacial damage. Compos Struct 2006;74:237–46.

[31] Abdullah SS, Bokti S, Wong K, Johar M, Chong W, Dong Y. Mode II and mode III delamination of carbon fiber/epoxy composite laminates subjected to a four-point bending mechanism. Compos B Eng 2024;270:111110.

[32] Li S, Liu X, Li R, Su Y. Shear deformation dominates in the soft adhesive layers of the laminated structure of flexible electronics. Int J Solids Struct 2017;110:305–14.

[33] Viet N, Zaki W, Umer R. Interlaminar shear stress function for adhesively bonded multi-layer metal laminates. Int J Adhes Adhes 2018;82:14–20.

[34] Atashipour SR, Challamel N, Girhammar UA, Folkow PD. Flexible N-layer composite beam/column elements with interlayer partial interaction imperfection–a novel approach to structural stability and dynamic analyses. Compos Struct 2025;367:119219.
[35] Cole R, Bateh E, Potter J. Fasteners for composite structures. Composites 1982;13:233–40.
[36] Borba NZ, Kötter B, Fiedler B, dos Santos JF, Amancio-Filho S. Mechanical integrity of friction-riveted joints for aircraft applications. Compos Struct 2020;232:111542.
[37] Liew K, Pan Z, Zhang L. An overview of layerwise theories for composite laminates and structures: Development, numerical implementation and application. Compos Struct 2019;216:240–59.
[38] Duong VA, Diaz AD, Chataigner S, Caron J-F. A layerwise finite element for multilayers with imperfect interfaces. Compos Struct 2011;93:3262–71.
[39] Moreira R, Rodrigues JD. A layerwise model for thin soft core sandwich plates. Comput Struct 2006;84:1256–63.
[40] Kharazi M, Ovesy H, Mooneghi MA. Buckling analysis of delaminated composite plates using a novel layerwise theory. Thin-Walled Struct 2014;74:246–54.
[41] Loja M, Barbosa J, Soares CM. Dynamic behaviour of soft core sandwich beam structures using kriging-based layerwise models. Compos Struct 2015;134:883–94.
[42] Wei L, Shen HJ. A refined layerwise finite element modeling of delaminated composite laminates with piezoelectric layers. Thin-Walled Struct 2018;131:792–804.
[43] Filippi M, Carrera E. Bending and vibrations analyses of laminated beams by using a zig-zag-layer-wise theory. Compos B Eng 2016;98:269–80.
[44] Demasi L. Partially layer wise advanced zig zag and HSDT models based on the generalized unified formulation. Eng Struct 2013;53:63–91.
[45] Eijo A, Oñate E, Oller S. Delamination in laminated plates using the 4-noded quadrilateral QLRZ plate element based on the refined zigzag theory. Compos Struct 2014;108:456–71.
[46] Tafsirojjaman T, Dogar AUR, Liu Y, Manalo A, Thambiratnam DP. Performance and design of steel structures reinforced with FRP composites: a state-of-the-art review. Eng Fail Anal 2022;138:106371.
[47] She G-L, Ding H-X. Nonlinear primary resonance analysis of initially stressed graphene platelet reinforced metal foams doubly curved shells with geometric imperfection. Acta Mech Sin 2023;39:522392.
[48] Li Y-P, She G-L. Nonlinear dynamic response of graphene platelets reinforced cylindrical shells under moving loads considering initial geometric imperfection. Eng Struct 2025;323:119241.
[49] Cetkovic M. Influence of initial geometrical imperfections on thermal stability of laminated composite plates using layerwise finite element. Compos Struct 2022;291:115547.
[50] Gurvich M, Clavette P, Kim S, Zafiris G, Phan N, Rahman A. Effect of Geometrical Imperfections on Structural Integrity of Laminated Composite Structures: Experimental Approach and Characterization. Proceedings of the American Society for Composites, 33rd Technical Conference 2018.
[51] Hilburger MW, Starnes Jr JH. Effects of imperfections of the buckling response of composite shells. Thin-Walled Struct 2004;42:369–97.
[52] Messager T. Buckling of imperfect laminated cylinders under hydrostatic pressure. Compos Struct 2001;53:301–7.
[53] Li Y-W, Elishakoff I, Starnes Jr JH, Bushnell D. Effect of the thickness variation and initial imperfection on buckling of composite cylindrical shells: Asymptotic analysis and numerical results by BOSOR4 and PANDA2. Int J Solids Struct 1997;34:3755–67.
[54] Zhang S, Zhang L, Wang Y, Tao J, Chen X. Effect of ply level thickness uncertainty on reliability of laminated composite panels. J Reinf Plast Compos 2016;35:1387–400.
[55] Wagner HN, Hühne C, Janssen M. Buckling of cylindrical shells under axial compression with loading imperfections: an experimental and numerical campaign on low knockdown factors. Thin-Walled Struct 2020;151:106764.
[56] Arbocz J. The effect of imperfect boundary conditions on the collapse behavior of anisotropic shells. Int J Solids Struct 2000;37:6891–915.
[57] Debski H, Teter A. Effect of load eccentricity on the buckling and post-buckling states of short laminated Z-columns. Compos Struct 2019;210:134–44.
[58] Khayal OMES. Literature review on imperfection of composite laminated plates. Journal of microscopy and ultrastructure 2017;5:119–22.
[59] Tho NC, Cong PH, Zenkour AM, Doan DH, Van Minh P. Finite element modeling of the bending and vibration behavior of three-layer composite plates with a crack in the core layer. Compos Struct 2023;305:116529.
[60] Ladevèze P, Lubineau G, Violeau D. A computational damage micromodel of laminated composites. Int J Fract 2006;137:139–50.
[61] Chen W, Cai J, Ye G. Exact solutions of cross-ply laminates with bonding imperfections. AIAA J 2003;41:2244–50.
[62] Chen W, Ying J, Cai J, Ye G. Benchmark solution of laminated beams with bonding imperfections. AIAA J 2004;42:426–9.
[63] Librescu L, Schmidt R. A general linear theory of laminated composite shells featuring interlaminar bonding imperfections. Int J Solids Struct 2001;38:3355–75.
[64] Ye J, Chen X, Zhai Z, Li B, Zi Y, He Z. Effects of thermal stress and imperfect interfacial bonding on the mechanical behavior of composites subjected to off-axis loading. Mater Sci Eng A 2010;527:7530–7.
[65] Talebitooti R, Daneshjou K, Tarkashvand A. Study of imperfect bonding effects on sound transmission loss through functionally graded laminated sandwich cylindrical shells. Int J Mech Sci 2017;133:469–83.
[66] Diaz AD, Chataigner S, Caron J-F. A layerwise finite element for multilayers with imperfect interfaces. Compos Struct 2011;93:3262–71.
[67] Garg N, Chakladar ND, Prusty BG, Song C, Phillips AW. Modelling of laminated composite plates with weakly bonded interfaces using scaled boundary finite element method. Int J Mech Sci 2020;170:105349.
[68] Zhang D-D, Ren J-J, Gu J, Li L-J, Zhang J-Y, Xiong W-H, et al. Nondestructive testing of bonding defects in multilayered ceramic matrix composites using THz time domain spectroscopy and imaging. Compos Struct 2020;251:112624.
[69] Kapuria S, Dhanesh N. Free edge stresses in composite laminates with imperfect interfaces under extension, bending and twisting loading. Int J Mech Sci 2016;113:148–61.
[70] Li D, Liu Y. Three-dimensional semi-analytical model for the static response and sensitivity analysis of the composite stiffened laminated plate with interfacial imperfections. Compos Struct 2012;94:1943–58.
[71] Feng X, Fan X, Li Y, Zhang H, Zhang L, Gao Y. Static response and free vibration analysis for cubic quasicrystal laminates with imperfect interfaces. European Journal of Mechanics-A/Solids 2021;90:104365.
[72] Yan W, Wang J, Chen W. Cylindrical bending responses of angle-ply piezoelectric laminates with viscoelastic interfaces. App Math Model 2014;38:6018–30.
[73] Wang Z-X, Qiao P, Xu J. Vibration analysis of laminated composite plates with damage using the perturbation method. Compos B Eng 2015;72:160–74.
[74] Atashipour SR, Girhammar UA, Challamel N. Stability analysis of three-layer shear deformable partial composite columns. Int J Solids Struct 2017;106:213–28.
[75] Atashipour SR, Challamel N, Girhammar UA. On buckling of layered composite heavy columns—Effect of interlayer bonding imperfection. Int J Solids Struct 2023;260:112030.
[76] Girhammar UA, Pan DH. Exact static analysis of partially composite beams and beam-columns. Int J Mech Sci 2007;49:239–55.
[77] Li D. Layerwise theories of laminated composite structures and their applications: a review. Arch Comput Meth Eng 2021;28:577–600.
[78] Hoff NJ. Bending and buckling of rectangular sandwich plates. Washington, USA: NACA (National Advisory Committee for Aeronautics), Technical Note TN No. 2225, 1950.
[79] Rzhanitsyn AR. Built-up rods and plates (in Russian). Moscow, Russia, 1986.
[80] Challamel N, Atashipour SR, Girhammar UA, Barroso VS, Andrade A, Boutin C, et al. A historical overview on static and dynamic analyses of sandwich or partially composite beams and plates. Math Mech Solids 2025;30:1608–43.
[81] Andrade ABVS, Providência P, Challamel N. A linear two-dimensional mathematical model for thin two-layer plates with partial shear interaction, with a view towards application to laminated glass. Thin-Walled Struct 2023;182:110255.
[82] Barroso VS, Andrade A, Providência P, Challamel N. A von Kármán-type model for two-layer laminated glass plates, with applications to buckling and free vibration under in-plane edge loads. Compos Struct 2023;322:117287.
[83] Boutin C. High-contrast multi-layered plates – Statics, Dynamics and Buckling, in: “Mechanics of High-Contrast Elastic Solids”, Advanced Structured Materials Springer, 2023.
[84] Shen XWY, Liu Y. Unlocking slip-mediated bending in multilayers: Efficient modeling and solutions with high precision and simplicity. International Journal of Solids Structures 2024;302:112971.
[85] Bolotin VV. On the theory of layered plates. Izv Akad Nauk SSSR Otd Tekh Nauk, Mekh Mashinostr 1963;3:65–72.
[86] Bolotin VV, Novichkov YN. Mechanics of multilayer structures (in Russian). Mashinostroenie, Moscow. 1980;376.
[87] Shaat M, Gao X-L, Li K, Littlefield A. New analytical model for thermomechanical responses of multi-layered structures with imperfect interfaces. Acta Mech 2023;234:5779–818.
[88] Shaat M, Gao X-L, Battentier A, Massué N. New analytical model for multi-layered composite plates with imperfect interfaces under thermomechanical loading. Acta Mech 2024;235:7083–120.
[89] Wu T, Wang G, Wang J, Wang Y, Xu R. Variational principles of laminated plates considering interlayer slip. Compos Struct 2022;281:114937.
[90] Shen X, Wei Y. Interlayer-Slip-Mediated Large Deflection Bending of Multilayer Two-Dimensional Structures: Theory and Application. J Mech Phys Solids 2025.106192.
[91] Bedford A. Hamilton's principle in continuum mechanics. Austin, TX, USA: Springer, 2021.
[92] Challamel N, Girhammar UA. Variationally-based theories for buckling of partial composite beam–columns including shear and axial effects. Eng Struct 2011;33:2297–319.
[93] Atashipour SR, Mohammadi Z, Folkow PD. A direct approach for three-dimensional elasto-static and elasto-dynamic solutions in curvilinear cylindrical coordinates with application to classical cylinder problems. European Journal of Mechanics-A/Solids 2022;95:104646.
[94] Hosseini-Hashemi S, Atashipour SR, Fadaee M. On the buckling analysis of isotropic, transversely isotropic, and laminated rectangular plates via Reddy plate theory: an exact closed-form procedure. Proc Inst Mech Eng C J Mech Eng Sci 2012;226:1210–24.
[95] McCutcheon WJ. Method for predicting the stiffness of wood-joist floor systems with partial composite action: Department of Agriculture, Forest Service, Forest Products Laboratory, 1977.
[96] Godonou P. Design of timber structures, Volume 2: Rules and formulas according to Eurocode 5. 3:2022 ed. Stockholm, Sweden: Swedish Wood, 2022.

[97] Civalek Ö. Three-dimensional vibration, buckling and bending analyses of thick rectangular plates based on discrete singular convolution method. Int J Mech Sci 2007;49:752–65.
[98] Reddy J, Phan N. Stability and vibration of isotropic, orthotropic and laminated plates according to a higher-order shear deformation theory. J Sound Vib 1985; 98:157–70.
[99] Srinivas S, Rao CJ, Rao A. An exact analysis for vibration of simply-supported homogeneous and laminated thick rectangular plates. J Sound Vib 1970;12: 187–99.
[100] Shiau L, Wu T. A high precision higher order triangular element for free vibration of general laminated plates. J Sound Vib 1993;161:265–79.
[101] Defense USDo. Military Handbook: Metallic Materials and Elements for Aerospace Vehicle Structures: US Department of Defense, 1990.
[102] Reddy JN. Mechanics of laminated composite plates and shells – Theory and analysis. Boca Raton, USA: CRC Press, 2004.